MASTERARBEIT | MASTER'S THESIS

Titel | Title

Metabolic Control of Inflammatory Processes

verfasst von | submitted by

Rebecca Schmidt BSc

angestrebter akademischer Grad | in partial fulfilment of the requirements for the degree of

Master of Science (MSc)

Wien | Vienna, 2026

Studienkennzahl lt. Studienblatt | Degree programme code as it appears on the student record sheet:	UA 066 862
Studienrichtung lt. Studienblatt | Degree programme as it appears on the student record sheet:	Masterstudium Chemie
Betreut von | Supervisor:	Univ.-Prof. Dr. Christopher Gerner
Mitbetreut von | Co-Supervisor:	Dr. Andrea Bileck MSc

Abstract

Chronic inflammation plays a role in age-related and inflammatory diseases, including cardiovascular diseases and cancer. Mitochondrial dysfunction is a key contributor to chronic inflammation and age-related diseases. Oxidative stress and inflammatory signaling can reinforce each other in a self-enhancing cycle, amplifying mitochondrial damage and inflammatory responses. Mitochondrial dysfunction often arises from oxidative damage to mitochondria, which disrupts energy metabolism and promotes inflammatory signaling. Oxidative stress contributes to aging by progressive accumulation of oxidative damage. Fibroblasts are central mediators of inflammation that secrete inflammatory signaling molecules and matrix-remodeling factors. Persistent activation of fibroblasts sustains chronic inflammation, making fibroblasts therapeutic targets for inflammatory diseases. This thesis investigates how oxidative stress-induced mitochondrial damage affects inflammatory responses in fibroblasts and how these effects differ with biological age. Oxidative stress and mitochondrial damage were induced using tert-butyl hydroperoxide (TBHP), while inflammation was triggered by the cytokine interleukin-1β (IL-1β). Adult primary fibroblasts (NHDF) were compared to embryonic Detroit 551 fibroblasts to assess age-related differences. Global proteomic profiling of the cellular proteome and secretome was performed using label-free quantitative mass spectrometry. IL-1β successfully induced inflammatory signaling and regulated known inflammation-associated proteins. TBHP triggered oxidative stress and altered redox-associated and mitochondrial proteins, confirming mitochondrial perturbation. The two fibroblast models displayed distinct basal proteomes, with NHDF cells possessing higher levels of proteins involved in prevention of oxidative stress and greater tolerance to TBHP, while Detroit 551 cells showed delayed adaptation to oxidative stress. Oxidative pre-stress prior to IL-1β stimulation affected inflammatory responses in a protein-specific manner, particularly after 48 h, suggesting that oxidative stress modulates inflammatory response in fibroblasts, in a time-delayed fashion. Overall, this thesis demonstrates that fibroblasts exhibit age-related differences in the response to oxidative stress and inflammatory stimuli, and that oxidative stress-induced mitochondrial damage modulates inflammatory responses.

Zusammenfassung

Chronische Entzündungen tragen zu altersbedingten und inflammatorischen Krankheiten, wie beispielsweise Krebs oder Herz-Kreislauf-Erkrankungen, bei, wobei mitochondriale Dysfunktion eine zentrale Rolle spielt. Oxidative Schäden an Mitochondrien führen zu mitochondrialer Dysfunktion, welche zu einem gestörten Energiemetabolismus und der Aktivierung entzündlicher Signalwege führt. Dabei verstärken sich entzündliche Signalübertragung und oxidativer Stress gegenseitig, was in einem selbstverstärkenden Kreislauf von mitochondrialem Schaden, oxidativem Stress und Entzündung resultiert. Altern und oxidativer Stress sind miteinander verbunden, da oxidative Schäden mit der Zeit akkumulieren können. Fibroblasten sind zentrale Mediatoren von entzündlichen Prozessen, die inflammatorische und Matrix-Remodellierungs-Faktoren sekretieren. Anhaltend aktivierte Fibroblasten tragen wesentlich zur Aufrechterhaltung chronischer Entzündungen bei und stellen ein potenzielles therapeutisches Ziel dar. Diese Masterarbeit untersucht die Effekte von oxidativ Stress-induzierten mitochondrialen Schäden auf die Entzündungsantwort in Abhängigkeit vom biologischen Zellalter. Zur Induktion von oxidativem Stress und mitochondrialem Schaden wurde das Peroxid tert-Butylhydroperoxid (TBHP) verwendet, und die Entzündungsreaktion wurde mit dem Zytokin Interleukin-1β (IL-1β) hervorgerufen. Um altersbedingte Unterschiede festzustellen, wurden adulte Fibroblasten (NHDF) mit embryonalen (Detroit 551) verglichen. Veränderungen im Zell- sowie sekretorischen Proteom wurden mittels quantitativer Massenspektrometrie untersucht. Die Entzündungsantwort wurde in Fibroblasten erfolgreich ausgelöst und durch bekannte Entzündungs-assoziierte Proteine bestätigt. Die Regulation von Mitochondrialen Proteinen und Redox-assoziierte Proteine bestätigten, dass TBHP oxidativen Stress und mitochondriale Störungen auslöst. Die adulten und embryonalen Fibroblasten unterschieden sich sowohl in ihrem Proteom als auch in ihrer Toleranz gegenüber TBHP, wobei NHDF über höhere Mengen antioxidativer Proteine verfügten und höhere TBHP-Konzentrationen tolerierten, während Detroit-551-Zellen erst zeitlich verzögerte Anpassungen zeigten. Die oxidative Vorbelastung durch TBHP vor der IL-1β-Stimulation beeinflusste die inflammatorische Antwort proteinspezifisch, insbesondere nach 48 Stunden, was darauf hindeutet, dass oxidativer Stress die Entzündungsreaktion in Fibroblasten zeitverzögert moduliert. Zusammenfassend wurde gezeigt, dass Fibroblasten altersabhängige Unterschiede in der Reaktion auf oxidativen Stress und entzündliche Reize aufweisen und dass durch oxidativen Stress verursachte mitochondriale Schäden die Entzündungsreaktionen modulieren.

Danksagung

Zuerst möchte ich mich bei Univ.-Prof. Dr. Christopher Gerner und Dr. Andrea Bileck für die Betreuung meiner Masterarbeit und das wirklich spannende Thema bedanken. Besonderer Dank gilt Dr. Andrea Bileck auch für die Einschulung in der Zellkultur.

Ich danke außerdem den Arbeitsgruppen von Univ.-Prof. Dr. Christopher Gerner und Ass.-Prof. Dr. Samuel Matthias Meier-Menches für die freundliche Aufnahme und das angenehme Arbeitsumfeld. Vielen Dank auch an Thomas Iellici für den hilfreichen Input, die Unterstützung und die netten Gespräche. Ein ganz besonderer Dank gilt auch meinen beiden Mit-Masterstudentinnen Valentina Heuschneider und Sofie Damian für die gemeinsamen Experimente und Stunden in der Zellkultur, die vielen lustigen Gespräche und unverzichtbaren gemeinsamen Kaffeepausen, ohne euch wäre diese Zeit nur halb so lustig gewesen.

Mein Dank gilt auch all meinen Freundinnen und Freunden, die mir während des Studiums begleitet und unterstützt haben. Besonders danken möchte ich meinen Freunden, die mich seit dem Bachelorstudium mit Kaffee, gemeinsamen Lerneinheiten und kollektivem Auslassen über das Studium begleitet haben, vor allem Robin Pfister, Katharina Himmler, Isabel Eder und Vera Brieskorn, meinen Mit-TutorInnen vom DCCC Ersti-Tut. Danke für die lustigen Spieleabende und die vielen gemeinsamen Stunden.

Auch möchte ich den DnD- und Spieleabend-Leuten für die wilkommene Ablenkung vom Alltag danken. Großer Dank geht auch an Lisa Pulferer und Julia Krottenthaler für die jahrelange Freundschaft, wertvollen Rat, ein offenes Ohr und viele schöne gemeinsame Erinnerungen, von gemeinsamen Urlauben und Cocktails bis hin zu Konzerten und unzähligen Gesprächen. Besonders danken möchte ich außerdem Alexandra Jexenflicker, die sich seit dem Start meiner Masterarbeit immer erkundigt hat wie es denn den Mitochondrien geht und stets ein offenes Ohr für mich hatte.

Vielen Dank auch an meine Arbeitsstelle und Kolleginnen für die große Flexibilität und die entgegenkommenden Arbeitszeiten, ohne die die erfolgreiche Fertigstellung meines Studiums in dieser Form nicht möglich gewesen wäre.

Zu guter Letzt, aber nicht weniger wichtig, möchte ich meinen Eltern Peter und Sabine Schmidt von ganzem Herzen danken. Danke für eure bedingungslose Unterstützung, eure aufbauenden Worte, eure Geduld und dafür, dass ihr mir jederzeit mit Rat und Tat zur Seite gestanden seid und euch mein Jammern immer angehört habt.

Danke!

Contents

Abbreviations

Abbr.	Abbreviation
2-CAM	2-chloroacetamide
acetyl-CoA	Acetyl coenzyme A
ACN	Acetonitrile
AKR1C2	Aldo-keto reductase family 1 member C2
ALDH1A1	Aldehyde dehydrogenase 1A1
ATP	Adenosine triphosphate
AUC	Area under curve
BCA	Bicinchoninic acid protein assay
BP	Biological process
BSA	Bovine serum albumin
CALB2	Calretinin
CC	Cellular component
CCL2	C-C motif chemokine ligand 2
CCS	Collisional cross section
COLs	Collagen alpha chains
CON	Control
CP	Ceruloplasmin
CXCL5	C-X-C motif chemokine 5
CXCL8	C-X-C motif chemokine ligand 8
DAMPs	Damage-associated molecular patterns
DC	Direct current
DDA	Data-dependent acquisition
DIA	Data-independent acquisition
DKK1	Dickkopf-related protein 1
DMEM	Dulbecco's Modified Eagle Medium
DMSO	Dimethyl sulfoxide
DNA	Deoxy ribonucleic acid
ECM	Extracellular matrix
EMEM	Eagle's Minimum Essential Medium
ER	Endoplasmic reticulum
ESI	Electrospray ionization
FA	Formic acid

FBS	Fetal bovine serum
FDR	False discovery rate
GCSH	Glycine cleavage system H protein
GO	Gene Ontology
GSH	Glutathione
IC_{50}	Half-maximal inhibitory concentration
ICAM1	Intracellular adhesion molecule 1
IL-17	Interleukin-17
IL-1β	Interleukin-1 beta
IL6	Interleukin-6
IMS	Ion mobility spectrometry
IPA	Isopropanol
LC	Liquid chromatography
LFQ	Label-free quantification
m/z	Mass-to-charge ratio
MF	Molecular function
MMP1	Interstitial collagenase
MMP3	Stromelysin-1
MMPs	Matrix metalloproteinases
MRPS34	Small ribosomal subunit protein mS34
MS/MS	Tandem mass spectrometry
MS1	Precursor ion scan
MS2	Fragment ion scan
mtDNA	Mitochondrial DNA
MTT	Thiazolyl Blue Tetrazolium Bromide
NADH	Nicotinamide adenine dinucleotide
NADPH	Nicotinamide adenine dinucleotide phosphate
NFKBIB	NF-kappa-B inhibitor beta
NF-κB	Nuclear factor kappa B
NHDF	Normal Human Dermal Fibroblasts
NINJ1	Ninjurin-1
Nrf2	Nuclear factor erythroid 2-related factor 2
P/S	Penicillin-Streptomycin
PASEF	Parallel Accumulation-Serial Fragmentation
PBS	Phosphate-buffered saline

PCA	Principal component analysis
PMPCB	Mitochondrial-processing peptidase subunit beta
PS	Phosphatidylserine
PSM	Peptide spectrum match
PTGS2	Prostaglandin G/H synthase 2
qTOF	Quadrupole time-of-flight
RF	Radio frequency
ROS	Reactive oxygen species
RP	Reversed phase
SASP	Senescence-associated secretory phenotype
SDC	Sodium deoxycholate
SDC4	Syndecan-4
SLC25A22	Mitochondrial glutamate carrier 1
SN	Secretome
TBHP	Tert-butyl hydroperoxide
TCEP	Tris (2-carboxyethyl) phosphine
TFA	Trifluoroacetic acid
TGF-β	Transforming growth factor beta
TIMS	Trapped ion mobility spectrometer
TNF	Tumor necrosis factor
TNFAIP8	Tumor necrosis factor alpha-induced protein 8
TNF-α	Tumor necrosis factor alpha
TXNIP	Thioredoxin-interacting protein
WCL	Whole cell lysate
XIC	Extracted ion current

1 Introduction

1.1 Inflammation

Inflammation is a normal, acute response to insult or injury. When this inflammation becomes dysregulated and persistent, it plays a vital role in chronic diseases such as cardiovascular diseases or cancers.[1,2]

1.1.1 Inflammatory Response and Resolution

Inflammatory response and wound healing are complex processes that consist of four phases: hemostasis, inflammation, proliferation and remodeling. During the inflammatory phase, neutrophils are recruited to the injury site by cytokines and growth factors derived from degraded platelets to establish homeostasis. They phagocytose bacteria or foreign bodies and secrete high levels of pro-inflammatory signaling molecules to further recruit immune cells. They are assisted by mast cells that break down the extracellular matrix (ECM), increase blood vessel permeability and secrete antimicrobial peptides. Subsequently, monocytes and macrophages are recruited to the injury site where they contribute to debris clearance by phagocytosis. Together with dendritic cells, they present antigens to trigger the adaptive immune response. After one day, neutrophils undergo apoptosis and are cleared by macrophages in a process called efferocytosis. Macrophages recognize the apoptotic signal molecule phosphatidylserine (PS) on the outside membrane of neutrophils, which functions as an “eat-me” signal. After efferocytosis, macrophages change their polarization from pro-inflammatory (M1 phenotype) to an anti-inflammatory, pro-regenerative phenotype (M2 phenotype). This transition is crucial for the resolution of the inflammation stage and initiation of tissue repair.[1]

1.1.2 Chronic Inflammation

Neutrophil cell death is essential for normal healing, as their clearance allows macrophages to transition from the pro-inflammatory M1 to the reparative M2 phenotype, which is associated with the production of anti-inflammatory mediators. Failure of this transition prevents proper resolution of inflammation. Unresolved inflammation becomes chronic and dysregulated. In chronic inflammation, neutrophils, monocytes and macrophages remain elevated. Persistent neutrophils, for example, release excessive amounts of proteases, reactive oxygen species (ROS) and neutrophil extracellular traps, leading to tissue damage. Overproduction of matrix metalloproteinases (MMPs) and inflammatory cytokines including tumor necrosis factor alpha (TNF-α), interleukin-1 beta (IL-1β) and interleukin-6 (IL-6) by immune cells damages the surrounding tissue and sustains inflammation. Fibroblasts also play a role in chronic inflammation, as they remain persistently activated, contributing to the sustained inflammatory environment and may promote progressive tissue dysfunction and fibrosis. Chronic inflammation is a central driver of several diseases, including rheumatoid arthritis,

atherosclerosis, and non-healing diabetic wounds. Persistent activation of immune and stromal cells can ultimately promote tissue fibrosis and long-term impairment of tissue function.[1,3]

1.1.3 Inflammation and Aging: Inflammaging

With advancing age, the damage from chronic, low-grade inflammations accumulates.[1] Aging is a complex biological process that is characterized by a progressive decline in cellular and physiological function of an organism. It is accompanied by an increased susceptibility to chronic, age-related diseases such as cardiovascular disease, diabetes or cancer. Nine hallmarks of aging have been identified: genomic instability, telomere shortening, epigenetic modifications, mitochondrial dysfunction, loss of proteostasis, dysregulated nutrient sensing, stem cell exhaustion, cellular senescence and altered cellular communication. These hallmarks are linked to chronic inflammation.[4] Aged mammals exhibit a pro-inflammatory phenotype that shows increased expression of genes linked to inflammation and immune response, elevated levels of cytokines such as IL6, as well as TNF-α and C-reactive protein, accumulation of damage-associated molecular patterns (DAMPs) and activation of nuclear factor kappa B (NF-κB) signaling, a central regulator of inflammatory responses. In 2000 *Franceschi et al.* introduced a term called inflammaging to describe this aged low-grade pro-inflammatory phenotype. Inflammaging is considered a biomarker for multimorbidity and common in most age-related diseases. This low-grade inflammatory state leads to disturbed immune homeostasis and immune function with an impaired ability to resolve inflammation.[4,5] As neutrophils age, their ability to phagocytose is reduced, they are more likely to undergo apoptosis without triggering inflammation, resulting in the production of ROS, thereby contributing to additional cellular damage. Macrophages show reduced efferocytosis, due to ROS cleaving the PS receptors. The reduced clearance of neutrophils in turn intensifies the cycle of inflammation and aging.[1]

Another central mechanism of inflammaging is cellular senescence. The cell cycle of senescent cells is permanently arrested, but they remain metabolically active and develop a senescence-associated secretory phenotype (SASP). SASP factors, such as IL-6, IL-1β, TNF-α, C-C motif chemokine ligand 2 (CCL2), C-X-C motif chemokine ligand 8 (CXCL8) and MMPs, can alter neighboring cells, recruit and activate immune cells and remodel surrounding tissue, facilitating more age-related damage and aging. This creates a positive feedback loop, where aged immune cells are recruited but cannot remove senescent cells efficiently. This leads to more senescent cells and secreted SASP factors, which further enhances and sustains chronic inflammation.[1,4,5]

Inflammaging contributes to a wide range of age-related diseases and is linked to increased oxidative stress, as elevated ROS levels and mitochondrial dysfunction promote cell damage and senescence.[4,5] As fibroblasts are involved in inflammatory processes, they represent a relevant cell type in inflammation and aging.[3]

1.2 Fibroblasts

Fibroblasts are commonly used in *in vitro* model systems to study various biological processes and diseases like wound healing, inflammation, oxidative stress and skin aging.[6]

1.2.1 Characteristics of Fibroblasts

Fibroblasts are diverse mesenchymal cells found in most tissues that differ functionally and transcriptionally across organs. They produce, maintain and remodel the complex ECM in connective tissues and support organ and tissue functions in which they provide signaling niches and positional cues. Major matrix components, including collagens, elastin and fibronectin, are deposited by fibroblasts, while they remodel the ECM through processes like crosslinking, glycosylation, and proteolysis. Fibroblasts shape the structural microenvironment, promote angiogenesis, establish chemokine gradients and engage in crosstalk with immune cells. In response to tissue damage or mechanical stress, fibroblasts can adopt a contractile myofibroblast phenotype. Besides their commonly known role of structural matrix production, fibroblasts actively contribute to intercellular communication by the secretion of a broad range of soluble mediators. Healthy fibroblasts help maintain tissue homeostasis and support wound healing through ECM production and interactions with the immune system. In chronic inflammatory diseases, fibroblasts can become persistently activated and promote chronic inflammation and tissue damage. They contribute to the secretion of pro-inflammatory cytokines, the establishment of chemokine gradients, and the recruitment of immune cells into affected tissues.[6,7]

1.2.2 Normal Human Dermal Fibroblasts

Normal Human Dermal Fibroblasts (NHDF) are primary fibroblasts derived from the dermis of an adult donor. They are spindle-shaped, adherent cells cultured under standard cell culture conditions. As primary cells, they have a finite lifespan and undergo senescence after a limited number of passages. They are widely employed in biomedical research, including research on wound healing, skin aging and response to pathogens.[8,9]

1.2.3 Detroit 551

The Detroit 551 (ATCC CCL-110, RRID: CVCL_2434) cell line consists of human fibroblasts derived from the skin of a normal White female embryo and was deposited by C.S. Stulberg. Detroit 551 are a finite fibroblast cell line with adherent growth and a lifespan of approximately 25 passages before they become senescent. They are used in a broad spectrum of biomedical research and are a useful study system for cytokine responses.[10,11]

1.2.4 Fibroblast Activation, Stress and Aging

As fibroblasts actively modulate immune responses, they are potential therapeutic targets for chronic inflammatory diseases. [7] Fibroblasts often persist and do not undergo apoptosis after inflammatory activation, which further reinforces inflammatory signaling, leading to persistent inflammation and promotion of long-term tissue dysfunction.[6,7]

Fibroblasts have distinct phenotypes depending on their state. Homeostatic fibroblasts are activated in inflamed tissues by various cytokines and recognition signals, which include tumor necrosis factor (TNF), interleukin-17 (IL-17), IL-1β, lipopolysaccharide (LPS), and DAMPs. These inflammatory stimuli induce a pro-inflammatory fibroblast phenotype, whereas mechanical cues and transforming growth factor beta (TGF-β) signaling promote differentiation toward a contractile myofibroblast phenotype. Myofibroblasts are crucial in wound healing and tissue repair, but when their activation persists, they accumulate ECM and form stress fibers, resulting in fibrosis and scar formation. Inflammatory fibroblasts and myofibroblasts are distinct activation states. Chronic inflammatory signaling can, however, promote the transition from inflammatory to myofibroblast phenotype, linking chronic inflammation to fibrosis. Inflammatory fibroblasts retain immune cells in inflamed tissue and amplify inflammation.[6,7]

Inflammatory fibroblasts secrete cytokines (IL-6, IL-1β, TNF), chemokines (CXCL1, CXCL2, CXCL5, CXCL12, CCL2, CCL19), adhesion molecules, MMPs and eicosanoids, and are regulated, among others, by NF-κB and DAMP signaling. Myofibroblasts, in contrast, secrete ECM proteins (collagens, fibronectin), matrix-remodeling enzymes, and immunomodulatory mediators such as TGF-β and CCL2.[2,3,7,12]

Proteomic profiling has revealed fibroblasts' hallmarks of inflammation, including innate immune response, cell adhesion and migration, cell proliferation and differentiation, response to oxidative stress, angiogenesis and reorganization of the ECM, as well as processes related to monosaccharide metabolism.[2]

1.3 Oxidative Stress and Reactive Oxygen Species

Oxidative stress stems from an imbalance of oxidative- and anti-oxidative processes like excessive ROS production. It plays a role in the pathogenesis of various inflammatory diseases and can trigger and mediate cell death.[13,14]

1.3.1 Oxidative Stress and Aging

Oxidative stress is known to contribute to aging. The link of aging and oxidative stress has first been proposed in 1955 by Harman as the free radical theory of aging. It postulated that the process of aging and shorter lifespan are a result of accumulated oxidative damage by free radicals to the cells macromolecules resulting in functional decline. This theory was later revised in 1972 by Harmann and called the mitochondrial free radical theory of aging. It identified mitochondria as the predominant source of intracellular ROS and suggested that mitochondrial deoxyribonucleic acid (DNA), due to its proximity to ROS production sites and its limited repair capacity, is particularly vulnerable to oxidative damage. Damage to mitochondria results in further ROS production, leading to a vicious cycle of more oxidative stress. Modern understanding has become more nuanced, shifting the view of ROS from a harmful byproduct to having both beneficial as well as pathological effects. As physiological ROS are important in signaling, aging is not just linked to ROS itself, but rather to elevated levels of ROS. As antioxidant defense and mitochondrial efficiency decline with age, their repair mechanisms and mitophagy are also impaired, therefore proteins, lipids, and nucleic acids are damaged progressively and cellular function is lost. Oxidative stress connects several consequences of aging, such as mitochondrial dysfunction, impaired proteostasis, genomic instability, and the development of cellular senescence.[4,15]

1.3.2 Sources of ROS

ROS can arise from both endogenous and exogenous sources. Exogenous ROS are generated by environmental factors such as radiation, ultraviolet light, chemicals, metals, xenobiotics, pollutants, drugs and alcohol metabolism. Endogenous ROS are byproducts of cellular processes, including inflammation and infection where activated immune cells like neutrophils and macrophages produce ROS. Mitochondria are the major intracellular source of ROS through electron leakage from the electron transport chain.[4,15]

1.3.3 Physiological Roles of ROS in Signaling, Homeostasis and Hormesis

At physiological levels, ROS are important in signaling as second messengers. Superoxide and hydrogen peroxide regulate redox-dependent signaling mechanisms, mostly by oxidation of the thiolate anion ($Cys\text{-}S^-$) to the sulfenic acid intermediate (Cys-SOH). ROS also aids host defense acting in signaling pathways such as NF-κB signaling pathway or nuclear factor erythroid 2-related factor 2 (Nrf2)-mediated signaling pathways. Redox-dependent signaling involves processes like gene expression, metabolism, as well as cell proliferation and differentiation. Both too high and too low ROS levels have pathological effects. This ROS signaling is required for cell homeostasis and includes cell cycle progression, wound healing and aiding immune response, too low levels impair their physiological signaling. Too high levels, on the other hand, lead to irreversible damage on macromolecules and organelles, amplifying aging and disease progression. The theory of mitohormesis describes that moderate ROS levels might activate compensatory mechanisms to protect the cell and its organelles from oxidative damage and aging phenotype.[4,15]

1.3.4 Mechanisms of Oxidative Damage

Oxidative damage develops when ROS exceeds cells' antioxidative capacity. This results in damage to lipids, proteins and DNA, which can impair structural integrity, signal transduction and survival. Oxidative stress is one of the main sources of accumulated DNA damage. DNA damage has been linked to increased age and DNA repair capacities decline with age as well. ROS can oxidize DNA or lead to hard to repair double strand breaks and can ultimately result in cell cycle arrest or cell death. Mitochondrial DNA is especially prone to damages and is a factor in mitochondrial loss of function. [4,15] While normal protein oxidation is essential for redox signaling, particularly the oxidation of cysteine, excessive oxidation from ROS can lead to fragmentation, cross-linking and changes in 3D structure of proteins. This influences physiological properties, enzyme activity and signaling and can further lead to unfolding of proteins and accumulation of aggregated proteins. [15] Polyunsaturated fatty acids are highly susceptible to ROS. Excessive free radicals start a chain reaction that results in lipid peroxides and aldehydes that form various reactive species like aldehydes. This so called lipid peroxidation results in damages to organelles by decreasing membrane fluidity and leading to membrane permeabilization. [4,15] Lipid peroxidation has been linked to mitochondrial membrane permeability and ferroptosis. [14] ROS can also alter calcium channels and calcium homeostasis. Perturbed calcium homeostasis leads to mitochondrial loss of function and drives cell death signaling.[15–17]

1.3.5 Cellular Responses to Oxidative Stress and Aging

The oxidative stress response involves numerous redox-sensitive proteins, including antioxidant systems (SODs, catalase, GPXs, PRDXs, TXN/TXNRD), stress regulators such as HO-1, Nrf2 and sirtuins, as well as ROS-producing enzymes like NOX2/NOX4, XO, MPO and MAO. Changes in glutathione GSH levels, GPX4 activity and lipid ROS serve as key molecular markers for oxidative damage and ferroptosis. Excessive or persistent ROS overwhelm antioxidant defenses, which results in oxidative damage to lipids, proteins and nucleic acids. This causes the activation of stress responses, such as the upregulation of antioxidant and detoxifying enzymes, activation of DNA repair and protein quality control, as well as impaired mitochondrial dynamics. Sustained oxidative stress could also lead to cell cycle arrest. [4,15] Oxidative stress can influence inflammatory signaling pathways, such as NF-κB signaling. Both too low and too high levels of ROS impair cellular function.[4,7,15]

1.3.6 tert-Butyl Hydroperoxide as an Oxidative Stressor

Oxidative stress can be induced experimentally to research stress responses and associated cell death. This is commonly done by inorganic peroxides like hydrogen peroxide (H_2O_2) or organic peroxides like tert-butyl hydroperoxide (TBHP) or cumene hydroperoxide. Organic peroxides like TBHP differ from H_2O_2. H_2O_2 is hydrophilic and diffuses slowly into cells through aquaporins, leading to widespread oxidative damage in the cell. Organic peroxides like TBHP on the other hand, are more lipophilic and target membranes directly, and preferentially membrane-rich organelles like mitochondria and inducing lipid peroxidation, loss of membrane integrity as well as loss of function. Additionally, TBHP exhibits higher intracellular stability than H_2O_2, which results in more persistent oxidative stress and sustained redox imbalance. Unlike H_2O_2, which induces apoptosis or unspecific necrosis, TBHP is known to induce ferroptosis. TBHP-induced ferroptosis is characterized by iron-dependent lipid peroxidation, lipid ROS accumulation as well as mitochondrial iron overload and dysfunction. In fibroblasts (NHDF), it was shown that TBHP induced oxidative stress, including alterations in cellular redox balance, induction of antioxidant stress markers and loss of mitochondrial membrane potential, accompanied by impaired energy metabolism.[13,14,18]

1.4 Mitochondria and Mitochondrial Dysfunction

Since mitochondria are profoundly affected by oxidative stressors like TBHP and play essential roles in both inflammation and aging, they represent a critical interface between metabolic dysfunction and chronic cellular stress.[5,18]

1.4.1 Structure and Function

Mitochondria originated through endosymbiosis from prokaryotic ancestors to eukaryotes and are essential for the evolution of complex organisms. They are highly complex cell organelles that constantly change shape, divide, fuse and fission. Mitochondria are associated with the cytoskeleton and interact with the endoplasmic reticulum (ER) to facilitate lipid transfer and their fission. Structurally, mitochondria possess two membranes, an inner and an outer membrane. The inner membrane separates the intermembrane space from the mitochondrial matrix and forms folds called cristae to enlarge the area for oxidative phosphorylation. While the inner membrane is selective and holds complexes for the electron transport chain, the outer membrane is freely permeable. The matrix contains mitochondrial DNA (mtDNA), proteins and ribosomes. The intermembrane space encloses the same small molecules as the cytoplasm and cytochrome c. In the matrix, pyruvate and fatty acids are converted to acetyl coenzyme A (acetyl-CoA) and enter the citric acid cycle for energy production where it is oxidized to CO_2 and H_2O. Nicotinamide adenine dinucleotide (NADH) and flavin adenine dinucleotide ($FADH_2$) then transfer their bound electrons to the electron transport chain in the inner membrane, where a proton gradient is utilized by ATP synthase to generate the adenosine triphosphate (ATP) phosphate bond. This yields around 15 times more ATP than glycolysis alone.[19]

Besides energy production, mitochondria play essential roles in cellular metabolism. They buffer the redox potential in the cytosol ($NADH/NAD^+$ ratio), provide nicotinamide adenine dinucleotide phosphate (NADPH), synthesize iron-sulfur clusters critical for electron transfer and genome stability, produce phospholipids such as cardiolipin for cell membrane biosynthesis and regulate calcium homeostasis. Calcium overload can trigger apoptosis. Additionally, the intrinsic pathway of apoptosis depends on mitochondria as well.[19,20]

1.4.2 ROS Induces Mitochondrial Damage

The mitochondrial respiratory chain is a main source for endogenous ROS. Given the close proximity to ROS, mitochondria are primary targets of oxidative damage. Excessive ROS damages mitochondrial membranes, proteins and mitochondrial DNA, thereby impacting mitochondrial structure and function. This damage compromises mitochondrial membrane integrity and promotes mitochondrial leakage, triggering the release of mitochondrial damage-associated molecular patterns (DAMPs) and further ROS generation, establishing a self-amplifying cycle of mitochondrial dysfunction and oxidative stress. As damaged mitochondria generate increased levels of ROS, mitochondrial injury is reinforced and not resolved. Released mitochondrial DAMPs include cardiolipin, mtDNA, N-formyl peptides and cytochrome c. Beyond being a marker of mitochondrial damage, cytochrome c also functions as a key mediator of mitochondrial apoptosis and contributes to inflammatory signaling. Due to their bacterial origin, mitochondrial components resemble pathogen-associated molecules and are thus recognized

by immune receptors, promoting a sustained inflammatory response, linking mitochondrial oxidative damage to chronic inflammation.[5,15,21]

1.4.3 Mitochondrial Dysfunction

Mitochondrial dysfunction describes a state where mitochondria fail to maintain energy production, redox homeostasis and signaling. It is characterized by decreased ATP production, potassium efflux, disturbed calcium homeostasis, altered NADH/NAD^+ homeostasis and increased mitochondrial ROS production. These alterations impair mitochondrial function compromises redox-dependent signaling pathways, while mitochondrial ROS promote oxidative damage. Disturbed calcium homeostasis further drives the loss of mitochondrial function and integrity. Damaged mitochondria are usually removed via lysosomes in a process called mitophagy, a form of mitochondrial quality control. When larger amounts of mitochondria are impaired, mitophagy is impaired as well, leading to the accumulation of damaged mitochondria and inflammatory responses in a so-called feedforward loop.[5,21]

1.4.4 Mitochondria in Regulated Cell Death

To ensure an organism's health, damaged, infected or dysfunctional cells are removed in a controlled manner. One form of regulated cell death is apoptosis, which is a programmed process in which cells destroy themselves and are removed by phagocytotic cells. During apoptosis cells shrink, condense and fragment their components and package them into apoptotic bodies. This process depends on the activation of caspases by an apoptotic signal and is generally considered non-inflammatory, as cellular contents remain enclosed. Apoptosis can be triggered by two pathways an extrinsic pathway and an intrinsic one. The extrinsic one is triggered by signaling proteins binding to surface death receptors, while the intrinsic pathway, also called mitochondrial pathway, is triggered by the release of mitochondrial proteins, such as cytochrome c, into the cytoplasm. The intrinsic pathway depends on the integrity of the mitochondrial outer membrane, linking mitochondrial integrity to cell death. Another form of cell death is necrosis, which is an acute response where cells swell and burst and induce an inflammatory response that is often a result of energy depletion. There is a form of mitochondrial regulated necrosis, called mitochondrial permeability transition driven necrosis, caused by calcium overload, oxidative damage and energy depletion, linking mitochondrial oxidative stress to inflammation. Another form of necrosis is ferroptosis, which is characterized by iron-dependent lipid peroxidation, lipid ROS accumulation, lipid damage and membrane disruption. While ferroptosis itself is not mediated by mitochondria, it is linked to mitochondrial function, as they play a role in iron metabolism, lipid peroxidation and exhibit changed morphology in ferroptotic cells.[14,20–22]

1.4.5 Mitochondria and Inflammation

Mitochondria play a central role in inflammatory processes. Due to their endosymbiotic origin, their components resemble bacterial or pathogen molecules. Mitochondrial damage results in the release of mitochondrial DAMPs that match pathogen-associated patterns, which are recognized by pattern recognition receptors and initiate an inflammatory response. Mitochondrial dysfunction is closely linked to the activation of inflammasomes. Mitochondrial ROS and mtDNA are inflammasome activators, which trigger the release of cytokines and recruit immune cells. As mitophagy is impaired during mitochondrial dysfunction, dysfunctional mitochondria are not efficiently removed, resulting in persistent ROS production, continuous DAMP release and sustained inflammatory signaling.[5,21]

1.5 Proteomics

1.5.1 Proteomics Techniques and Applications

Proteins are biopolymers that carry out a wide range of essential biological functions in living organisms including structural roles, catalysis of chemical reactions, and signaling to regulate biological processes. Their abundance, structure and modifications reflect on a cell's functional state and can provide insights into molecular mechanisms in health and disease. To investigate these complex and dynamic protein networks and interactions, the field of proteomics has emerged. Proteomics focuses on the large-scale study of protein structure and function of all proteins in a cell, tissue or organism, the proteome, regarding composition, abundance differences, structure, functions and interactions. Proteomics has a wide range of applications in biomedical research to provide insights on how protein expression, structure and interactions change over time or in response to internal or external stimuli. There are different types of proteomics with different focuses. Expression proteomics examines qualitative and quantitative differences in protein levels between conditions, whereas structural proteomics aims to determine the structure of proteins and protein complexes. Functional proteomics investigates the functions of proteins including signaling pathways and interaction networks. Researching post-translational modifications with branches such as phosphoproteomics and glycoproteomics further expands the scope of proteomics by revealing additional layers of cellular regulation and signaling. These approaches are valuable tools for studying aging, various diseases such as cancer or cardiovascular diseases, as well as drug discovery, personalized medicine and biomarker discovery.[23]

1.5.2 Shotgun Proteomics

Mass spectrometry-based proteomics can be divided into two strategies, top-down proteomics and bottom-up or shotgun proteomics. In top-down proteomics, intact proteins and peptides are analyzed directly, allowing for the characterization of distinct proteoforms. In contrast, bottom-up proteomics uses peptides from protein digestion. This provides a higher depth of proteome coverage and is suitable for complex samples such as cell lysates. In the shotgun approach, protein samples are enzymatically digested, most commonly using a combination of trypsin and LysC. Both enzymes are serine proteases, with trypsin cleaving after lysine and arginine residues except when followed by proline, and LysC cleaving specifically after lysine residues. The resulting peptides are then separated by liquid chromatography (LC) and analyzed by tandem mass spectrometry (MS/MS). Quantification can be achieved by label-free approaches or isotopic labeling. After acquisition, peptide spectra are matched to candidate spectra derived from a protein database. The matches are scored by a search algorithm, with the best-scoring candidate peptide being called a peptide spectrum match (PSM). Identified spectra are then used to infer protein identities and abundance. To assess the statistical confidence of a PSM, peptide spectra are searched against a decoy database of shuffled or reverse sequences to estimate the proportion of false hits, which is then used to calculate the false discovery rate (FDR).[23]

1.5.3 Data-dependent Acquisition

Data acquisition is crucial for proteomics and involves the collection of precursor ions (MS1) and fragment ions (MS2). There are two acquisition strategies data-dependent acquisition (DDA) and data-independent acquisition (DIA). In DDA the MS2 scans are influenced by the MS1 data. In untargeted DDA, MS1 spectra are acquired iteratively to detect precursor ions. The most intense precursor ions are selected for fragmentation in the following MS2 scans. To avoid repeated fragmentation, precursor masses are put on a dynamic exclusion list that excludes ions from reselection for a defined time period. A limitation of this approach is that precursor selection is stochastic, which can lead to variability between measurements. Targeted DDA focuses on the fragmentation of predefined mass-to-charge ratio (m/z) values of peptides of interest, which decreases overall proteome coverage but increases the likelihood of consistent identification of target proteins. In contrast, in DIA precursor ions are fragmented regardless of MS1 intensities, which improves reproducibility but increases complexity.[23]

1.5.4 Label-free Quantification

In quantitative proteomics, changes in protein abundance are essential to identify differences in protein abundances to understand underlying biological processes. [23,24] There are various methods to assess peptide abundance and abundance changes across samples, such as peptide labeling with isobaric tags, tandem mass tags and label-free quantification (LFQ). In contrast to stable isotope-based labeling, LFQ does not require additional preparation steps and can be done with spectral counting or extracted ion current (XIC)-based approaches. LFQ is suitable for samples that cannot be labeled. It can be performed using software packages such as MaxQuant. High mass resolution is crucial for accurate quantification. One widely used implementation of LFQ is in the MaxQuant software package, where "delayed normalization" is used, which assumes that most of the proteome does not differ between conditions and thus can be used as a relative standard. This relative standard is used to calculate normalization coefficients *via* Levenberg-Marquardt optimization in order to minimize variation in the stable proteome. LFQ values are calculated across LC-MS/MS experiments using the area under curve (AUC) from the XICs.[24]

1.5.5 Secretome Profiling

The secretome is a complex set of molecules secreted by living cells and can be studied in tissue-derived proximal fluids or cell culture-conditioned media. Secretome proteins play essential roles in cell signaling, communication and migration, including growth factors, proteases, cytokines, chemokines and extracellular matrix proteins. The composition of the secretome is highly dynamic and reflects the physiological or environmental state cells are in.[25,26] Secretomics encompasses the global analysis of proteins produced by cells, tissues or organisms in a condition and time dependent manner. Proteomic profiling of the secretome has become a valuable approach for biomarker and drug target discovery. Secreted proteins are released through classical pathways, like signal peptides, as well as non-classical and exosomal routes. Through these mechanisms, secreted proteins participate in intercellular cross-talk and numerous biological processes such as immune responses, development, adhesion, proteolysis, homeostasis, and extracellular matrix organization.[25,27] Secretome analysis faces several challenges. One major difficulty arises from typically low concentrations of secreted proteins due to their high dilution in body fluids or culture media. Contamination is another critical issue, as cytoplasmic or other non-secreted proteins released during cell lysis and cell death can mask the secretome profile. In cell culture studies, serum proteins such as albumin and serotransferrin from fetal bovine serum (FBS) also mask secretome proteins. These serum proteins also often persist despite extensive washing steps and their composition varies between serum batches. To minimize this interference, cells are often incubated in serum-deprived medium. Serum starvation, however, introduces additional obstacles, as the lack of serum can result in metabolic stress, reduced

proliferation, altered gene expression and signaling as well as apoptosis. Apoptosis also results in the release of intracellular proteins into the medium, where they can mask the secretome or be misaccounted for secreted proteins. This also restricts the experimental design, as the cells viability is often limited to around 24 hours.[25,26]

Another challenge is the dynamic nature of protein secretion itself. Secretion rates depend on cell proliferation and can change under different conditions. In addition, proteins are often released through non-classical mechanisms, often *via* exosomes. The exosomal secretions of proteins that are normally considered intracellular, which adds a layer of complexity to the microenvironment and complicates secretome analysis.[25,26] One exemplary application of secretomics is the study of senescent cells. Even though senescent cells permanently halt their cell cycle, they still remain metabolically active and secrete a set of characteristic factors known as SASP. The SASP includes pro-inflammatory cytokines, chemokines, growth factors and proteases. While it can aid tissue repair and regeneration, chronic SASP secretion drives inflammation and tissue dysfunction contributing to age-related pathologies. Senescent cells also release exosomes and microvesicles in addition to the SASP, propagating senescence to neighboring cells in the tissue microenvironment.[27]

1.5.6 LC-MS/MS

Complex peptide samples require separation prior to MS analysis. Peptides are first separated by liquid chromatography to reduce complexity and are then further ionized and analyzed by MS.[23]

1.5.6.1 Nano Liquid Chromatography

LC is a separation technique commonly used in mass spectrometry-based proteomics to minimize ion suppression, a phenomenon where over-abundant peptides mask low-abundant ones. Reversed phase (RP) LC is commonly used in proteomics, separation is based on the binding of peptides in aqueous solvent to C18 material *via* non-polar interactions determined by their hydrophobicity, which are disrupted by increasing concentrations of organic solvent. Due to the complex nature of the proteome and the often-limited amount of available sample, nano-scale liquid chromatography (nanoLC) is widely used in proteomics. NanoLC uses lower flow rates and smaller internal column diameters to increase sensitivity. To protect the analytical column, and for desalting as well as contaminant removal, samples are often first loaded onto a pre-column or trapping column.[23,28]

1.5.6.2 Nano Electrospray Ionization

Electrospray ionization (ESI) is a soft ionization technique enabling the transfer of analytes from liquid to gas phase. The LC eluent is sprayed through a narrow nozzle under a high voltage, resulting in a mist of charged droplets. As the solvent evaporates, the droplets shrink and electrostatic repulsion increases. When this repulsion exceeds the surface tension, a Coulomb explosion occurs, resulting in even smaller droplets. Small enough droplets lead to ions being transferred into the gas phase. This

process is aided by a nebulizer gas, like nitrogen, acting as a drying gas and breaking liquids into drops. Nano-ESI operates at reduced flow rates compared to conventional ESI, resulting in smaller initial droplets, which increases ionization efficiency. The mobile phase is typically acidified to promote protonation of analytes. In proteomics, tryptic peptides have one positive charge at the N-terminal amine and an additional charge on the side chain of the C-terminal lysine or arginine residue, facilitating ionization. Due to the smaller droplet size and reduced dilution effects, nano-ESI enables the detection of low-abundant peptides. It also exhibits improved tolerance toward aqueous solvents and moderate salt concentrations compared to conventional ESI.[29]

1.5.6.3 timsTOF Pro

In proteomic profiling, peptides are eluted from the LC and electrosprayed into MS, where their collision-induced fragments are identified by database identification. The depth is limited by chromatographic separation, sensitivity and sequencing speed of the mass spectrometer. Bruker Daltonics developed the timsTOF Pro to provide an additional dimension of separation using a trapped ion mobility spectrometer (TIMS) coupled orthogonally to a quadrupole time-of-flight mass analyzer (qTOF). TOF mass analyzers separate ions based on their m/z, by measuring the time required for ions to travel a fixed distance after acceleration to the same kinetic energy. TOF analyzers have a high acquisition rate but lack sensitivity at high scanning speeds, however, they are compatible with ion mobility spectrometry (IMS). In IMS, ions are separated by their ion mobility, which is related to their collisional cross section (CCS) in the gas phase. In the case of TIMS, ions are trapped stationary in a radio frequency (RF) tunnel with a direct current (DC) and a gas flow. Larger ions are slowed down more by the gas flow, as they have a larger CCS, and are thus retained longer than smaller ions. Ions are released by gradually lowering the electrical field for sequential analysis. The accumulation and mobility analysis in TIMS can be separated by using a longer TIMS tunnel. In this dual TIMS setup, ions are trapped in the first part of the TIMS tunnel and resolved by mobility in the second part of the TIMS tunnel. Low mobility ions are released first, as they require a lower electrical field to overcome the opposing gas flow. This simultaneous accumulation and ion mobility analysis allows parallel storage and separation, which improves duty cycle and sensitivity. The Parallel Accumulation-Serial Fragmentation (PASEF) technology uses a dual TIMS. As interfering background ions are separated by ion mobility, the signal-to-noise ratio of the qTOF increases. TIMS adds an additional fourth dimension to the data, while PASEF technology increases efficiency. In DDA PASEF technology also increases the number of precursors that can be targeted, which enables scanning low abundant precursors multiple times to increase signal-to-noise ratios.[30–32]

2 Aims and Objectives of this Thesis

As mitochondrial dysfunction is a key contributor to chronic inflammation and age-related diseases, this thesis aims to explore how oxidative stress-induced mitochondrial damage affects inflammatory processes in fibroblasts, and whether these effects differ between fibroblasts of different biological age. Mitochondrial damage was induced in fibroblasts by oxidative stress using TBHP. Inflammation was induced using the cytokine interleukin 1-beta. To assess age-related differences in cellular responses, primary adult fibroblasts (NHDF) were compared to embryonic fibroblasts (Detroit 551). Proteomic profiling of both the cellular proteome and the secretome was performed using mass spectrometry to identify molecular changes associated with mitochondrial dysfunction and inflammation, including the release of cytokines and stress response markers.

3 Materials and Methods

3.1 Experimental Design

3.1.1 Short-term Comparison Experiment

To compare short-term proteomic responses of differently aged fibroblasts to inflammatory stimulation, oxidative stress, and their combined effects, a short-term comparison experiment was performed. Two human fibroblast models, embryonic Detroit 551 and adult NHDF were used. The overall experimental setup can be seen in the schemes in Figure 1.

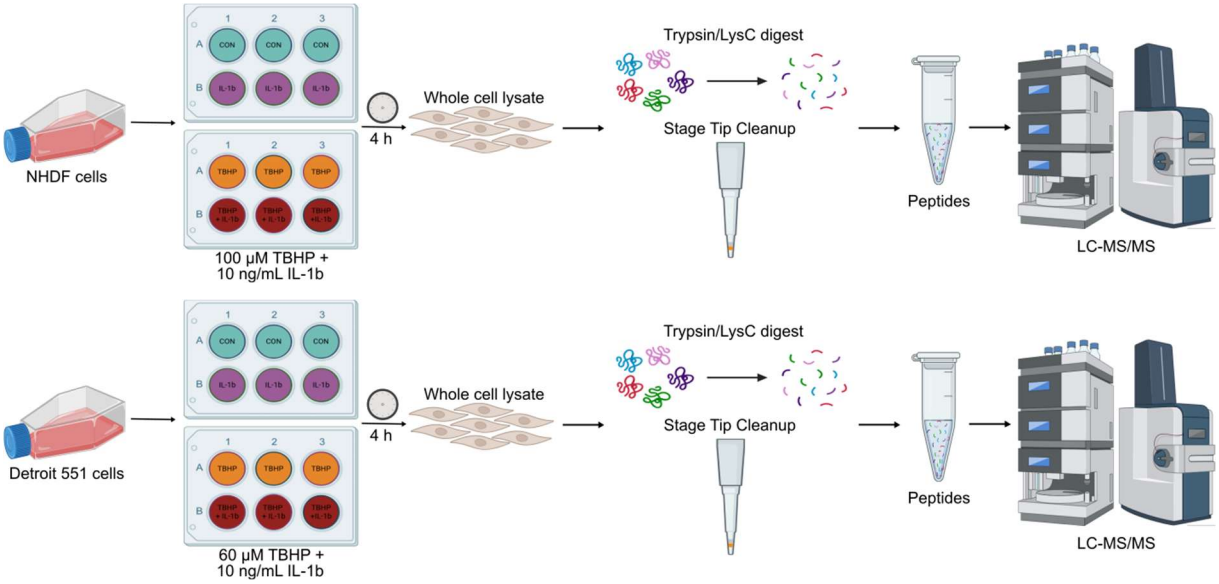

Figure 1 Overview of the short-term comparison experimental design. NHDF and Detroit 551 fibroblasts were treated with IL-1β, TBHP, or a combination of TBHP pre-treatment followed by IL-1β stimulation. Cells were harvested after 4 h for whole-cell lysate proteomics. Graph created with BioRender.com.[33]

There were four experimental conditions: untreated control (CON), IL-1β treated cells (IL-1b), TBHP treated cells (TBHP), and TBHP pre-stress followed by IL-1β stimulation (TBHP + IL-1b). At the start of the experiment, oxidative stress was induced by subjecting the TBHP and TBHP + IL-1β conditions to TBHP-containing medium, while the CON and IL-1β conditions underwent a normal medium change. After 1h of TBHP exposure, 10 ng/mL of L-1β (IL-1 beta human, Sigma-Aldrich, recombinant, expressed in *E. coli*; dissolved in sterile PBS) was added to the IL-1β and TBHP + IL-1β conditions. TBHP concentrations were selected close to the respective IC_{50} values for each cell type to induce comparable levels of oxidative stress while accounting for differences in stress tolerance between NHDF and Detroit 551 fibroblasts. Cells were harvested after a total incubation time of 4 h, to capture early proteomic changes associated with oxidative stress, inflammation, and their combination. Whole cell lysates were collected for proteomic analysis. General cell culture procedures as well as sample processing are described in the following sections.

3.1.2 Time-course Experiment

To investigate how oxidative pre-stress modulates inflammatory responses over time, a time-course experiment was performed in embryonic Detroit 551 fibroblasts. The overall experimental setup can be seen in the scheme in Figure 2.

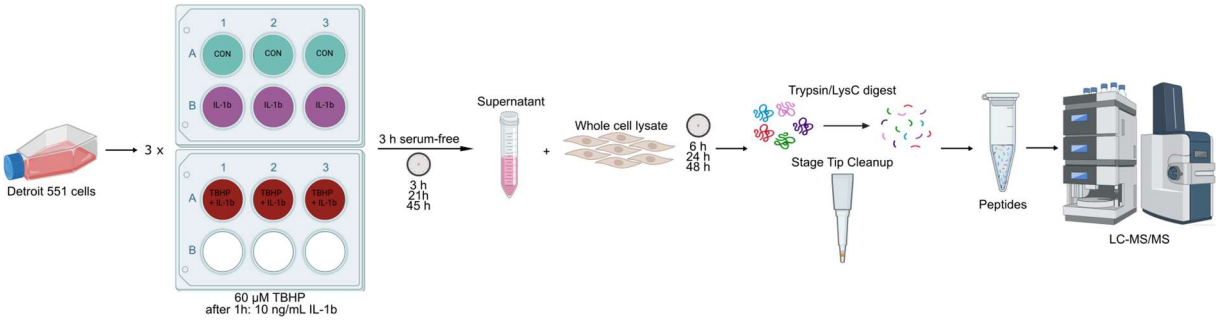

Figure 2 Overview of the Detroit 551 time-course experimental design. Cells were stimulated with IL-1β or a combination of TBHP pre-treatment followed by IL-1β stimulation. Cells were harvested at multiple timepoints and whole-cell lysates and secretomes were analyzed. Graph created with BioRender.com.[33]

There were three experimental conditions: untreated control (CON), IL-1β treated cells (IL-1b) and TBHP pre-stress followed by IL-1β stimulation (TBHP + IL-1b). At the start of the experiment (t=0 h), oxidative pre-stress was induced by exposing the TBHP + IL-1β condition to medium containing 60 µM TBHP, while CON and IL-1β conditions underwent a medium change. After 1 h of TBHP pre-treatment, inflammatory stimulation was induced by adding 10 ng/mL IL-1β to the IL-1β and TBHP + IL-1β conditions. Cells were sampled at multiple timepoints (6 h, 24 h, and 48 h). To enable the analysis of the secretome, cells were incubated in serum-free medium 3 h prior to sampling. Cells and culture medium were harvested at the respective timepoints and processed as described in the following sections.

3.2 Cell Culture

All cell culture procedures were performed in an incubator (Thermo Scientific, HERACELL 150i CO2 Incubator) at 37 °C and 5 % CO_2 in a humidified environment and in flow cabinets (Thermo Scientific, HERASAFE KS). The culture media was preheated to 37 °C using a water bath (huber 110A).

Two different cell lines were used for the proteomics experiments, namely NHDF (provided by (Verena Paulitschke from the Department of Dermatology of the Medical University of Vienna, Austria), and Detroit 551 (CCl-110, purchased from the American Type Culture Collection (ATCC)). NHDF cells were cultured in RPMI-1640 Medium with L-glutamine and sodium bicarbonate (Sigma-Aldrich), supplemented with 10 % Fetal Bovine Serum (FBS, gibco) and 1 % Penicillin-Streptomycin (P/S, Sigma-Aldrich, 10,000 units penicillin and 10 mg streptomycin/mL). Detroit 551 cells were cultured in Minimum Essential Medium Eagle with Earle's salts (EMEM), L-glutamine and sodium bicarbonate

supplemented with 10 % FBS and 1 % P/S. Both cell lines (NHDF passage number (p) 18 and Detroit 551 p 19) were thawed and slowly pipetted into a 15 mL falcon tube containing 9 mL of the respective culture medium and then centrifuged at 1100 rpm for 5 min (Thermo Scientific HERAEUS MEGAFUGE 16R). After centrifugation, the medium was removed from the pelleted cells and 1 mL of fresh culture medium was added to resuspend the cells. The cell suspension was then pipetted into a T75 cell culture flask (Sarstedt) containing 9 mL of fresh culture medium.

Every two days, the cell's confluency was checked under a light microscope (Zeiss Primo Vert equipped with a AxioCam ERc5s camera) connected to the Software ZEN (2011 version, blue edition) at 40x magnification. The culture medium was replaced by fresh culture medium every two days, until the cells reached full confluence. At this point, they were subcultured by washing the cells with 10 mL of phosphate buffered saline (PBS, sterile filtered, 137 mM NaCl, 2.7 mM KCl, 10 mM Na_2HPO_4 and 1.8 mM KH_2PO_4 in H_2O) and incubating them with 3 mL of 0.25 % Trypsin-EDTA (gibco) for 4 min (Detroit 551 cells) or 6 min (NHDF cells) and tapping the flask against the palm of the hand to detach residual cells, before quenching trypsinization with 7 mL of the respective culture medium. Residual cells were washed from the T75 flasks by pipetting up and down. The detached cell suspension was transferred into 15 mL falcon tubes and centrifuged at 1100 rpm for 5 min to pellet the cells. The supernatant was then removed and the cell pellet was gently resuspended in 1 mL of culture medium. The cells were then either split to two T75 flasks (split ratio 1:2) or counted and seeded as described in the experiments' sections. Cells were counted by staining 10 µL of cell suspension with 10 µL of 0.4 % Trypan Blue solution (Sigma-Aldrich). 10 µL of the stained cell suspension was then pipetted onto an Automated Brightfield Cell Counter (DeNovix CellDrop BF) using the Trypan Blue Assay protocol adjusted for each cell line according to roundness, diameter and dilution factor. The cells were once counted manually using a Neubauer chamber to verify the Automated Brightfield Cell Counter settings and results.

To preserve cells for long-term storage, the cells were periodically frozen (NHDF: p 19, p 30, p 31, Detroit 551: p 13, p 14, p 17). Similarly to subculturing, the cells were detached from the flask with 3 mL of Trypsin-EDTA and pelleted by centrifugation at 1100 rpm for 5 min. The supernatant was removed and the cells were resuspended in 3 mL of freezing medium. The freezing medium consisted of the respective culture medium supplemented with 5 % Dimethyl sulfoxide (DMSO, puriss. Sigma-Aldrich). 1 mL of the cell suspension was pipetted into Cryovials and placed in a Freezing Container and placed at –80 °C for two days before moving the cells for final storage in a liquid nitrogen tank.

NHDF cells were used from passage numbers p 18 to p 32 and Detroit 551 cells were used from passage numbers p 13 to p 17.

3.2.1 MTT Cell Viability Assay

To assess cell viability after treatment with TBHP, the colorimetric MTT assay was employed. NHDF and Detroit 551 cells were seeded in 96-well plates (Sarstedt) at a density of 10,000 cells per well in 100 µL of culture medium one day prior to treatment. Each treatment condition was performed in six technical replicates. The outer wells of the plates were filled with sterile PBS to avoid evaporation. Additionally, wells only containing 200 µL of culture medium and untreated cells served as blanks. TBHP-containing medium at twice the target concentration was prepared immediately before treatment and 100 µL were added to each well to achieve the target concentration. Two concentration ranges (7.8 - 1000 µM and 6.25 - 200 µM) consisting of eight points were tested with an incubation time of 24 h. Following the treatment, 20 µL of MTT solution (5 mg/mL Thiazolyl Blue Tetrazolium Bromide, ≥97.5%, Sigma-Aldrich) was added to each well and incubated for 3 h at 37 °C. Afterwards, the supernatant was carefully removed and the formazan crystals were dissolved with 100 µL of DMSO (Sigma-Aldrich). The absorbance was measured at 570 nm using a Thermo Scientific MULTISKAN GO plate reader (ScanIt software 3.2.0.35 RE, 570 nm, single wavelength, fast reading) and the raw data was exported to Microsoft Excel (2010) for blank correction and calculation. For data analysis, $\log_{10}$-transformed TBHP concentrations were plotted against normalized viability using GraphPad Prism (version 6.07). Nonlinear regression (log[inhibitor] vs. normalized response – variable slope) was applied to generate dose-response curves and interpolate unknown values, and calculate half-maximal inhibitory concentrations (IC_{50}).

3.2.2 Whole Cell Lysate

For 6-well plate experiments, the culture medium was either removed or collected for secretome-proteomics. The cells were washed with 1 mL of PBS and then lysed by adding 80 µL of SDC buffer (102 mM Sodium deoxycholate 98 % and 100 mM (Tris(hydroxymethyl)-aminomethane)-HCl pH 8.5 in H_2O) and scraped with a cell scraper (SARSTEDT) to detach the cells from the wells. The suspension was then transferred into microcentrifuge tubes. To ensure that all cells were scraped, this was repeated with 50 µL of SDC buffer. After checking under the light microscope that all cells were detached, the solution was heated to 95 °C for 5 min using a Thermoshaker (eppendorf Thermomixer compact). After cooling to room temperature, the samples were spun down and stored at - 20 °C until further processing. To isolate the proteins, the samples were thawed, heated to 95 °C for 5 min, cooled down and spun down. The samples were transferred into 15 mL falcon tubes and sonicated three times at 90 % for 1 sec with an ultrasonic homogenizer (UW 2070, BANDELIN electronic). After spinning down and transferring the samples back to the microcentrifuge tubes, the samples were stored at - 20 °C before protein concentration was quantified as described in the Bicinchoninic acid protein assay section. The procedure for T25 flask experiments was similar, with the exception of only scraping once with 250 µL of SDC buffer.

3.2.3 Processing of the Cell Culture Medium for Secretome Proteomics

To remove cells and cellular components from the culture medium, the medium was transferred from the cell culture flask into a falcon tube and centrifuged for 5 min at 3,500 rpm and 4 °C. The resulting supernatant was pipetted onto four times the supernatant's volume (8 mL for 6 well plates and 10 mL for T25 flasks) of ice-cold ethanol (EtOH abs., 99.8 %, Fisher Scientific). The falcon tubes were inverted once, sealed with parafilm and stored at -20 °C for at least one day. To pellet precipitated proteins, the samples were centrifuged at 5,000 rpm at 4 °C (acceleration 9, deceleration 9, Thermo Scientific Heraeus Megafuge 16R) for 5 min. The supernatant was discarded and the pellet was air-dried for 15 min followed by drying for 25 min in a vacuum desiccator. Pellets were resuspended in a total of 200 µL SDC buffer and solubilized by sonication for 5 min at 100 % power in an ultrasonic bath. The protein concentration was determined as described in the Bicinchoninic acid protein assay section.

3.3 Sample Preparation

3.3.1 Bicinchoninic Acid Protein Assay (BCA)

To assess the protein content of the samples, they were thawed at room temperature and subsequently heated to 95 °C for 5 min using a Thermoshaker (Eppendorf ThermoMixer C) set to 1400 rpm. Afterwards, they were cooled to room temperature and briefly centrifuged (accuSpin Micro 17, Fisher Scientific) to remove condensate from the lid. For calibration, a ten-point calibration curve (0 - 9 µg/µL) was prepared by pipetting defined volumes of a 1 µg/µL Bovine Serum Albumin (BSA) (Carl Roth) stock into the wells of a 96-well plate (Sarstedt). To account for matrix effects, 1 µL of SDC lysis buffer was added to each standard. The samples were prepared by pipetting 9 µL of water into the wells prior to adding 1 µL of the sample. The working reagent was freshly prepared by mixing BCA reagent A (29 mM Bicinchoninic acid, 188.7 mM Sodium carbonate, 8.25 mM Sodium tartrate and 113 mM Sodium bicarbonate) and BCA reagent B (200 mM $CuSO4 \cdot 5H_2O$) in a ratio of 50:1. Two hundred µL of working reagent were added to each well and mixed using a plate shaker (Vortexer IKA Works, Thermo Fisher) at 1100 rpm for 1 min. After incubation at 60 °C for 30 min, the extinction at 562 nm was measured by a Plate Reader (MULTISKAN GO plate reader equipped with ScanIt software 3.2.0.35 RE, 562 nm, single wavelength, fast reading) and exported into Microsoft Excel (2010) for further processing. The protein concentrations were calculated from the linear regression of the calibration curve.

3.3.2 In Solution Digest

For digestion, 20 µg of the protein samples were adjusted to a final volume of 90 µL with SDC lysis buffer. To reduce the proteins 2 µL of 500 mM Tris (2-carboxyethyl) phosphine (TCEP) (Thermo Fisher Scientific, Bond-Breaker™ TCEP Solution, pH 7) were added to the samples and incubated on a Thermoshaker (Eppendorf TMX comfort) at 45 °C for 5 min at 1200 rpm. Afterwards, the alkylation was

carried out by adding 5 µL of 800 mM 2- chloracetamide (2-CAM) (Alfa Aesar) and incubating at 45 °C for 5 min at 1200 rpm using a Thermoshaker. Prior to the addition of 2 µL of 0.1 µg/µL trypsin/lysC (Promega, in resuspension buffer), the samples were cooled on ice. The digestion was carried out at 37 °C for 16 h at 1200 rpm.

3.3.3 StageTip Cleanup

For desalting of the peptide solution, 200 µL StageTips packed with three disks of SDP-RPS material were used. The StageTips were packed with a syringe and conditioned directly before use by adding 150 µL of Loading Buffer (1 % trifluoroacetic acid (TFA) in isopropanol (IPA)) and centrifuging for 5 min at 1,000 g (Thermo Scientific HERAEUS MEGAFUGE 16R). After each centrifugation step, the waste tube was emptied. Following the in-solution digest, the samples were placed in a vacuum concentrator (GeneVac miVac DUO concentrator) at 45 °C for approximately 30 min and then cooled to room temperature. One hundred twenty µL of Loading Buffer was added to the samples, and mixed by pipetting up and down before being transferred onto the StageTips. To minimize loss, the sample tubes were washed with 40 µL of Loading Buffer each. After centrifugation at 1,000 g for 7 min, the flowthrough was discarded from the waste tubes and the StageTips were washed with 100 µL of Loading Buffer and centrifuged at 1,500 g for 7 min. Then, the flowthrough was discarded again and the StageTips were washed with 100 µL of Wash Buffer (5 % acetonitrile (ACN) and 0.2 % TFA in VWR water) and centrifuged at 1,500 g for 8 min. After washing, the StageTips and adapters were placed into sample tubes containing glass inserts. The peptides were then eluted into the inserts via 30 µL of Elution Buffer (60 % ACN and 0.0014 % NH_3 in VWR water) and centrifuging at 1,500 g for 8 min. The elution step was repeated. Afterwards, the samples were dried in a vacuum concentrator at 45 °C for 1 h. The samples were stored at -20 °C until reconstitution and measurement.

3.3.4 Peptide Reconstitution

After the StageTip Cleanup, the peptides were reconstituted by pipetting up- and down with 5 µL of 10 fmol/µL Standard Peptide Mix (in 30 % formic acid (FA)) and 40 µL of MS Loading Buffer (97.95 % H_2O, 2 % acetonitrile and 0.05 % TFA). The glass inlets were then placed in sample tubes containing 400 µL of water (LC-MS grade VWR chemicals) and sonicated in an ultrasonic bath (SONREX DIGITAL 10 P, BANDELIN electronic) for 5 min at 40 % power. After sonication, the samples were centrifuged for 5 min at 5,000 g to collect the liquid at the bottom. The glass inserts were then transferred into labeled MS glass vials and measured *via* nanoLC-MS/MS.

3.4 nanoLC-MS/MS

The reconstituted samples were separated by nanoLC-MS/MS performed on a Dionex UltiMate™ 3000 RSLCnano system (Thermo Fisher Scientific) equipped with a pre-column (Acclaim™ PepMap™ C18 100,

Thermo Fisher Scientific) and an analytical column (Aurora series emitter column, 1.6 µm C18, 25 cm · 75 µm, IonOpticks) coupled to a timsTOF Pro (Bruker Daltonics) mass spectrometer running in PASEF and DDA mode. 5 µL of each sample were loaded onto the pre-column using eluent A (99.9 % water, 0.1% formic acid (FA)) at a flow rate of 10 µL/min and eluted onto the analytical column using a gradient from 12 % to 42 % eluent B (79.9 % acetonitrile, 20 % water, 0.1 % FA) in eluent A over 90 min (for whole cell lyastes) or 55 min (supernatants) at a flow rate of 300 nL/min. This resulted in a total runtime of 140 min (whole cell lysates) or 85 min (supernatants) per sample, including washing and equilibration steps. For the m/z scans, the range was set from 100 to 1700 for both MS1 and MS2 spectra. Ion mobility separation was performed using a 100 ms ramp with inverse reduced ion mobility values (1/k0) ranging from 0.6 to 1.6 Vs/cm². Each cycle included 10 PASEF MS/MS scans, resulting in a total cycle time of 1.16 seconds.

3.5 Data Processing

The generated data was processed using the MaxQuant v 1.6.17.0 software package[34] with the Andromeda search engine.[35] Proteins were identified and quantified label-free using the SwissProt human database (version from December 14, 2019, with 20,380 entries). The false discovery rate (FDR) was set to 1% for both peptide-spectrum matches (PSMs) and proteins. "Match between runs" was enabled with a 0.7-minute matching window and a 20-minute alignment window. The MS/MS mass tolerance was set to 40 ppm, allowing up to two missed cleavages. Proteins were considered identified if at least one unique peptide was found. Carbamidomethylation of cysteine was used as a fixed modification, while methionine oxidation and N-terminal acetylation were treated as variable modifications.

For further processing, Perseus version 1.6.14.0.[36] was used. LFQ values and samples description from the MaxQuant protein groups results file were used for data processing. Gene Ontology (GO) annotations were added in Perseus using the UniProt "Majority protein IDs" column. Peptides only identified by site, matching the reverse sequences and potential contaminants were filtered out. The LFQ values were then log2-transformed and all proteins that were not found at least 70 % in one of the groups were filtered out. Missing values were imputed from a normal distribution (downshift: 1.8, width: 0.3). To assess sample clustering a Principal component analysis (PCA) was performed. Differential protein expression between the different groups was analyzed using a two-sided t-test with 250 randomizations, a permutation-based false discovery rate (FDR) of 0.05 and an S_0 value of 0.1.

Using the Perseus plain matrix export feature, all matrices relevant for plotting were exported and plotted using R and RStudio (version R 4.5.0[37]) using the packages tidyverse[38] (for data manipulation and visualization), readxl[39] and openxlsx[40] (for Excel input/output), ggrepel[41] (for non-overlapping text labels in plots), and stringr[42] (for string operations). For functional enrichment, the clusterProfiler

package[43] was employed to analyze overrepresented GO biological processes (BP), molecular function (MF) and cellular component (CC) and mapped using the org.Hs.eg.db annotation database[44]. All results were exported into Excel workbooks.

4 Results

4.1 Oxidative Stress Responses to TBHP in Fibroblasts

4.1.1 TBHP Reduces Fibroblast Viability

To assess the reaction of Detroit 551 and NHDF cells to TBHP, MTT assays (Figure 3) were performed. The IC_{50} values calculated from normalized cell viability and log_{10}-transformed TBHP concentrations using GraphPad Prism.

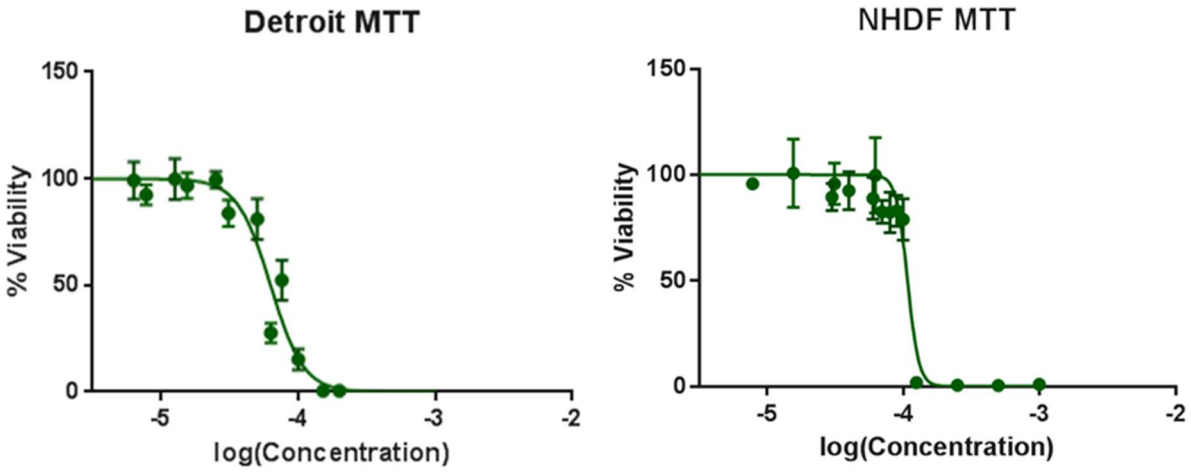

Figure 3 24 h MTT log-dose *vs* response graphs of Detroit (left) and NHDF (right) cells; the IC_{50} were calculated to be 62 ± 2 µM (Detroit) and 108 ± 3 µM (NHDF)

Both log-dose response curves show an inverse sigmoidal shape, indicating a concentration dependent decline in cell viability. However, the Detroit curve on the left exhibits a more gradual decline in viability. In contrast, the NHDF curve on the right shows greater variability between the replicates and retains a more constant viability in the 6.25 – 100 µM concentration range and a sharp drop at the 125 µM concentration. This could suggest a more abrupt cellular response compared to the gradual decline in Detroit cells. With IC_{50} values being 108 ± 3 µM for NHDF cells and 62 ± 2 µM for Detroit cells, NHDF cells are able to tolerate approximately 50 µM of TBHP more than Detroit 551 cells before reaching half-maximal viability loss.

4.1.2 Baseline Proteomic Differences in Detroit 551 and NHDF Related to Oxidative Stress Response

To examine baseline proteome differences between the cell lines, and to identify proteome differences that might explain the higher TBHP resistance of NHDF cells, the time-course Detroit 551 experiment and the NHDF experiment were compared to each other and visualized *via* Principal Component Analysis (PCA) (Figure 4).

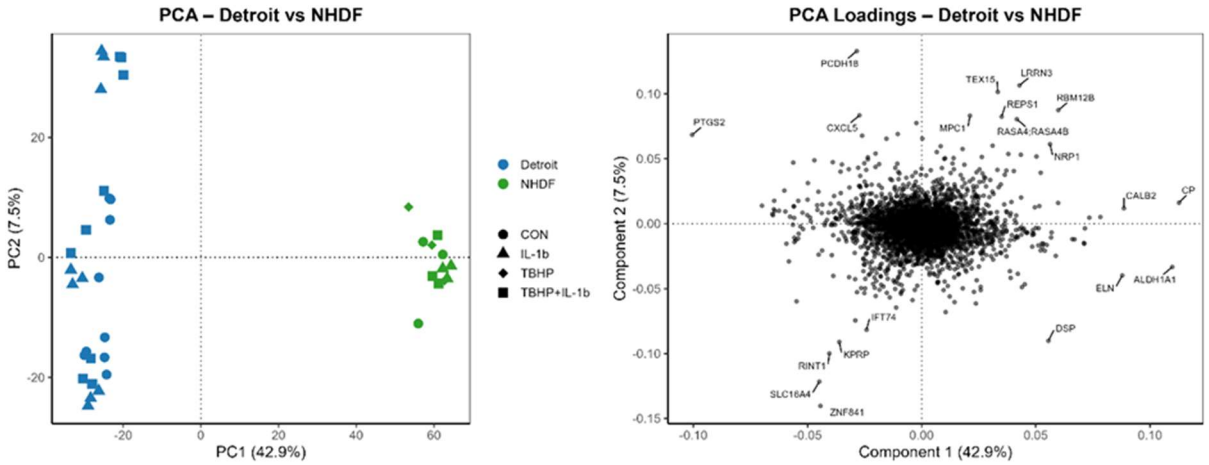

Figure 4 PCA (left) and corresponding loadings plot (right) of the proteomics data from the Detroit 551 time-course experiment and the NHDF 4 h experiment. Samples are colored by cell line (Detroit 551 in blue and NHDF in green) and shaped according to treatment condition (control, IL-1β, TBHP, TBHP + IL-1β).

In the PCA (Figure 4) the Detroit 551 samples and NHDF samples are separated unambiguously by the first principal component (PC1), indicating distinct differences between the proteomes of both cell lines. Treatment conditions and timepoints are distributed along PC2. The loadings plot shows how strongly certain proteins contribute to the separation of Detroit 551 and NHDF. Proteins with high positive loadings (such as CP, CALB2, ALDH1A1 and ELN), are responsible for the shift of NHDF cells to the right side of the PCA plot, whereas proteins with negative loadings (such as PTGS2) contribute to Detroit 551 shift towards the left side.

To investigate potential protein drivers of the observed differences in oxidative stress response, proteins related to oxidative stress were examined more in detail, as can be seen in Figure 5.

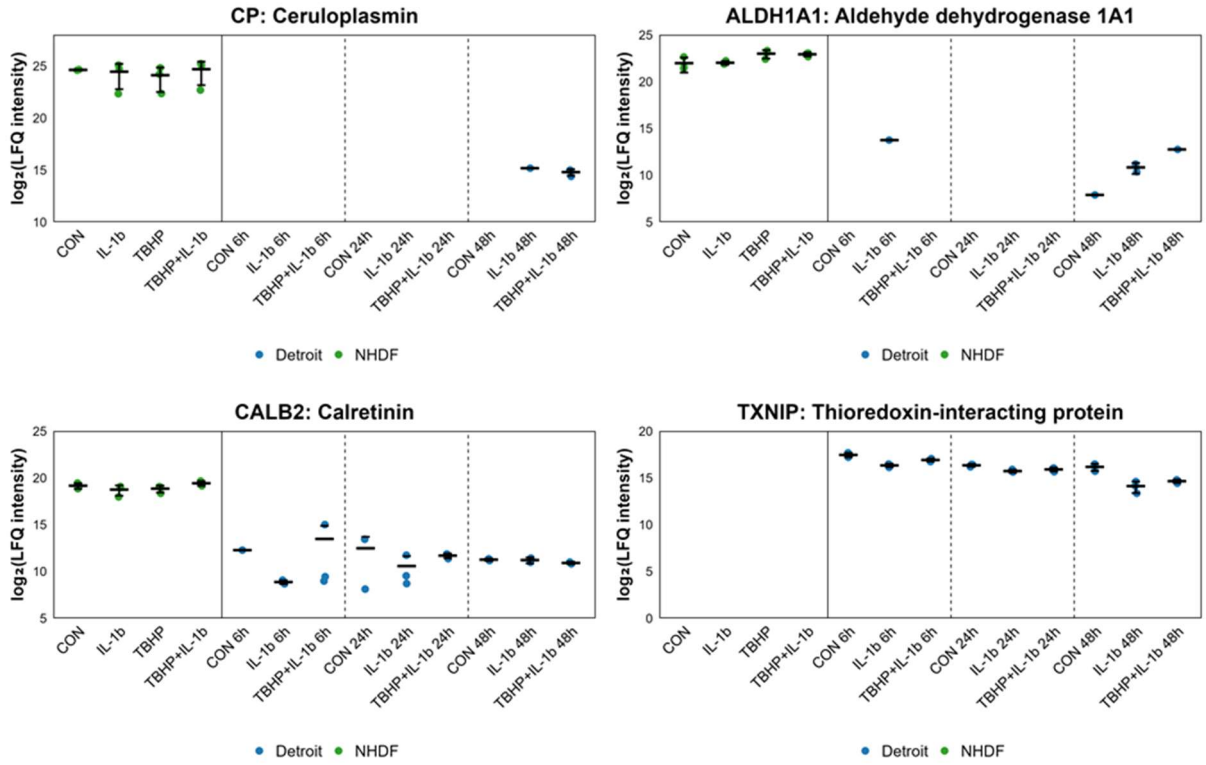

Figure 5 Dot plots of specific proteins showing mean log_2 label-free quantification (LFQ) values for the Detroit 551 time-course experiment and the NHDF 4 h experiment. Samples are colored by cell line (Detroit 551 in blue and NHDF in green). Cell lines are separated with a line, the dashed lines separate the timepoints of the Detroit 551 time-course experiment (6 h, 24 h and 48 h).

As can be seen in Figure 5, the protein Ceruloplasmin (CP) showed high log_2 LFQ values in NHDF cells with similar values across all conditions. In Detroit 551 cells, CP was detected only at later time points (48 h), and at lower intensities compared to NHDF. Aldehyde dehydrogenase 1A1 (ALDH1A1) showed a similar pattern. It is present at high levels in all NHDF conditions but showed lower and less consistent detection in Detroit 551 samples. Calretinin (CALB2) showed consistently higher abundance across all NHDF conditions compared to Detroit 551 cells. Thioredoxin-interacting protein (TXNIP), however, was only detected in Detroit 551 cells. TXNIP levels remained relatively stable across the treatments and timepoints, but after 48 h it shows a slight decrease in both the IL-1β and TBHP + IL-1β treatments.

To compare both cell lines responses to treatment with IL-1β, TBHP and TBHP + IL-1β, the 4 h Detroit 551 experiment and the NHDF experiment were compared to each other and visualized *via* PCA (Figure 6).

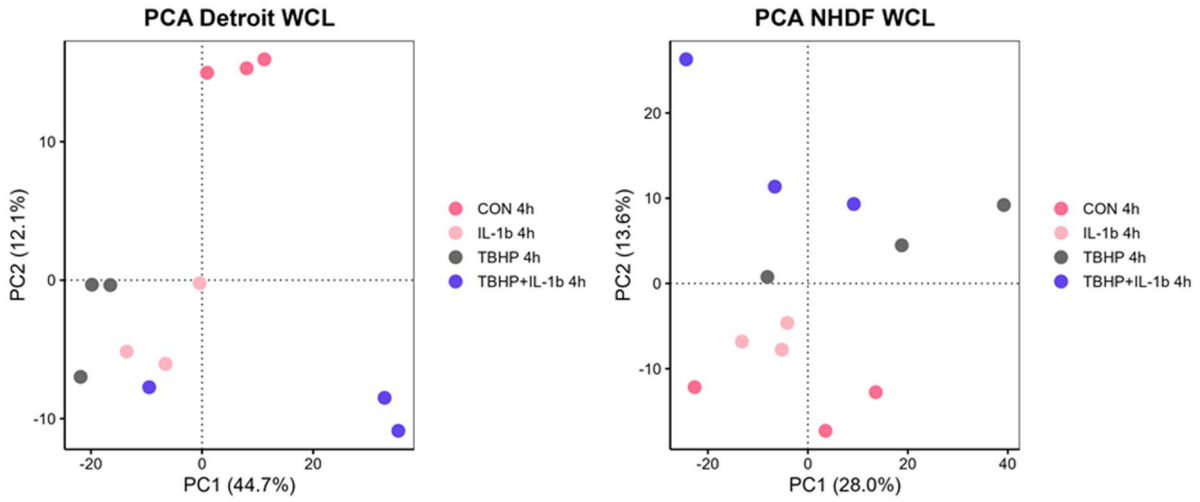

Figure 6 PCA of the whole cell lysate (WCL) proteomics data from the comparison experiment for Detroit 551 (left) and NHDF (right). Samples are colored according to treatment condition (control, IL-1β, TBHP, TBHP + IL-1β).

Both PCAs in Figure 6, but especially the NHDF cells show a high variability between the replicates, as they do not cluster together. In the Detroit 551 PCA the control clusters separately from all treatment conditions, IL-1β and TBHP cluster together. For TBHP + IL-1β, two of three replicates cluster away from the other treatment conditions, while one replicate clusters with IL-1β and TBHP.

4.1.3 Proteomic Response to TBHP-induced Oxidative Stress

To identify which proteins are significantly regulated upon TBHP treatment after 4 h, differential protein expression of the comparison experiment was determined using a two-sided t-test, and the results were visualized in Volcano plots seen in Figure 7.

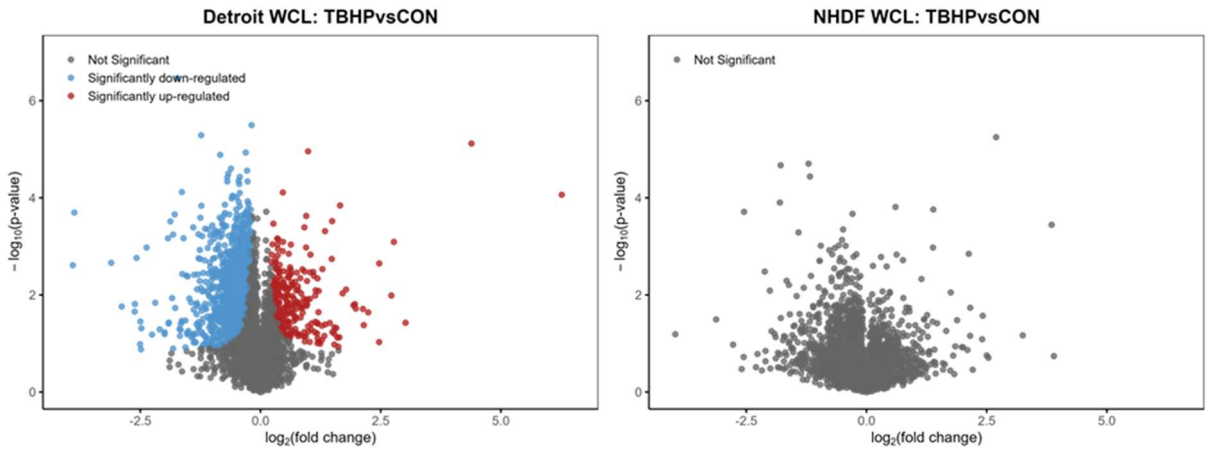

Figure 7 Volcano plots for the TBHP *vs* control comparison for Detroit 551 (left) and NHDF (right) based on a two-sided t-test (FDR < 0.05). Significantly upregulated proteins are shown in red, significantly downregulated proteins in blue, and non-significant proteins in grey.

In Detroit 551 cells, a total of 1413 out of 5034 quantified proteins were significantly regulated in the TBHP *vs* control comparison. Out of these, 238 proteins were significantly upregulated and 1175 were downregulated. In contrast, NHDF cells showed no significantly regulated proteins.

To assess which biological processes (BP) and molecular functions (MF) are affected by TBHP treatment, a Gene Ontology (GO) enrichment analysis was conducted, to identify terms that are statistically overrepresented among the significantly regulated proteins compared to the background proteome. Figure 8 shows the GO enrichment for BP and Figure 9 for MF of the Detroit comparison experiment.

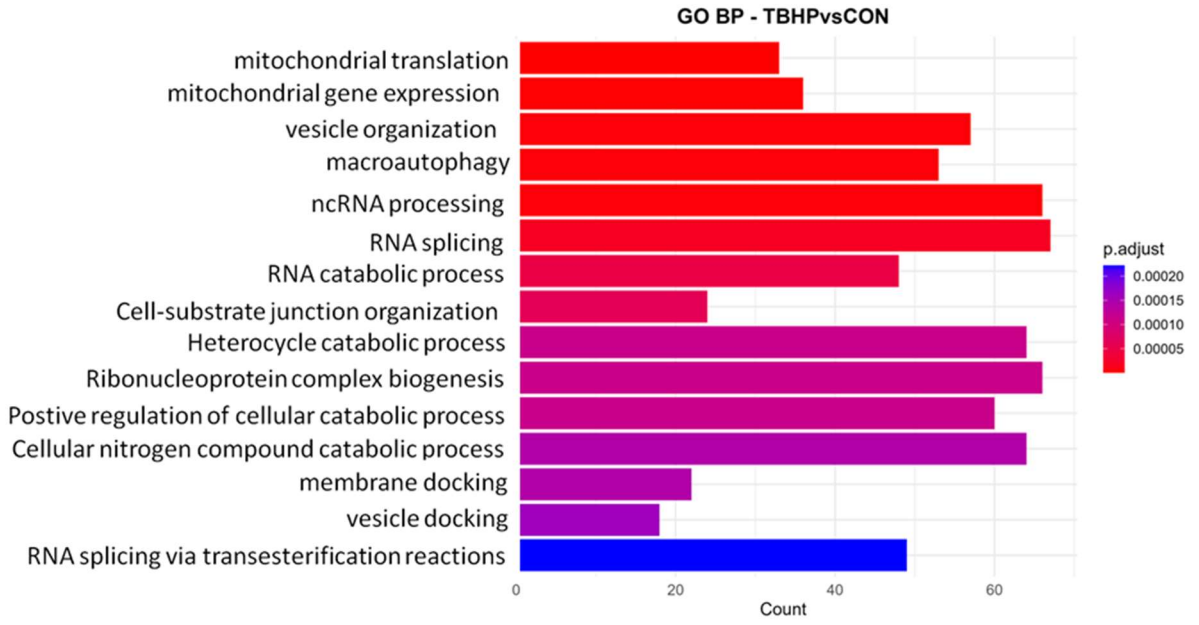

Figure 8 Gene Ontology (GO) Enrichment for the significantly regulated proteins for Detroit 551 TBHP vs CON comparison for biological processes (BP)

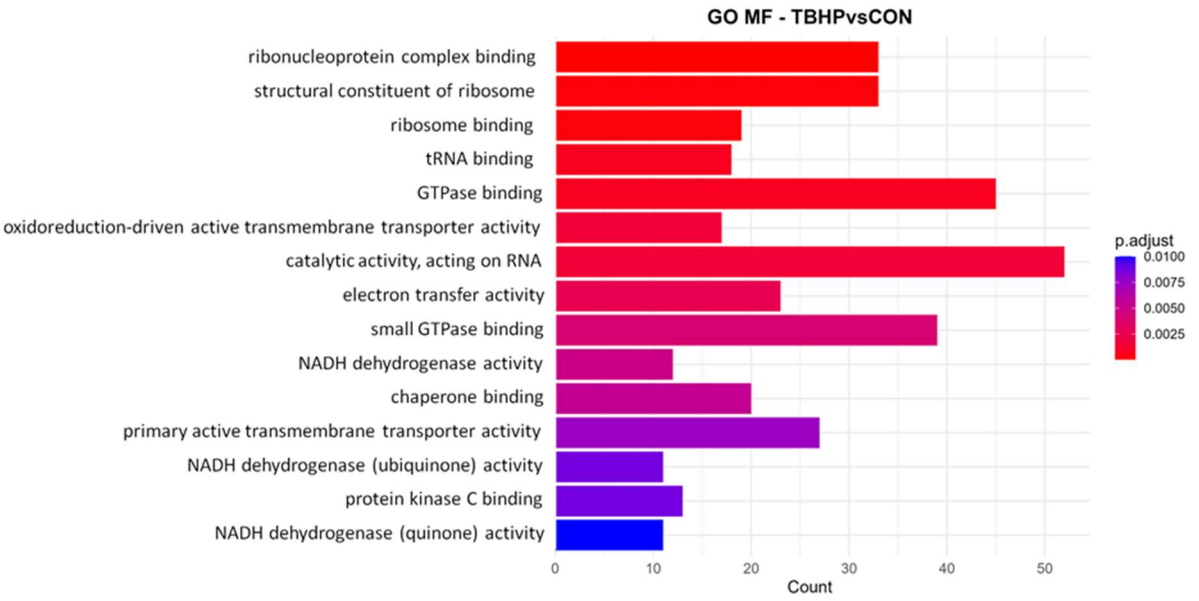

Figure 9 Gene Ontology (GO) Enrichment for the significantly regulated proteins for Detroit 551 TBHP vs CON comparison for molecular function (MF)

The GO Enrichment analysis (Figure 8 and Figure 9) revealed several overrepresented BP and MF in Detroit 551 as a response to TBHP, including mitochondrial translation, mitochondrial gene expression, various catabolic processes, RNA processing and splicing as well as oxidoreduction-driven active transmembrane transporter activity and NADH dehydrogenase activity.

Mitochondrial proteins and proteins associated with oxidative stress response were explored further.

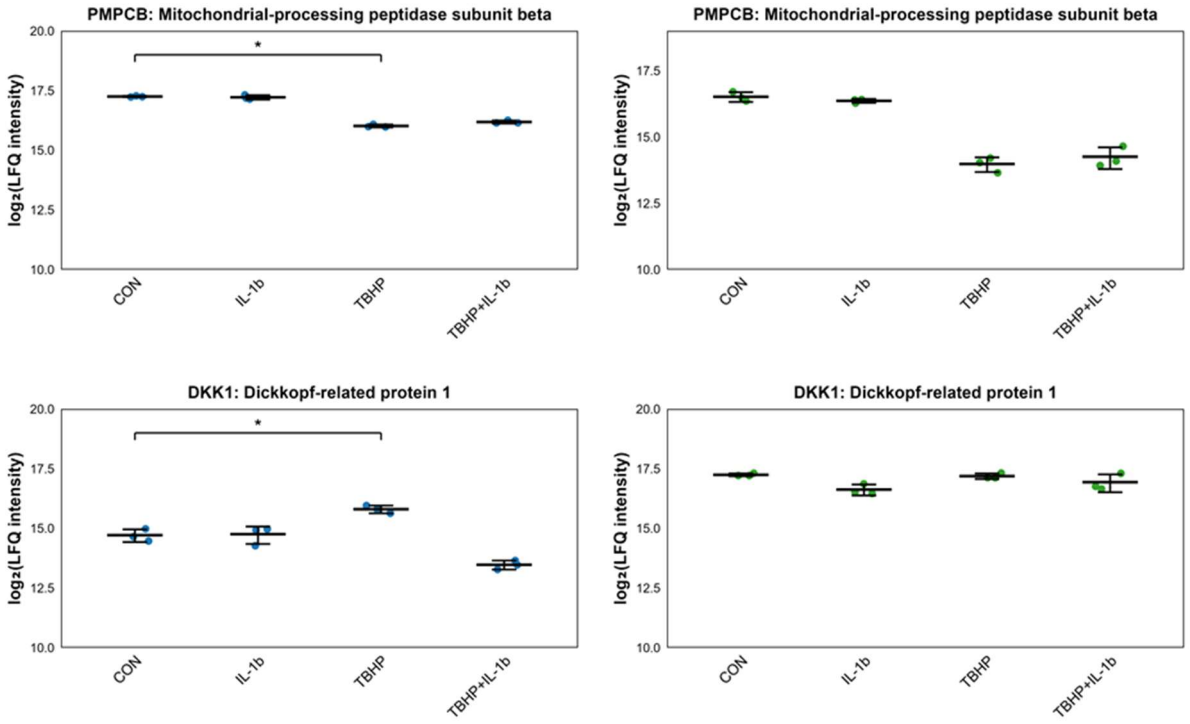

Figure 10 Dot plots of specific proteins showing mean log_2 label-free quantification (LFQ) values for the NHDF (right, colored in green) and the Detroit 551 (left, colored in blue) 4 h experiments. A bracket with an asterisk indicates a significant regulation between the conditions the bracket connects.

In Detroit 551 cells, as seen in Figure 10, mitochondrial-processing peptidase subunit beta (PMPCB) is significantly downregulated upon TBHP stimulation compared to control. IL-1β levels are similar to the control's levels, while TBHP + IL-1β levels are similar to TBHP levels. NHDF show a similar pattern. Dickkopf-related protein 1 (DKK1) in contrast, is significantly upregulated after TBHP treatment, while its levels are similar to the control in IL-1β samples. In the combination treatment however, DKK1 abundances are lower than control and IL-1β. This differs for NHDF cells, as DKK1 levels are not changed by TBHP treatment compared to control, while its levels decrease both in the IL-1β and TBHP + IL-1β groups. While both cell lines have a similar response with PMPCB, their responses differ for DKK1.

4.2 Inflammatory Responses to IL-1β Stimulation in Fibroblasts

4.2.1 Early Inflammatory Proteomic Response to IL-1β (4 h)

To identify which proteins are significantly regulated upon IL-1β treatment, differential protein expression of the comparison experiment was determined using a two-sided t-test and the results were visualized in Volcano plots seen in Figure 11.

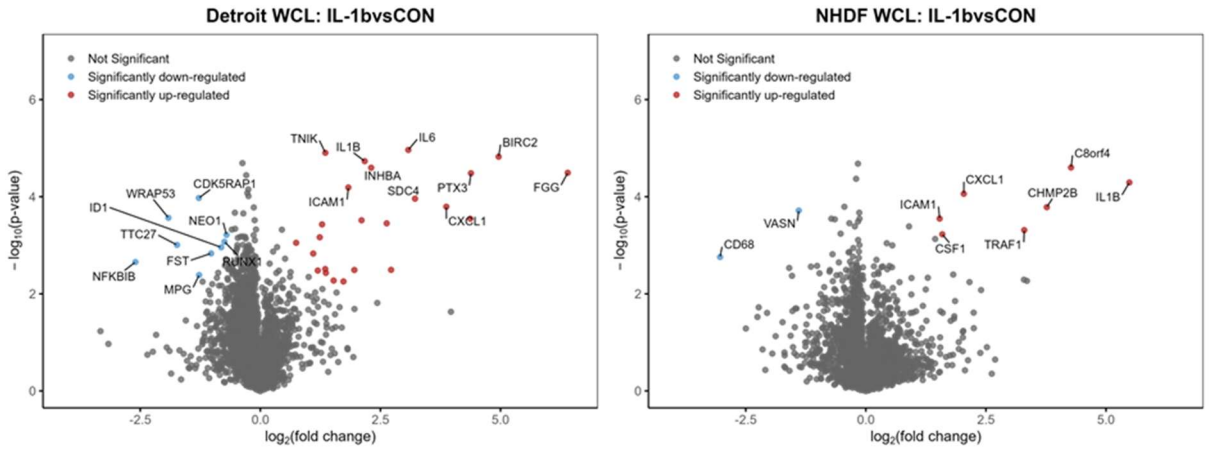

Figure 11 Volcano plots for the IL-1β *vs* control comparison for Detroit 551 (left) and NHDF (right) based on a two-sided t-test (FDR < 0.05). Significantly upregulated proteins are shown in red, significantly downregulated proteins in blue, and non-significant proteins in grey.

In Detroit 551 cells, a total of 33 out of 5034 quantified proteins were significantly regulated in the IL-1β *vs* control comparison, with 24 proteins being significantly upregulated and 9 downregulated. In NHDF cells 9/4613 proteins were significantly regulated, out of these 7 were upregulated and 2 downregulated. Detroit 551 and NHDF share regulated proteins such as IL1B, CXCL1 and ICAM1, while others are uniquely regulated in Detroit 551 and NHDF. VASN, for example, is downregulated in NHDF but not regulated in Detroit 551. The other regulated 5 proteins in NHDF C8orf4, CHMP2B, TRAF1, CSF1 and CD68 were not detected in Detroit 551. In contrast, 14 proteins regulated in Detroit 551 such as PTX3 and HERC5 were not detected in NHDF. Other 15 regulated proteins in Detroit 551 such as BIRC2 and TNFAIP2 were found in NHDF, but were not significantly regulated.

Proteins associated with inflammatory stress response were further explored (Figure 12).

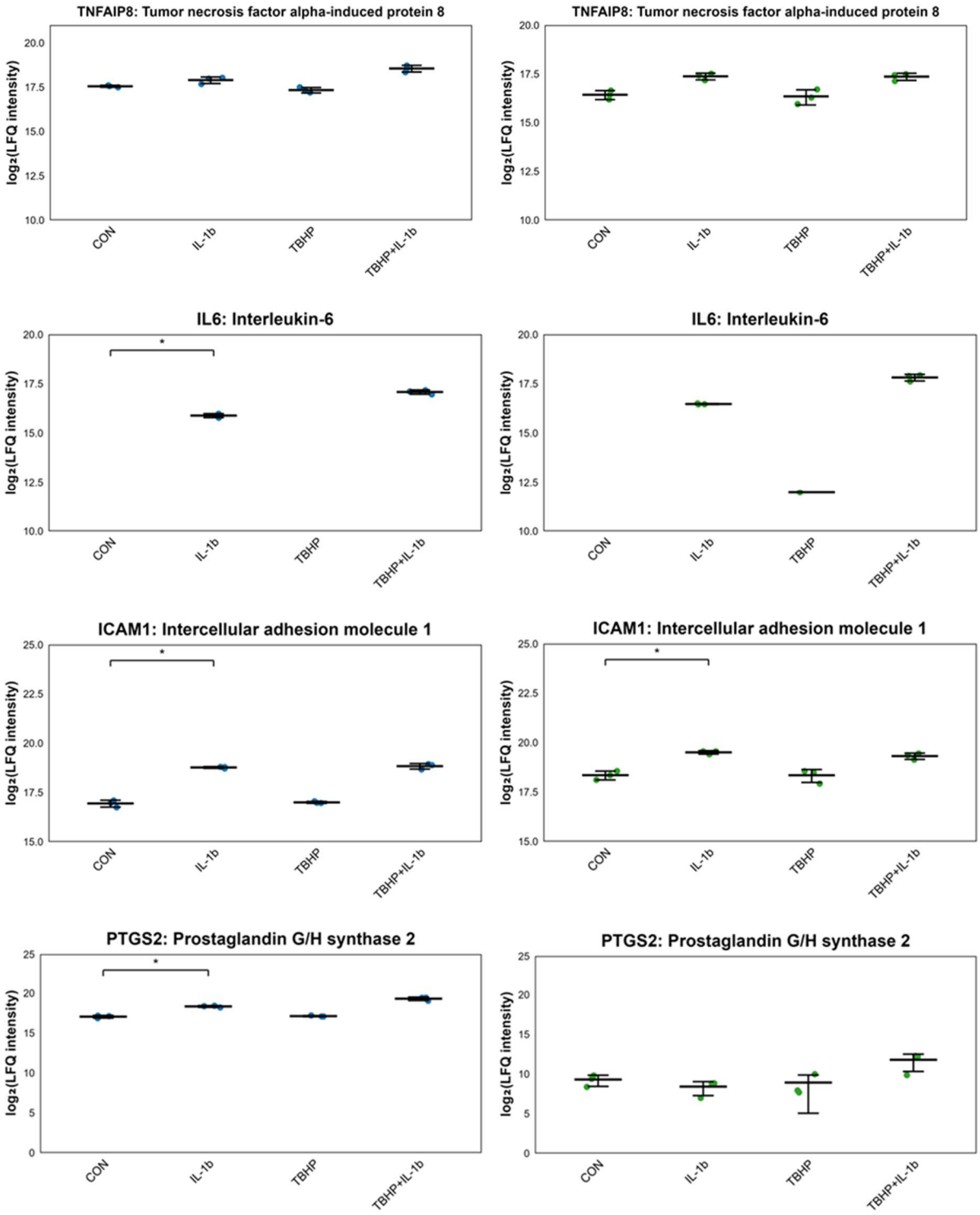

Figure 12 Dot plots of specific proteins showing mean log_2 label-free quantification (LFQ) values for the NHDF (right, colored in green) and the Detroit 551 (left, colored in blue) 4 h experiments. A bracket with an asterisk indicates a significant regulation between the conditions the bracket connects.

Figure 12 shows Tumor necrosis factor alpha-induced protein 8 (TNFAIP8) increased in both cell lines upon IL-1β stimulation compared to control. The abundances of TBHP and control group are similar in both cell lines. In NHDF the TBHP + IL-1β and IL-1β group have similar abundances, while TNFAIP8 levels are higher in Detroit 551 in TBHP + IL-1β compared to IL-1β. Interleukin-6 (IL6) is significantly upregulated after inflammatory stimulation compared to the control condition in Detroit 551 cells. IL6 is not detected in the TBHP condition, but its abundance is higher in the TBHP + IL-1β condition than in IL-1β alone, although this difference is not statistically significant. A similar pattern is observed in NHDF cells, IL6 is absent in the control and not consistently detected in the TBHP condition. Similarly, the IL6 levels are higher in TBHP + IL-1β condition compared to IL-1β. In contrast, Intracellular adhesion molecule 1 (ICAM1) is significantly elevated in the IL-1β condition compared to the control and TBHP conditions. The ICAM1 levels of the combination of TBHP + IL-1β and IL-1β are similar. Another significantly upregulated protein upon inflammatory stimulation in Detroit 551 is Prostaglandin G/H synthase 2 (PTGS2). As observed in IL-6, PTGS2 levels are even more elevated in TBHP + IL-1β, though this difference is not statistically significant, while PTGS2 levels of control and TBHP are similar. In contrast, PTGS2 levels in NHDF are similar across all conditions except TBHP + IL-1β, where an increase is visible, but not statistically significant.

Additionally, GO enrichments for BP for Detroit 551 and NHDF cells were conducted to compare both cell lines inflammatory processes (Figure 13 and Figure 14).

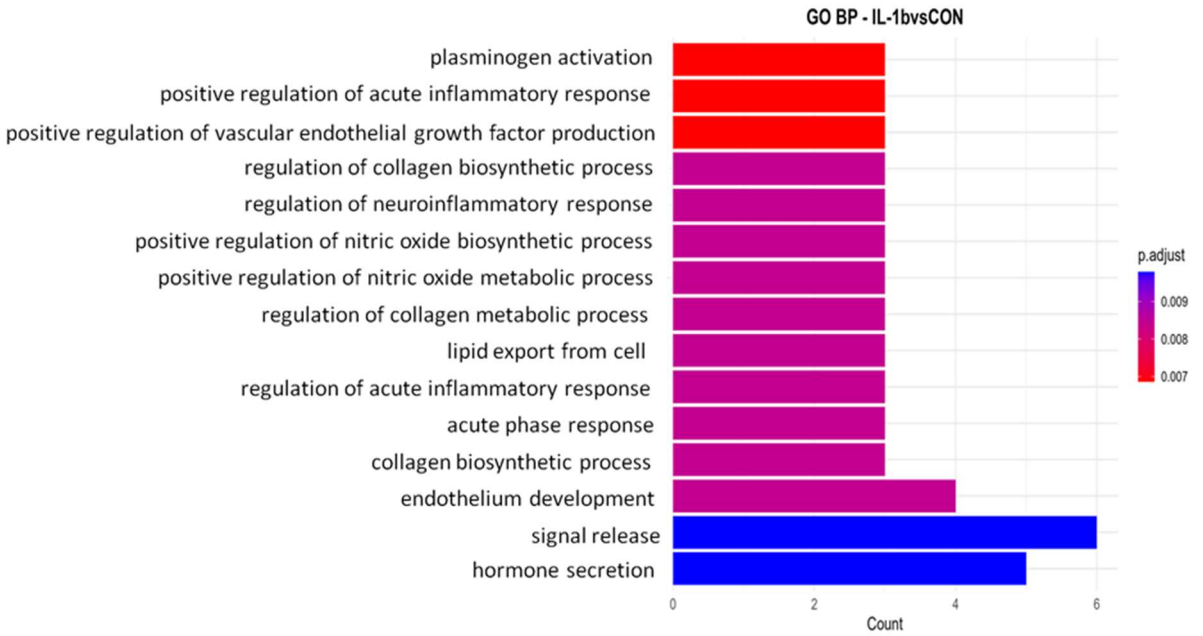

Figure 13 Gene Ontology (GO) Enrichment for the significantly regulated proteins for Detroit 551 IL-1β vs CON comparison for biological processes (BP)

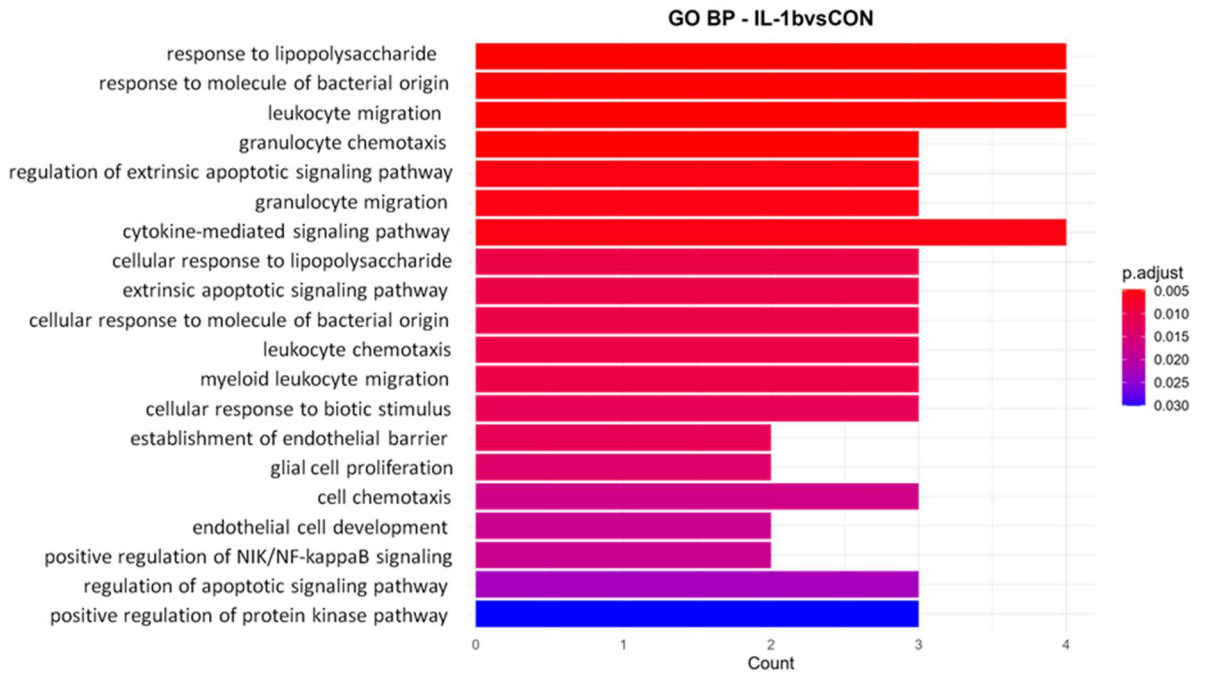

Figure 14 Gene Ontology (GO) Enrichment for the significantly regulated proteins for NHDF IL-1β vs CON comparison for biological processes (BP)

Comparison of the GO Enrichments of Detroit 551 and NHDF (Figure 13 and Figure 14) revealed primarily unique enriched terms. Both cell lines share endothelial developmental terms (endothelium development for Detroit 551, and endothelial cell development as well as establishment of endothelial barrier for NHDF).

In Detroit 551 enriched terms were predominantly inflammatory responses such as nitric oxide associated and collagen related processes. NHDF on the other hand, were enriched in immune cell associated processes (leukocyte and granulocyte migration) and signaling pathways (apoptotic signaling, positive regulation of protein kinase pathway and positive regulation of NF-κB signaling). Overall, both fibroblast cell lines differ in their enriched BP.

4.2.2 IL-1β-induced Inflammatory Response Over Time (6–48 h)

To assess how inflammatory stimulation with IL-1β changes over time upon TBHP pre-stress, both cell lysates and secretome samples were compared to each other and visualized *via* PCA, as shown in Figure 15

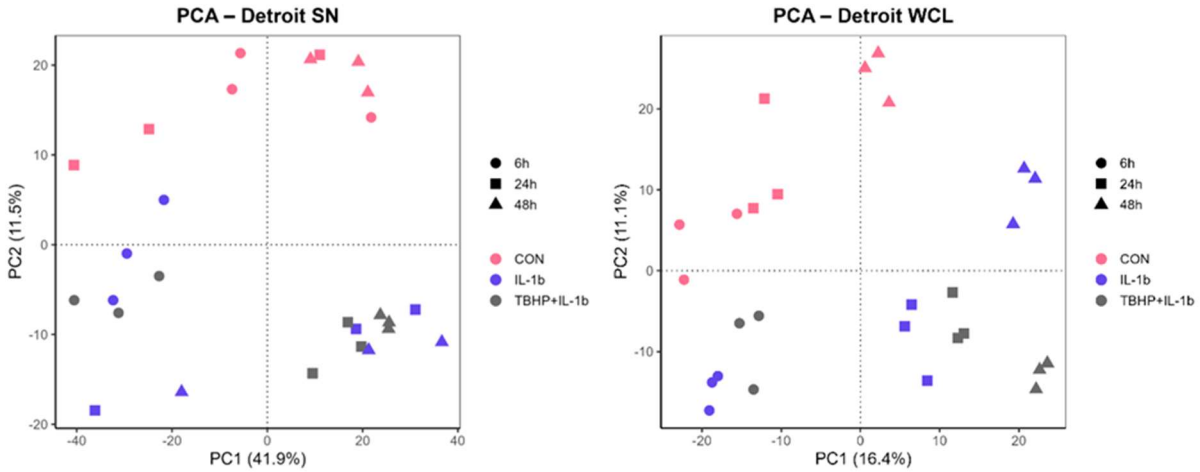

Figure 15 PCA of the secretome (SN, left) and whole cell lysate (WCL, right) proteomics data from the Detroit 551 time-course experiment. Samples are colored according to treatment condition (control, IL-1β, TBHP + IL-1β) and shaped according to timepoint (6 h, 24 h and 48 h).

The PCA of the SN in Figure 15 shows variability between the replicates, especially in the IL-1β condition after 24 h and 48 h. The control clusters away from both treatment groups. The 6 h samples of TBHP + IL-1β and IL-1β cluster together, while both the 24 h and 48 h TBHP + IL-1β and IL-1β samples cluster together. For the WCL the control is separated from both treatments. IL-1β and TBHP + IL-1β cluster according to timepoint, with IL-1β and TBHP + IL-1β being relatively close to each other, showing minor separation. After 48 h samples of both IL-1β and TBHP + IL-1β are clearly separated.

To identify which proteins are significantly regulated upon IL-1β treatment in Detroit 551 cells over time, differential protein expression of the comparison experiment was determined using a two-sided t-test and the results were visualized in Volcano plots seen in Figure 16 for the WCL and Figure 17 for the SN.

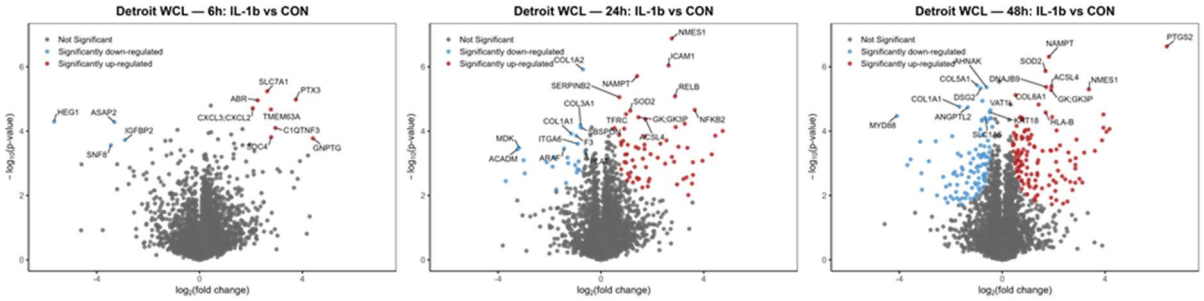

Figure 16 Volcano plots for the IL-1β *vs* control comparison for Detroit 551 time-course experiment WCL based on a two-sided t-test (FDR < 0.05) with the timepoints 6 h (left), 24 h (middle) and 48 h (right). Significantly upregulated proteins are shown in red, significantly downregulated proteins in blue, and non-significant proteins in grey. Highly regulated hits are labeled.

As seen in Figure 16, in the cell lysates of the Detroit 551 time-course experiment, at 6 h 12 proteins out of 4232 proteins in total were significantly regulated, with 8 being upregulated and 4 downregulated. Strongly regulated proteins include SDC4, CXCL3/2, IGFBP2 and PTX3. After 24 h 90 proteins were significantly regulated (65 upregulated, 25 downregulated), including proteins such as NFKB2, SOD2, and ICAM1 along with COL1A1 and COL3A1. At 48 h, IL-1β induced the strongest response, with 231 significantly regulated proteins (127 upregulated, 104 downregulated). Among the top upregulated proteins was PTGS2 along with NAMPT and SOD2. Overall, proteomic changes after IL-1β treatment showed a time-dependent increase in significantly regulated proteins.

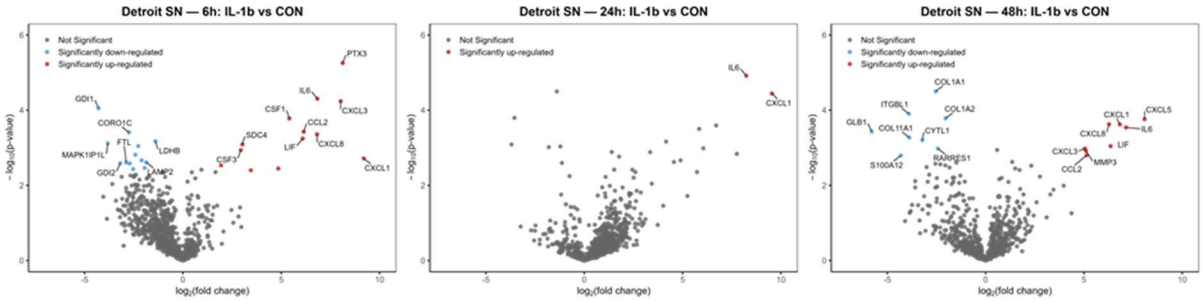

Figure 17 Volcano plots for the IL-1β *vs* control comparison for Detroit 551 time-course experiment SN based on a two-sided t-test (FDR < 0.05) with the timepoints 6 h (left), 24 h (middle) and 48 h (right). Significantly upregulated proteins are shown in red, significantly downregulated proteins in blue, and non-significant proteins in grey. Highly regulated hits are labeled.

As Figure 17 shows, after 6 h 26 out of 866 proteins are significantly regulated (13 upregulated and 13 downregulated), regulated proteins include MAPK1P1L, CCL2, CXCL1, CXCL3, CXCL8, IL6, LIF and PTX3. After 24, 2 proteins are significantly upregulated IL6 and CXCL1, whereas the number of regulated proteins increased again after 48 h to 16 significantly regulated proteins (8 upregulated and 8

downregulated), including proteins such as MMP3, LIF, CXCL11, CXCL 5, CXCL 8, COL1A1, COL11A1, COL1A2 and CCL2.

4.3 Inflammatory Responses Following Oxidative Pre-stress in Fibroblasts

4.3.1 Short-term Inflammatory Response after Oxidative Pre-stress (4 h)

To assess whether TBHP-induced oxidative stress modulates inflammatory responses, differential protein expression in NHDF cells and Detroit 551 cells was determined for the TBHP + IL-1β vs IL-1β comparison using a two-sided t-test, and the results were visualized in volcano plots seen in Figure 18.

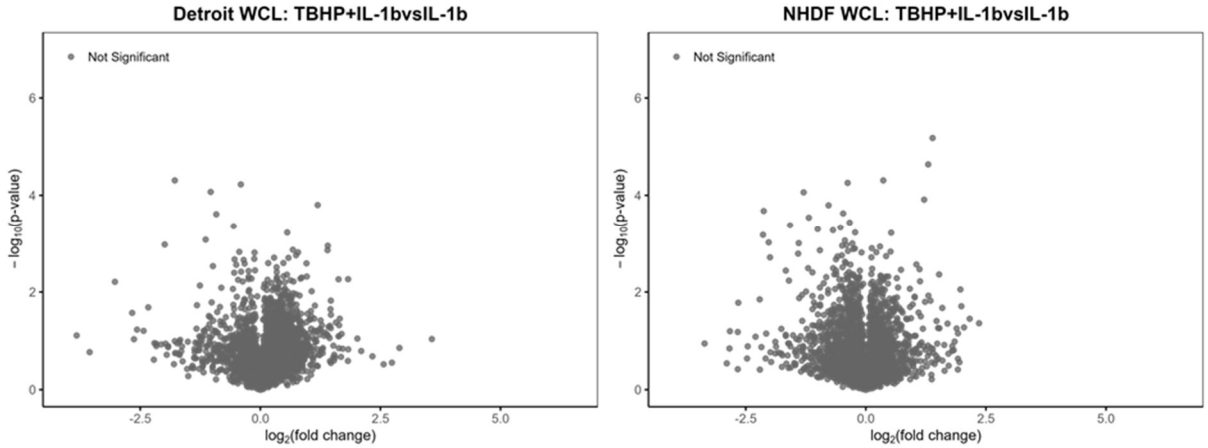

Figure 18 Volcano plots for the TBHP + IL-1β *vs* IL-1β comparison for Detroit 551 (left) and NHDF (right) based on a two-sided t-test (FDR < 0.05). Significantly upregulated proteins are shown in red, significantly downregulated proteins in blue, and non-significant proteins in grey.

No significantly regulated proteins were identified in the TBHP + IL-1β vs IL-1β comparison in either Detroit 551 and NHDF cells (Figure 18).

As the variability was quite high in NHDF and in the Detroit 551 TBHP + IL-1β group, proteins associated with inflammatory responses and oxidative stress were further explored to determine potential modulations in the TBHP + IL-1β group.

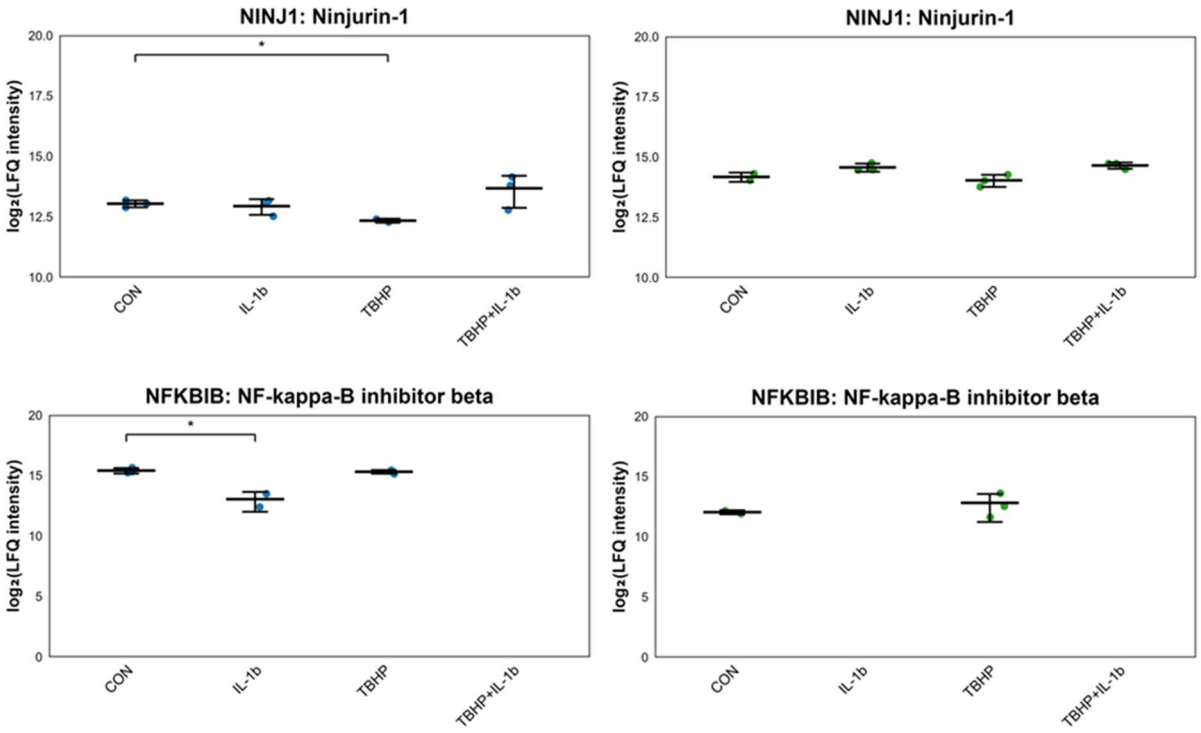

Figure 19 Dot plots of specific proteins showing mean log2 label-free quantification (LFQ) values for the NHDF (right, colored in green) and the Detroit 551 (left, colored in blue) 4 h experiments. A bracket with an asterisk indicates a significant regulation between the conditions the bracket connects.

In Detroit 551 cells (Figure 19), Ninjurin-1 (NINJ1) levels are significantly reduced upon TBHP treatment compared to control, while levels remain stable upon IL-1β treatment. The TBHP + IL-1β condition showed a slight, non-significant increase compared to IL-1β and control. In NHDF cells, NINJ1 levels remained relatively stable, while they appear slightly elevated in TBHP + IL-1β and IL-1β compared to control and TBHP. NF-kappa-B inhibitor beta (NFKBIB) is significantly downregulated upon IL-1β stimulation compared to control, while its levels remained similar to control upon TBHP treatment. In the TBHP + IL-1β group, NFKBIB was not detected. This is different in NHDF cells, as the NFKBIB levels of TBHP and control are still similar, but NFKBIB is not present in both TBHP + IL-1β and IL-1β.

4.3.2 Long-term Effects of Oxidative Pre-stress on Inflammatory Signaling (6–48 h)

To assess how TBHP-induced oxidative stress modulates inflammatory responses over time, differential protein expression in Detroit 551 cells was determined for the TBHP + IL-1β vs IL-1β comparison using a two-sided t-test and the results were visualized in Volcano plots seen in Figure 20 and Figure 23.

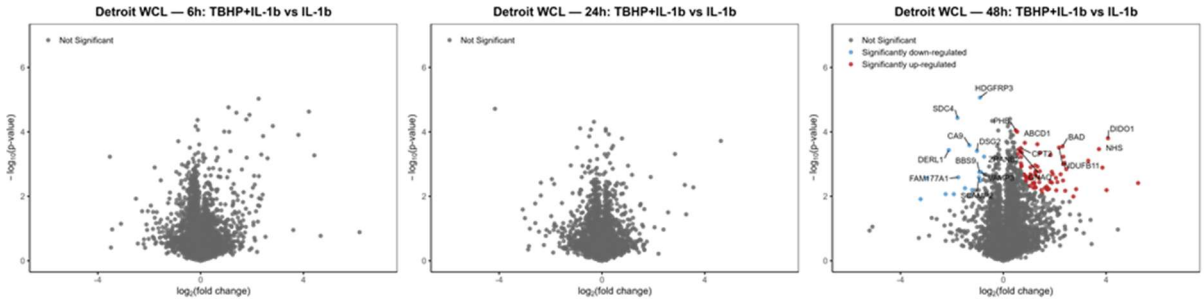

Figure 20 Volcano plots for the TBHP + IL-1β *vs* IL-1β comparison for Detroit 551 time-course experiment WCL based on a two-sided t-test (FDR < 0.05) with the timepoints 6 h (left), 24 h (middle) and 48 h (right). Significantly upregulated proteins are shown in red, significantly downregulated proteins in blue, and non-significant proteins in grey. Highly regulated hits are labeled.

Figure 20 shows, that after 6 h and 24 h no proteins are significantly different from the IL-1β group. After 48 h 91 of 4232 proteins were significantly regulated, 17 downregulated and 74 upregulated. This includes proteins such as NDUFAF2, NDUFB11, UQCRQ, DIDO1, BAD and SDC4.

To assess how inflammatory response is modulated by oxidative stress in the cell lysates, proteins associated with inflammatory response were further explored to determine potential modulations by TBHP + IL-1β. Additionally, proteins associated with mitochondrial stress were examined as well. (Figure 21)

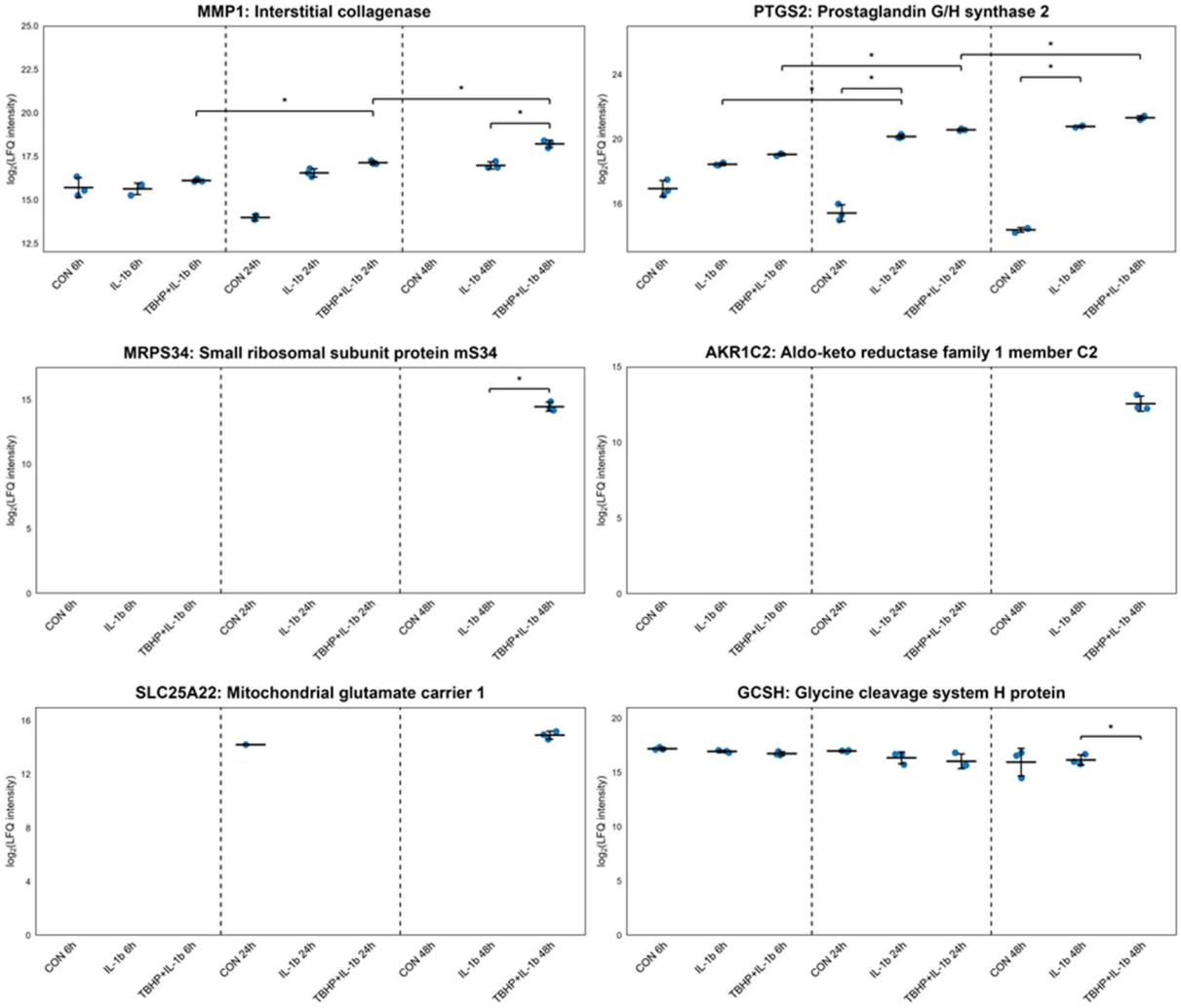

Figure 21 Dot plots of specific proteins showing mean log2 label-free quantification (LFQ) values for the Detroit 551 WCL time-course experiment. A bracket with an asterisk indicates a significant regulation between the conditions the bracket connects.

The abundances of interstitial collagenase (MMP1) are similar across all conditions at 6 h. In the control, MMP1 levels decrease over time, with MMP1 not being detected anymore at 48 h. At the same time, MMP1 levels increase in both IL-1β and TBHP + IL-1β groups. While MMP1 levels are slightly higher in TBHP + IL-1β compared to IL-1β at 24 h, MMP1 is significantly upregulated in TBHP + IL-1β compared to IL-1β after 48 h. A similar pattern can be seen for Prostaglandin G/H synthase 2 (PTGS2). PTGS2 levels also decrease for the control over time, while they are elevated and increase for both IL-1β and TBHP + IL-1β over time. PTGS2 levels are non-significantly higher in TBHP + IL-1β compared to IL-1β across all timepoints. Small ribosomal subunit protein mS34 (MRPS34), Aldo-keto reductase family 1 member C2 (AKR1C2) and Mitochondrial glutamate carrier 1 (SLC25A22) all show similar

patterns, as they are absent in all conditions and timepoints apart from TBHP + IL-1β at 48 h. SLC25A22 was however detected in one of the three replicates of control at 24 h. In contrast, Glycine cleavage system H protein (GCSH) shows a reverse pattern, as GCSH levels are at relatively similar levels across all conditions and timepoints, except TBHP + IL-1β at 48 h, where GCSH is absent.

Additionally, a GO enrichment for the TBHP + IL-1β comparison to IL-1β at 48 h for the WCL was conducted. (Figure 22)

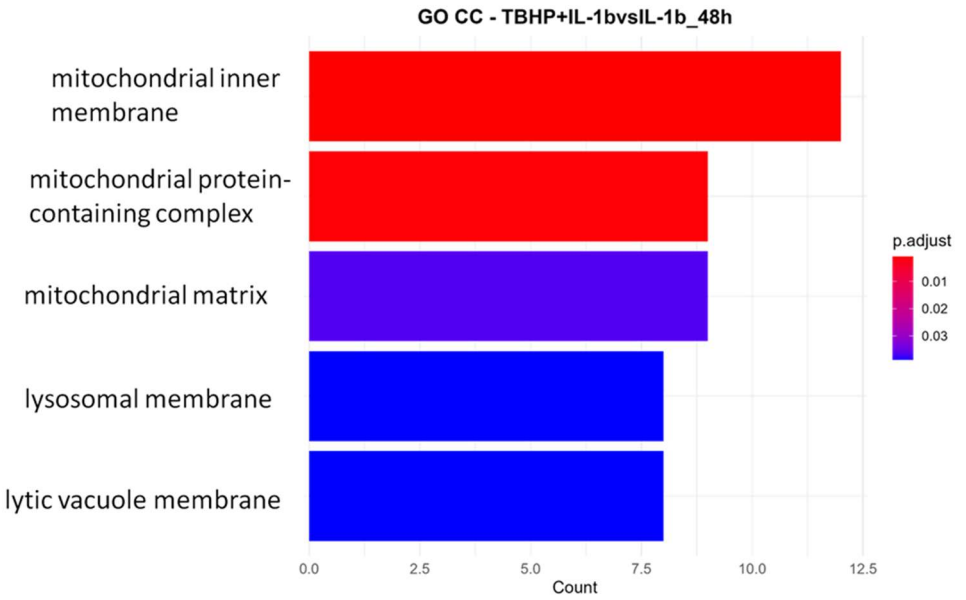

Figure 22 Gene Ontology (GO) Enrichment for the significantly regulated proteins for Detroit 551 TBHP + IL-1β vs IL-1β comparison for cellular components (CC)

As shown in Figure 22, several mitochondrial components were enriched, including the mitochondrial inner membrane, mitochondrial protein-containing complexes, and the mitochondrial matrix. Additionally, terms associated with lysosomal and lytic vacuole membranes were enriched.

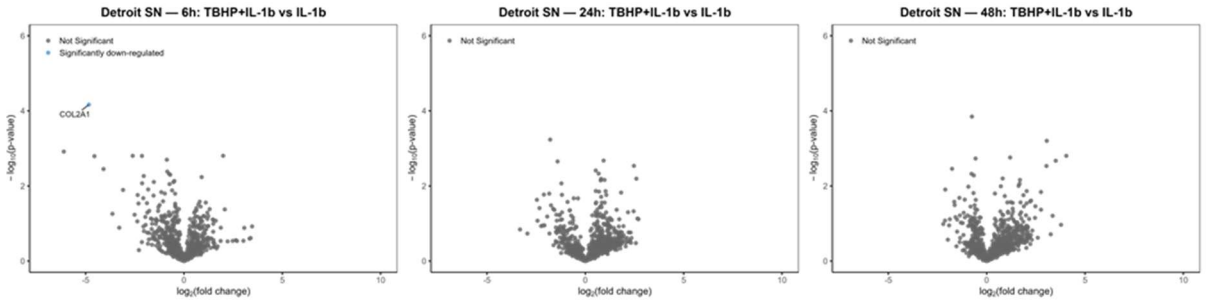

Figure 23 Volcano plots for the TBHP + IL-1β *vs* IL-1β comparison for Detroit 551 time-course experiment SN based on a two-sided t-test (FDR < 0.05) with the timepoints 6 h (left), 24 h (middle) and 48 h (right). Significantly upregulated proteins are shown in red, significantly downregulated proteins in blue, and non-significant proteins in grey. Highly regulated hits are labeled.

Figure 23 shows that in secretome samples only 1 out of 866 proteins is significantly downregulated after 6 h, namely COL2A1. After 24 h and 48 h, no proteins were significantly modulated by TBHP pre-stress.

To assess how inflammatory response is modulated by oxidative stress, proteins associated with inflammatory response were examined in Figure 24.

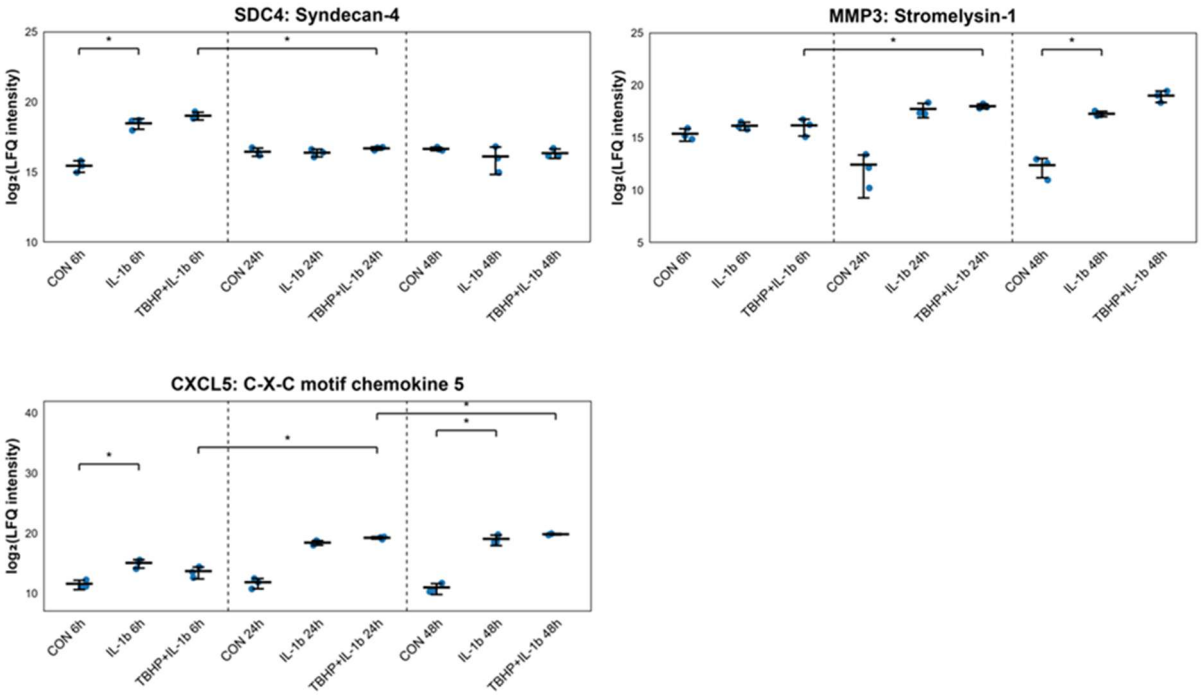

Figure 24 Dot plots of specific proteins showing mean log_2 label-free quantification (LFQ) values for the Detroit 551 SN time-course experiment. A bracket with an asterisk indicates a significant regulation between the conditions the bracket connects.

Figure 24 shows the temporal abundance changes of Syndecan-4 (SDC4), Stromelysin-1 (MMP3) and C-X-C motif chemokine 5 (CXCL5) in Detroit 551 cells secretome across 6 h, 24 h and 48 h for all treatment groups. For SDC4, IL-1β stimulation led to significantly higher abundances compared to the control at 6 h, while its levels are non-significantly elevated in TBHP + IL-1β. At 24 h SDC4 levels of control and IL-1β are at the same level, while TBHP + IL-1β SDC4 levels appear slightly higher. After 48 h, SDC4 abundances were similar across all conditions. MMP3 levels were similar across all conditions at 6 h, with IL-1β and TBHP + IL-1β appearing slightly higher. Over time, MMP3 levels decreased in the control, while its levels increased in IL-1β and TBHP + IL-1β. Especially after 48 h the abundance of MMP3 in TBHP + IL-1β is higher than in IL-1β. In CXCL5, IL-1β increased abundances significantly at 6 h compared to control, while CXCL5 levels barely increased for TBHP + IL-1β. Over time both TBHP + IL-1β and IL-1β CXCL5 levels increased compared to control, with TBHP + IL-1β abundances appearing slightly, non-significantly elevated compared to IL-1β.

As oxidative stress and chronic inflammation are known to modulate extracellular matrix remodeling, collagen and collagen-associated proteins were specifically examined and highlighted in the volcano plots (Figure 25, Figure S 1 and Figure S 2). A detailed overview of all identified collagen and collagen-associated proteins is provided in the supplementary material (Table S 12 and Table S 13).

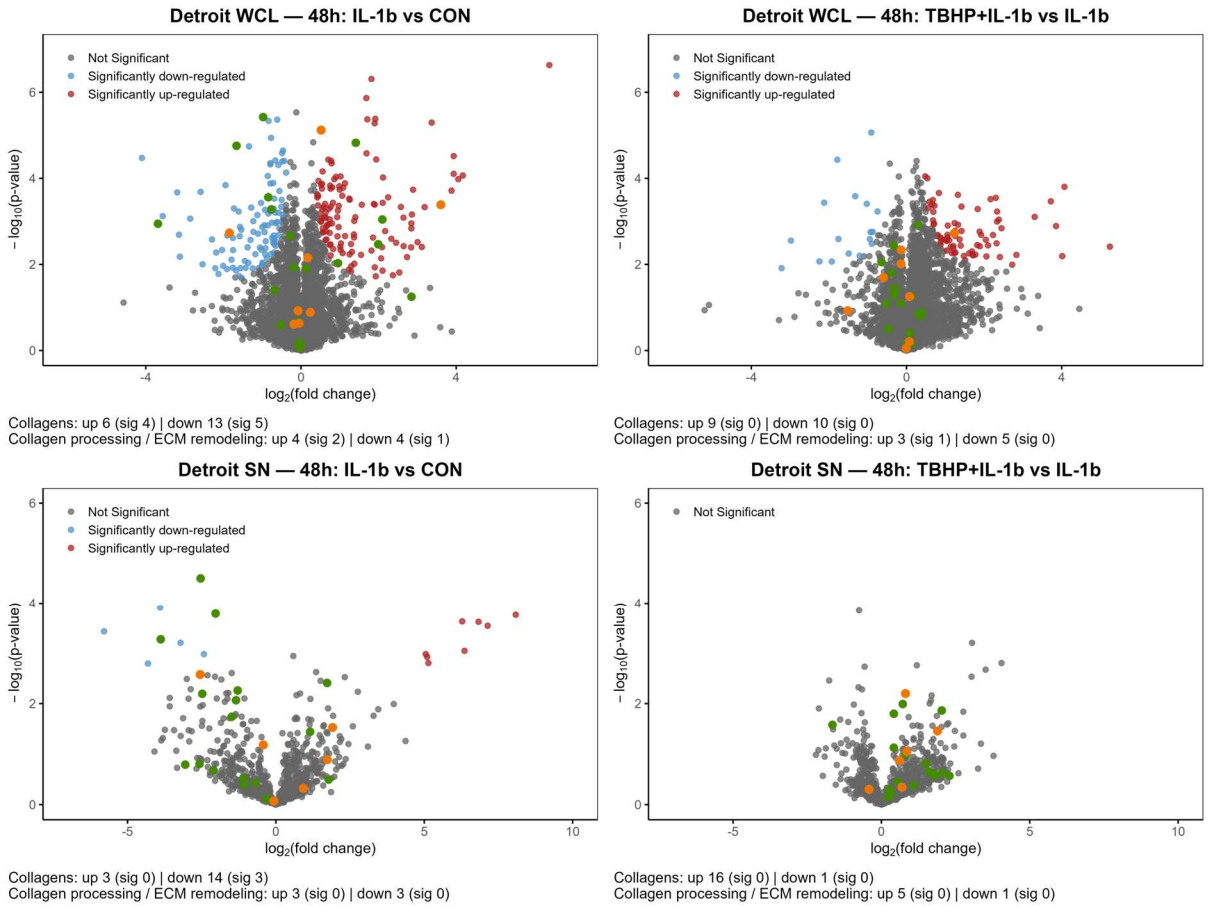

Figure 25 Volcano plots for the IL-1β *vs* CON (left) and TBHP + IL-1β *vs* IL-1β (right) comparison for the Detroit 551 time-course experiment WCL (top) and SN (bottom) at 48 h. Significantly upregulated proteins are shown in red, significantly downregulated proteins in blue, and non-significant proteins in grey. Collagens are highlighted in green, while proteins involved in collagen processing and ECM remodeling are shown in orange. Numbers below the plots indicate the numbers of collagens and collagen-/ECM-remodeling-related proteins showing positive (up) or negative (down) log_2 fold changes, numbers in the parentheses (sig) indicate how many of these were significant.

As seen in Figure 25, in the Detroit 551 time-course experiment, collagen and collagen-associated proteins showed a coordinated regulation in the 48 h TBHP + IL-1β *vs* IL-1β comparison. In the WCL of the TBHP + IL-1β vs IL-1β comparison, more of the collagens and collagen-/ECM-remodeling-related proteins are downregulated (15 downregulated, 12 upregulated), while in the SN the pattern is clearer with a total of 21 upregulated and two downregulated collagens and collagen-/ECM-remodeling-related proteins. Although these changes are non-significant, a uniform directional change in the secretome at 48 h is visible. In the secretome, PLOD2 and COL2A1 were decreased, while PLOD1, MMP1, MMP2, CTHRC1 and Collagen alpha chains (COLs) increased in TBHP + IL-1β *vs* IL-1β. For both IL-1β comparisons to the control, the distribution of both collagens and collagen-/ECM-remodeling-related proteins were distributed on both the positive and negative log_2FC sides of the volcano plot, without an apparent shift in one direction. At 6 h and 24 h, collagen-related proteins also displayed heterogeneous patterns with no directional trend in both WCL and SN (Figure S 1 and Figure S 2).

5 Discussion

5.1 Oxidative Stress Responses to TBHP in Fibroblasts

5.1.1 TBHP Reduces Fibroblast Viability

The embryonic Detroit 551 cell line and the adult NHDF cell line showed different dose-response behavior to TBHP in the MTT assay. This suggests cell line specific stress responses to TBHP. Detroit 551 cells showed a gradual decline in the dose-response curve with increasing TBHP concentrations, indicating a continuous and dose-dependent impairment of cellular metabolic activity possibly due to a limited capacity to buffer oxidative stress. Whereas NHDF cells showed stable viability until a critical TBHP concentration was reached, then the viability dropped to zero. This suggests that NHDF are able to buffer TBHP-induced oxidative stress up to a certain limit. Once the buffer capacity is exceeded, cells abruptly lose their metabolic activity. Additionally, the IC_{50}-value for TBHP is higher in NHDF cells, showing higher resistance. These differences could be due to the different biological age of the cell lines, suggesting that adult cells adapted to oxidative stress and have a higher baseline protective program compared to embryonic fibroblasts. NHDF likely adapted to cumulative oxidative stress and damage[4], resulting in higher anti-oxidative capacity until a threshold was reached.

5.1.2 Baseline Proteomic Differences in Detroit 551 and NHDF Related to Oxidative Stress Response

Detroit 551 and NHDF cells were clearly separated on PC1, indicating that embryonic and adult fibroblasts differ substantially in their baseline proteomes. These differences could be caused by their biological age, as adult NHDF may have adapted to environmental stimuli, whereas embryonic Detroit 551 may focus on growth and proliferation. The differences in their proteomic profiles already suggest that the two cell lines respond differently to a variety of stimuli, which could correspond to the different responses to TBHP-induced oxidative stress observed in the MTT assay, where NHDF cells exhibited greater resistance to TBHP than Detroit 551 cells.

Proteins involved in oxidative stress responses differed between Detroit 551 and NHDF. For example, CP, ALDH1A1 and CALB2 were consistently found at high abundances in NHDF across all conditions, while in Detroit 551 only CALB2 was consistently found at lower abundances and CP and ALDH1A1 were only found inconsistently and at the 48 h timepoint. CP is a glycoprotein with ferroxidase activity, that oxidizes Fe^{2+} to Fe^{3+} without releasing ROS.[45] Iron is a central player in ferroptosis and induces oxidative stress by producing ROS. TBHP is known to cause Fe^{2+} accumulation in mitochondria, lipid peroxidation and ROS accumulation.[14] The expression of CP could alleviate the oxidative stress response in NHDF cells by removing Fe^{2+} and prevent cell death. This fits well to the MTT results, with NHDFs viability remaining nearly constant, until a certain TBHP concentration is reached, where CP

cannot prevent ferroptosis anymore and viability drops to zero. ALDH1A1 oxidizes cytotoxic aldehydes that stem from lipid peroxidation.[46] A high baseline level in NHDF suggests that NHDF have a higher capacity to deal with lipid peroxidation products from TBHP-induced oxidative stress. CALB2 is a calcium binding protein that buffers intracellular calcium levels and is involved in calcium homeostasis, as well as modulating calcium dependent signaling.[47] Calcium mobilization and overload is a sign of mitochondrial damage, associated with oxidative stress and triggers cell death.[5] In contrast, TXNIP was predominantly detected in Detroit 551 cells. TXNIP inhibits thioredoxin, which controls ROS and redox homeostasis and regulates apoptosis.[48] High TXNIP levels in Detroit 551 and the resulting hindered redox buffering by thioredoxin could explain that Detroit 551 are able to tolerate less TBHP compared to NHDF. The decline of TXNIP, especially after 48 h, could indicate a late compensatory mechanism after treatment with IL-1β and TBHP + IL-1β.

The variability observed in the PCA is unfortunately a common phenomenon in cell culture experiments in both primary cells and established cell lines.[49] Variability can arise from culture history and prior subculture. Depending on the growth phase (lag, log or plateau phase) cells are in, they differ in metabolism, protein synthesis, proliferation and signaling. Cells that are in different phases contribute to variability in perturbation experiments.[50] However, as the cells were harvested when at full confluency and the starting population for each replicate was identical, variability arising from differences in subculture history was reduced. The variability seen in the PCA is likely due to normal biological heterogeneity in cell culture. Increasing the number of replicates would strengthen the statistical power of future experiments. Additionally, using cells from the same growth phase could further reduce biological variability.

5.1.3 Proteomic Response to TBHP-induced Oxidative Stress

The strong proteomic response observed in Detroit 551 cells with more than 1400 proteins being significantly regulated by TBHP treatment, indicates that embryonic fibroblasts are highly susceptible to oxidative stress, which is consistent with the MTT results and proteomic comparison of both cell lines. In contrast, NHDF cells showed no significant proteome changes, but they exhibited higher variability across their replicates, which could have masked TBHP-induced changes. As NHDF cells showed a higher antioxidant capacity and less susceptibility to TBHP, they likely would still respond less strongly to TBHP than Detroit 551.

PMPCB is a subunit of a mitochondrial processing protease that cleaves off the mitochondria targeting sequence of imported proteins. Knockdowns of PMPCB were shown to induce mitophagy.[51] The reduction of PMPCB in both cell lines in the TBHP and TBHP + IL-1β conditions indicates a mitochondrial stress response. Despite NHDF cells being able to buffer TBHP-induced oxidative stress responses better, the reduction of PMPCB is more pronounced, suggesting a stronger effect on their

mitochondria. As cells accumulate damages from oxidative stress while aging, mitochondrial function decreases, mitophagy is reduced and damaged mitochondria accumulate.[4,5,15] As a consequence, adult NHDF have likely accumulated damaged mitochondria, while those of embryonic Detroit 551 are presumably fully functional. This could explain the higher downregulation and stronger mitochondrial stress response in NHDF than Detroit 551, as undamaged mitochondria possibly tolerate mitochondrial stress better. DKK1 is an inhibitor of Wnt signaling, its overexpression under oxidative stress conditions has been associated with pro-apoptotic cellular responses.[52] Wnt signaling plays a role in fibroblast tissue regeneration. Transient Wnt signaling promotes regenerative healing, while chronic Wnt signaling leads to fibrosis.[6] As DKK1 inhibits Wnt signaling, fibroblast repair mechanisms are hindered. This up-regulation of DKK1 in Detroit 551 cells upon TBHP treatment could be a sign of an oxidative stress response. Its downregulation under combined oxidative and inflammatory stress may reflect an adaptive shift to preserve Wnt-dependent repair mechanisms. In contrast, NHDF show no DKK1 modulation upon TBHP oxidative stress, consistent with their antioxidative capacities. The slight downregulation of DKK1 may indicate enhanced Wnt signaling induced tissue repair.

The GO enrichment of BP and MF provides insights into the most affected processes by TBHP induced oxidative stress in Detroit 551 cells. Mitochondrial processes such as mitochondrial translation and mitochondrial gene expression indicate that TBHP majorly targets mitochondria. This is consistent with previous studies that describe that TBHP directly targets mitochondria.[13,14,18] Additionally, terms like oxidoreduction-driven transmembrane transporter activity and NADH dehydrogenase activity could indicate impaired mitochondrial function due to TBHP. Changes in NADH/NAD+ levels are signs of impaired mitochondrial respiration and decreased NADH dehydrogenase activity has been associated with excessive ROS production.[4] Terms associated with RNA processing, RNA splicing, ribonucleoprotein complex biogenesis, and various catabolic processes, could indicate that Detroit 551 cells are adjusting their protein production or repairing/replacing damaged proteins[53], which could be a compensatory mechanism to TBHP. Overall, the GO enrichment shows, that TBHP induces oxidative stress that targets mitochondria in Detroit 551 cells.

5.2 Inflammatory Responses to IL-1β Stimulation in Fibroblasts

5.2.1 Early Inflammatory Proteomic Response to IL-1β (4 h)

The comparison of IL-1β induced proteomic changes between Detroit 551 and NHDF cells showed that both fibroblasts responded with an inflammatory program with shared upregulated proteins such as IL1B, CXCL1 and ICAM1. IL-1β is upregulated as both cell lines were treated with it. But the known inflammatory mediators ICAM1 and CXCL1, are characteristic for inflammatory stimulation in fibroblasts.[2,3,7] Detroit 551 cells showed a stronger inflammatory response compared to NHDF cells with more than four times as many significantly regulated proteins. However, NHDF cells showed a higher variability in the replicates, which could have masked some of the responses. There were 15 uniquely regulated proteins in Detroit 551 including PTX3, PLAU and TNFAIP2. Although some of those have been reported to be induced upon IL-1β treatment also in NHDF cells, such as PTX3 and TNFAIP2[2,3], others were truly unique to Detroit 551 cells. This supports the theory that some proteomic changes were masked due to NHDFs higher variability. In contrast, NHDF showed other uniquely regulated proteins such as VASN, C8orf4 or CSF1, that have been previously reported to be regulated upon IL-1β stimulation.[2,3] Overall, Detroit 551 and NHDF cells seem to differ in their IL-1β induced inflammatory response, likely due to NHDFs higher variability. However, there are uniquely regulated proteins for each cell line, indicating that embryonic and adult fibroblasts respond differently to IL-1β.

One example highlighting differences in inflammatory responses between the two cell lines is the cell line specific detection of PLAU in Detroit 551 cells and CSF1 in NHDF cells. Urokinase-type plasminogen activator (PLAU) is associated with inflammatory response, wound healing and ECM remodeling.[54] Macrophage colony-stimulating factor 1 (CSF1) is secreted by fibroblasts to sustain macrophages during inflammation.[55] This could indicate that NHDF cells focus more on immune cell recruitment while Detroit 551 predominantly focus on ECM remodeling.

TNFAIP8 is an antiapoptotic protein induced by TNF-α. Its absence leads to an enhanced inflammatory response.[56] TNFAIP8 is not regulated by TBHP compared to the control, it is however upregulated upon IL-1β stimulation. In Detroit 551 this elevation is even higher in the TBHP + IL-1β condition, while NHDF show no additional increase. The upregulation suggests a protective response to limit an excessive inflammatory response. This protective response is enhanced by TBHP pre-stress in Detroit 551 cells, suggesting a compensatory, antiapoptotic protective mechanism, whereas NHDF cells buffer this stress without further TNFAIP8 induction.

The known inflammatory markers for IL-1β stimulation in fibroblasts IL6, ICAM1 and PTGS2[2,3], are significantly upregulated in the IL-1β group in Detroit 551 cells. In NHDF cells ICAM1 and IL6 are elevated as well, while PTGS2 levels remained unaffected. In both cell lines TBHP alone does not change abundances of these proteins, while in comparison to IL-1β, IL6 and PTGS2 are elevated in the

TBHP + IL-1β group, despite not being statistically significant. ICAM1 levels are comparable between IL-1β and TBHP + IL-1β in both cell lines. The patterns for IL6 and PTGS2 suggest that TBHP modulates and amplifies inflammatory responses in both cell lines. As ICAM1 levels are unaffected, this suggests that TBHP only modulates certain proteins and signaling pathways. This additionally supports the notion that embryonic and adult fibroblasts differ in both their oxidative stress response and inflammatory response.

Differences in the inflammatory response between Detroit 551 and NHDF cells are also visible in the GO BP enrichment. Both adult and embryonic fibroblasts share enriched terms associated with endothelial development, which is consistent with fibroblasts' inflammatory remodeling of the extracellular matrix.[6] Detroit 551 cells were enriched in nitric oxide (NO) and collagen-related processes, while NHDF cells were enriched in terms associated with immune cells and their recruitment. It was previously shown that NHDF cells play an important role in the recruitment of immune cells.[2] NO, a redox-active radical, and NO synthase are mediators of inflammatory signaling and linked to matrix remodeling.[57] Fibroblasts are known to secrete ECM and collagens during inflammatory matrix remodeling. [6,55] This suggests that embryonic and adult fibroblasts react differently to IL-1β-induced inflammation.

5.2.2 IL-1β-induced Inflammatory Response Over Time (6–48 h)

In the PCA, the control is clearly separated from both IL-1β-containing conditions. In the secretome, both TBHP + IL-1β and IL-1β cluster together according to timepoints, suggesting that the primary proteomic changes result upon IL-1β inflammatory stimulation with TBHP not having much of a modulatory effect. This is similar in the cell lysates at the 6 h and 24 h timepoints, however TBHP + IL-1β and IL-1β are clearly separated at the 48 h timepoint, suggesting that TBHP does modulate the inflammatory response primarily at later timepoints.

In the secretome, the variability between the replicates was more pronounced than in the cell lysates. This is expected because secreted proteins are generally low-abundant.[25,26] Together with normal biological heterogeneity[49,50], this contributes to the higher variability observed.

The number of significantly regulated proteins in the Detroit 551 cell lysates increased from 6 h to 48 h of well-described proteins associated with fibroblast inflammatory response such as SDC4, CXCL3/2, IGFBP2, PTX3, NFKB2, SOD2, ICAM1, PTGS2, NAMPT, COL1A1 and COL3A1.[2,3] Many of these proteins are also associated with the hallmarks of inflammation such as innate immune response, ECM reorganization, cell adhesion and migration, as well as response to oxidative stress.[2] This temporal pattern of differently regulated proteins aligns with different phases in the cycle of inflammation, starting with an acute response and transitioning towards regulated remodeling processes as the reaction progresses. [1]

IL-1β stimulation induced a temporally dynamic secretory response in Detroit 551 cells. At 6 h, several well-characterized inflammatory mediators such as CXCL1/3/8, CCL2, IL6, LIF and PTX3 were significantly regulated. At 24 h, the number of significantly regulated secreted proteins decreased to two (IL6 and CXCL1). The amount of significantly regulated proteins increased again with the upregulation of chemokines (CXCL5/8/11), LIF, CCL2 and the matrix-modifying enzyme MMP3, alongside the downregulation of collagens such as COL1A1, COL11A1 and COL1A2 at 48 h.[2,3] This pattern is compatible with the transition from early cytokine signaling toward later extracellular-matrix–related remodeling processes of inflammation[1] , despite the secretome samples having higher variability in the data.

5.3 Inflammatory Responses Following Oxidative Pre-stress in Fibroblasts

5.3.1 Short-term Inflammatory Response after Oxidative Pre-stress (4 h)

There were no significantly regulated proteins in the TBHP + IL-1β *vs* IL-1β comparison, likely due to the high variability in NHDF cells and in Detroit 551 cells TBHP + IL-1β group.

NINJ1 is involved in plasma membrane rupture during programmed cell death and promotes interactions between immune cells and endothelial cells. A previous study showed that NINJ1 controls ferroptosis by regulating cellular antioxidant capacity, with NINJ1 knockdown being protective against ferroptosis, while NINJ1 overexpression enhances ferroptosis.[58] TBHP-induced a downregulation of NINJ1 in Detroit 551 cells, while being slightly elevated in the TBHP + IL-1β combination but was not affected by IL-1β alone. This suggests a protective adaptation response of Detroit 551 cells to TBHP-induced oxidative stress and ferroptosis. The upregulation of NINJ1 after TBHP pre-stress and subsequent IL-1β stimulation, while IL-1β alone does not affect NINJ1 levels, indicates that the combined oxidative and inflammatory stress exceeds the cellular protective capacity, shifting the response towards ferroptotic cell death. The added stress from IL-1β surpassed Detroit 551's protective response shifting to cell death. This indicates that TBHP modulates signaling pathways linked to inflammation and cell death, and that additional inflammatory stress can convert an initially protective response into a pro-death phenotype. NHDF cells, however, reacted differently to TBHP treatment than Detroit 551 cells, as NINJ1 levels are at a similar level to the control, while being non-significantly elevated in both TBHP + IL-1β and IL-1β. This is consistent with NHDF cells higher antioxidative capacity and fits well with the MTT data. The increased NINJ1 levels in both inflammatory groups indicates that NHDF cells are more sensitive to inflammatory stimulation than Detroit 551 cells and are shifting towards ferroptosis.

NFKBIB inhibits NF-κ-B by binding to it. NF-κ-B is a central transcription factor in inflammation, that activates the expression of cytokines and adhesion molecules. NFKBIB downregulation is known upon inflammatory stimulation, so that NF-κ-B can drive inflammatory signaling.[59] In Detroit 551 cells,

NFKBIB is significantly downregulated upon inflammatory stimulation, while TBHP does not influence NFKBIB levels. In TBHP + IL-1β, however, NFKBIB is not detected anymore, which could indicate that TBHP oxidative pre-stress enhanced inflammatory signaling. In NHDF cells TBHP also did not change NFKBIB levels, in both IL-1β and TBHP + IL-1β groups NFKBIB is absent, indicating a stronger inflammatory response in NHDF compared to Detroit 551 upon IL-1β stimulation. This highlights that both fibroblast cell lines not only respond differently to TBHP-induced oxidative stress but also inflammatory stimulation.

5.3.2 Long-term Effects of Oxidative Pre-stress on Inflammatory Signaling (6–48 h)

As TBHP pre-stress did not alter the inflammatory response at 6 h and 24 h, but effects became apparent at 48 h, this suggests TBHP does not substantially modulate early inflammatory responses but affects later timepoints such as 48 h. The appearance of proteins related to mitochondrial function (e.g., NDUFAF2, NDUFB11, UQCRQ)[60], apoptosis and cell survival (BAD, DIDO1)[60] suggests a time-delayed effect of TBHP-induced oxidative stress that might trigger adaptive mechanisms. This fits well with TBHP and oxidative stress impacting mitochondrial function.[13,14,18]

MMP1 and PTGS2 are known inflammatory mediators upregulated upon IL-1β stimulation.[2,3] MMP1 cleaves collagens and is involved in matrix remodeling, which is part of wound healing.[60] PTGS2 converts arachidonic acid to prostaglandins and plays a central role in the inflammatory response.[60] TBHP + IL-1β at 48 h elevated MMP1 significantly and PTGS2 non-significantly compared to IL-1β, which indicates that TBHP modulates inflammatory response after 48 h. The proteins MRPS34 and SLC25A22 are mitochondrial proteins.[60] Their late induction after 48 h in the TBHP + IL-1β indicates a compensatory mitochondrial stress response or adaptive mechanism. This is consistent with the known TBHP damage to mitochondria.[13,14,18] AKR1C2 is a reductase involved in steroid metabolism and known to prevent ferroptosis by reducing end products of lipid peroxidation.[60] It followed the same pattern as MRPS34 and SLC25A22, further suggesting a time-delayed protective response to TBHP-induced mitochondrial damage and sustained oxidative stress.[13,14,18] GCSH is a mitochondrial protein responsible for the modification of mitochondrial enzymes involved in energy production.[60] Its complete absence after 48 h in the TBHP + IL-1β condition suggests an altered or impaired mitochondrial function. This highlights a delayed modulation of the inflammatory process by TBHP and a delayed mitochondrial and oxidative stress response and indicates impaired mitochondrial function.

The GO CC enrichment shows predominantly mitochondrial terms, suggesting that mitochondria are strongly affected. This fits well with the proteomic changes with the appearance of AKR1C2, MRPS34, SLC25A22 and absence of GCSH and supports the notion of a late mitochondrial stress response.

The secretome of Detroit 551 cells show no significant protein changes at 24 h and 48 h and only one single downregulated protein (COL2A1) at 6 h. This suggests that TBHP does not substantially alter the

secretome of embryonic fibroblasts. The secretome ,however, displayed higher variability in the replicates, which could have masked more subtle differences.[49,50]

Three proteins, namely SDC4, MMP3 and CXCL5 that have been shown to be upregulated upon IL-1β stimulation promote IL-1β-driven inflammatory activation in fibroblasts.[2,3] MMP3 and CXCL5 showed a non-significant elevation in TBHP + IL-1β compared to IL-1β, especially after 48 h, which again supports the idea that TBHP changes inflammatory response at later timepoints such as 48 h. SDC4 on the other hand showed a different pattern, as SDC4 levels were similar across all conditions at 24 h and 48 h, while it was upregulated upon inflammatory stimulation after 6 h, which indicates an early inflammatory response. Again, TBHP + IL-1β compared to IL-1β showed slightly elevated levels, though non-significant.

The uniform upregulation of collagens and collagen-associated proteins at 48 h in the secretome of the TBHP pre-stressed inflammatory stimulated cells, compared to inflammatory stimulated cells without pre-stress, indicates a time-delayed effect on the ECM. Although these changes are not significant, they differ from inflammatory stimulation compared to control and the 6 h and 24 h timepoints by showing a consistent directional regulation instead of a heterogeneous distribution pattern, which could still indicate a biologically relevant change. Proteins involved in collagen processing such as collagenases (MMP1 and MMP2), enzymes mediating collagen crosslinking (PLOD1 and PLOD2) and collagen-associated proteins (CTHRC1), which are involved in ECM remodeling[60], are regulated. Except from COL2A1 and PLOD2, all those proteins are upregulated in the secretome, which indicates enhanced ECM remodeling due to oxidative pre-stress prior to inflammatory stimulation. Even though a major function of fibroblasts is ECM remodeling in wound healing, which includes production of collagens, production of excessive quantities of ECM as well as excessive collagen deposition, especially collagen type I and type III have been linked to fibrosis.[6,17,55] The coordinated regulations of collagens and collagen-related proteins at the 48 h timepoint suggests that oxidative pre-stress alters matrix remodeling in fibroblasts. This could be an adaptive remodeling response but could also be associated with fibrosis. As this observed effect was not significant, it is unclear if this remodeling is excessive.

6 Conclusion and Outlook

This thesis characterized proteomic changes in embryonic Detroit 551 and adult NHDF cells upon TBHP-induced oxidative stress, IL-1β-induced inflammatory response and oxidative pre-stress prior to inflammatory stimulation. Additionally, proteomic changes over 48 h were characterized in Detroit 551 cells to see how TBHP modulates inflammatory response over time. Inflammatory stimulation was induced successfully by IL-1β and resulted in the regulation of already described inflammatory proteins in fibroblasts. TBHP successfully induced oxidative stress and modulated redox-associated and mitochondrial proteins, which indicates mitochondrial stress. Both fibroblast cell lines differed in their basal proteome, with NHDF cells possessing a higher amount of proteins preventative of oxidative stress and tolerated higher TBHP concentrations, while Detroit 551 cells adapted to oxidative stress at the 48 h timepoint. This suggests that adult fibroblasts may already be better adapted to oxidative stress. The oxidative pre-stress and subsequent IL-1β stimulation showed that prior oxidative stress can influence inflammatory responses. Some inflammatory proteins were elevated, while others remained unaffected, suggesting that TBHP modulates inflammatory processes in a protein-specific manner, or only modulates shared pathways between oxidative stress and inflammatory signaling, while independent pathways remain unaffected. The differences between inflammatory stimulation and inflammatory stimulation after prior oxidative stress were most pronounced after 48 h, indicating a time-delayed effect on inflammatory processes. Oxidative pre-stress prior to inflammatory stimulation could also be associated with a time-dependent change in collagens and related proteins, suggesting altered matrix remodeling in fibroblasts. This thesis highlights age-associated differences in fibroblast stress responses and confirmed TBHP-induced mitochondrial damage.

Based on this, future experiments could extend the timeframe beyond 48 h to capture long-term adaptations and mechanisms and see whether oxidative stress predisposes fibroblasts to more prolonged inflammatory signaling. Additionally, repeated TBHP exposure could model chronic oxidative stress and uncover cumulative effects of oxidative and mitochondrial damage. Increasing the number of biological replicates in future experiments would further improve statistical power and could uncover subtle regulatory changes that were masked by variability in the present dataset. Adding other types of analyses, such as eicosanoid profiling, phosphoproteomics or metabolomics, could give additional insight into lipid mediators, signaling activity, and metabolic changes. This could help to better understand how oxidative and inflammatory pathways work together and how oxidative stress shapes inflammatory responses in fibroblasts.

7 References

(1) Bender, E. C.; Tareq, H. S.; Suggs, L. J. Inflammation: A Matter of Immune Cell Life and Death. *Npj Biomed. Innov.* **2025**, *2* (1), 7. https://doi.org/10.1038/s44385-025-00010-4.

(2) Slany, A.; Bileck, A.; Kreutz, D.; Mayer, R. L.; Muqaku, B.; Gerner, C. Contribution of Human Fibroblasts and Endothelial Cells to the Hallmarks of Inflammation as Determined by Proteome Profiling. *Mol. Cell. Proteomics* **2016**, *15* (6), 1982–1997. https://doi.org/10.1074/mcp.M116.058099.

(3) Tahir, A.; Bileck, A.; Muqaku, B.; Niederstaetter, L.; Kreutz, D.; Mayer, R. L.; Wolrab, D.; Meier, S. M.; Slany, A.; Gerner, C. Combined Proteome and Eicosanoid Profiling Approach for Revealing Implications of Human Fibroblasts in Chronic Inflammation. *Anal. Chem.* **2017**, *89* (3), 1945–1954. https://doi.org/10.1021/acs.analchem.6b04433.

(4) Maldonado, E.; Morales-Pison, S.; Urbina, F.; Solari, A. Aging Hallmarks and the Role of Oxidative Stress. *Antioxidants* **2023**, *12* (3), 651. https://doi.org/10.3390/antiox12030651.

(5) Dela Cruz, C. S.; Kang, M.-J. Mitochondrial Dysfunction and Damage Associated Molecular Patterns (DAMPs) in Chronic Inflammatory Diseases. *Mitochondrion* **2018**, *41*, 37–44. https://doi.org/10.1016/j.mito.2017.12.001.

(6) Plikus, M. V.; Wang, X.; Sinha, S.; Forte, E.; Thompson, S. M.; Herzog, E. L.; Driskell, R. R.; Rosenthal, N.; Biernaskie, J.; Horsley, V. Fibroblasts: Origins, Definitions, and Functions in Health and Disease. *Cell* **2021**, *184* (15), 3852–3872. https://doi.org/10.1016/j.cell.2021.06.024.

(7) Wei, K.; Nguyen, H. N.; Brenner, M. B. Fibroblast Pathology in Inflammatory Diseases. *J. Clin. Invest.* **2021**, *131* (20). https://doi.org/10.1172/jci149538.

(8) *Primary Dermal Fibroblast; Normal, Human, Adult (HDFa) - PCS-201-012 | ATCC*. https://www.atcc.org/products/pcs-201-012 (accessed 2025-01-30).

(9) Waise, S.; Parker, R.; Rose-Zerilli, M. J. J.; Layfield, D. M.; Wood, O.; West, J.; Ottensmeier, C. H.; Thomas, G. J.; Hanley, C. J. An Optimized Method to Isolate Human Fibroblasts from Tissue for Ex Vivo Analysis. *Bio-Protoc.* **2019**, *9* (23), e3440. https://doi.org/10.21769/BioProtoc.3440.

(10) *Detroit 551 - CCL-110 | ATCC*. https://www.atcc.org/products/ccl-110 (accessed 2025-12-28).

(11) Sugarman, B. J.; Aggarwal, B. B.; Hass, P. E.; Figari, I. S.; Palladino, M. A.; Shepard, H. M. Recombinant Human Tumor Necrosis Factor-Alpha: Effects on Proliferation of Normal and Transformed Cells in Vitro. *Science* **1985**, *230* (4728), 943–945. https://doi.org/10.1126/science.3933111.

(12) Janker-Bortel, P.; Martinez-Val, A.; Hagn, G.; Skos, L.; Olsen, J. V.; Gerner, C. Phosphoproteomics Highlights Complex Resource Management upon Inflammatory Stimulation of Fibroblasts. bioRxiv October 11, 2024. https://doi.org/10.1101/2024.10.11.617591.

(13) Wenz, C.; Faust, D.; Linz, B.; Turmann, C.; Nikolova, T.; Bertin, J.; Gough, P.; Wipf, P.; Schröder, A. S.; Krautwald, S.; Dietrich, C. T-BuOOH Induces Ferroptosis in Human and Murine Cell Lines. *Arch. Toxicol.* **2018**, *92* (2), 759–775. https://doi.org/10.1007/s00204-017-2066-y.

(14) Chen, Y.; Guo, X.; Zeng, Y.; Mo, X.; Hong, S.; He, H.; Li, J.; Fatima, S.; Liu, Q. Oxidative Stress Induces Mitochondrial Iron Overload and Ferroptotic Cell Death. *Sci. Rep.* **2023**, *13* (1), 15515. https://doi.org/10.1038/s41598-023-42760-4.

(15) Luo, J.; Mills, K.; Le Cessie, S.; Noordam, R.; Van Heemst, D. Ageing, Age-Related Diseases and Oxidative Stress: What to Do Next? *Ageing Res. Rev.* **2020**, *57*, 100982. https://doi.org/10.1016/j.arr.2019.100982.

(16) Ermak, G.; Davies, K. J. A. Calcium and Oxidative Stress: From Cell Signaling to Cell Death. *Mol. Immunol.* **2002**, *38* (10), 713–721. https://doi.org/10.1016/S0161-5890(01)00108-0.

(17) Rotariu, D.; Babes, E. E.; Tit, D. M.; Moisi, M.; Bustea, C.; Stoicescu, M.; Radu, A.-F.; Vesa, C. M.; Behl, T.; Bungau, A. F.; Bungau, S. G. Oxidative Stress – Complex Pathological Issues Concerning the Hallmark of Cardiovascular and Metabolic Disorders. *Biomed. Pharmacother.* **2022**, *152*, 113238. https://doi.org/10.1016/j.biopha.2022.113238.

(18) Pinho, S. A.; Oliveira, P. J.; Cunha-Oliveira, T. Heterogeneous Redox Responses in NHDF Cells Primed to Enhance Mitochondrial Bioenergetics. *Biochim. Biophys. Acta BBA - Mol. Basis Dis.* **2025**, *1871* (1), 167495. https://doi.org/10.1016/j.bbadis.2024.167495.

(19) Alberts, B.; Johnson, A.; Lewis, J.; Morgan, D.; Raff, M.; Roberts, K.; Walter, P. Energy Conversion: Mitochondria and Chloroplasts. In *Molecular Biology of the Cell*; Garald Science, 2014; pp 755–780.
(20) Alberts, B.; Johnson, A.; Lewis, J.; Morgan, D.; Raff, M.; Roberts, K.; Walter, P. Cell Death. In *Molecular Biology of the Cell*; Garald Science; pp 1021–1030.
(21) Marchi, S.; Guilbaud, E.; Tait, S. W. G.; Yamazaki, T.; Galluzzi, L. Mitochondrial Control of Inflammation. *Nat. Rev. Immunol.* **2023**, *23* (3), 159–173. https://doi.org/10.1038/s41577-022-00760-x.
(22) Tang, D.; Chen, X.; Kang, R.; Kroemer, G. Ferroptosis: Molecular Mechanisms and Health Implications. *Cell Res.* **2021**, *31* (2), 107–125. https://doi.org/10.1038/s41422-020-00441-1.
(23) Jiang, Y.; Rex, D. A. B.; Schuster, D.; Neely, B. A.; Rosano, G. L.; Volkmar, N.; Momenzadeh, A.; Peters-Clarke, T. M.; Egbert, S. B.; Kreimer, S.; Doud, E. H.; Crook, O. M.; Yadav, A. K.; Vanuopadath, M.; Hegeman, A. D.; Mayta, M. L.; Duboff, A. G.; Riley, N. M.; Moritz, R. L.; Meyer, J. G. Comprehensive Overview of Bottom-Up Proteomics Using Mass Spectrometry. *ACS Meas. Sci. Au* **2024**, *4* (4), 338–417. https://doi.org/10.1021/acsmeasuresciau.3c00068.
(24) Cox, J.; Hein, M. Y.; Luber, C. A.; Paron, I.; Nagaraj, N.; Mann, M. Accurate Proteome-Wide Label-Free Quantification by Delayed Normalization and Maximal Peptide Ratio Extraction, Termed MaxLFQ. *Mol. Cell. Proteomics* **2014**, *13* (9), 2513–2526. https://doi.org/10.1074/mcp.m113.031591.
(25) Makridakis, M.; Vlahou, A. Secretome Proteomics for Discovery of Cancer Biomarkers. *J. Proteomics* **2010**, *73* (12), 2291–2305. https://doi.org/10.1016/j.jprot.2010.07.001.
(26) Méndez, O.; Villanueva, J. Challenges and Opportunities for Cell Line Secretomes in Cancer Proteomics. *PROTEOMICS – Clin. Appl.* **2015**, *9* (3–4), 348–357. https://doi.org/10.1002/prca.201400131.
(27) Samiminemati, A.; Aprile, D.; Siniscalco, D.; Di Bernardo, G. Methods to Investigate the Secretome of Senescent Cells. *Methods Protoc.* **2024**, *7* (4), 52. https://doi.org/10.3390/mps7040052.
(28) Mitulovic, G.; Mechtler, K. HPLC Techniques for Proteomics Analysis--a Short Overview of Latest Developments. *Brief. Funct. Genomic. Proteomic.* **2006**, *5* (4), 249–260. https://doi.org/10.1093/bfgp/ell034.
(29) Karas, M.; Bahr, U.; Dülcks, T. Nano-Electrospray Ionization Mass Spectrometry: Addressing Analytical Problems beyond Routine. *Fresenius J. Anal. Chem.* **2000**, *366* (6), 669–676. https://doi.org/10.1007/s002160051561.
(30) Meier, F.; Beck, S.; Grassl, N.; Lubeck, M.; Park, M. A.; Raether, O.; Mann, M. Parallel Accumulation−Serial Fragmentation (PASEF): Multiplying Sequencing Speed and Sensitivity by Synchronized Scans in a Trapped Ion Mobility Device. *J Proteome Res* **2015**.
(31) Meier, F.; Brunner, A.-D.; Koch, S.; Koch, H.; Lubeck, M.; Krause, M.; Goedecke, N.; Decker, J.; Kosinski, T.; Park, M. A.; Bache, N.; Hoerning, O. Online Parallel Accumulation–Serial Fragmentation (PASEF) with a Novel Trapped Ion Mobility Mass Spectrometer. *Mol. Cell. Proteomics* **2018**, *17* (12), 2534–2545. https://doi.org/10.1074/mcp.TIR118.000900.
(32) Meier, F. Trapped Ion Mobility Spectrometry and Parallel Accumulation-Serial Fragmentation in Proteomics. *Mol. Cell. Proteomics* **2021**, *20*, 100138.
(33) *BioRender*. BioRender. https://biorender.com/ (accessed 2022-01-10).
(34) Cox, J.; Mann, M. MaxQuant Enables High Peptide Identification Rates, Individualized p.p.b.-Range Mass Accuracies and Proteome-Wide Protein Quantification. *Nat. Biotechnol.* **2008**, *26* (12), 1367–1372. https://doi.org/10.1038/nbt.1511.
(35) Cox, J.; Neuhauser, N.; Michalski, A.; Scheltema, R. A.; Olsen, J. V.; Mann, M. Andromeda: A Peptide Search Engine Integrated into the MaxQuant Environment. *J. Proteome Res.* **2011**, *10* (4), 1794–1805. https://doi.org/10.1021/pr101065j.
(36) Tyanova, S.; Temu, T.; Sinitcyn, P.; Carlson, A.; Hein, M. Y.; Geiger, T.; Mann, M.; Cox, J. The Perseus Computational Platform for Comprehensive Analysis of (Prote)Omics Data. *Nat. Methods* **2016**, *13* (9), 731–740. https://doi.org/10.1038/nmeth.3901.
(37) Posit Team. RStudio: Integrated Development Environment for R, 2025. https://www.posit.co/ (accessed 2025-11-04).

(38) Wickham, H.; Averick, M.; Bryan, J.; Chang, W.; McGowan, L. D.; François, R.; Grolemund, G.; Hayes, A.; Henry, L.; Hester, J.; Kuhn, M.; Pedersen, T. L.; Miller, E.; Bache, S. M.; Müller, K.; Ooms, J.; Robinson, D.; Seidel, D. P.; Spinu, V.; Takahashi, K.; Vaughan, D.; Wilke, C.; Woo, K.; Yutani, H. Welcome to the Tidyverse. *J. Open Source Softw.* **2019**, *4* (43), 1686. https://doi.org/10.21105/joss.01686.

(39) Wickham, H.; Bryan, J.; Posit; attribution), P. (Copyright holder of all R. code and all C. code without explicit copyright; code), M. K. (Author of included R.; code), K. V. (Author of included libxls; code), C. L. (Author of included libxls; code), B. C. (Author of included libxls; code), D. H. (Author of included libxls; code), E. M. (Author of included libxls. Readxl: Read Excel Files, 2025. https://cran.r-project.org/web/packages/readxl/index.html (accessed 2025-11-04).

(40) Schauberger, P.; Walker, A.; Braglia, L.; Sturm, J.; Garbuszus, J. M.; Barbone, J. M.; Zimmermann, D.; Kainhofer, R. Openxlsx: Read, Write and Edit Xlsx Files, 2025. https://cran.r-project.org/web/packages/openxlsx/index.html (accessed 2025-11-04).

(41) Slowikowski, K. Ggrepel: Automatically Position Non-Overlapping Text Labels with "Ggplot2," 2016, 0.9.6. https://doi.org/10.32614/CRAN.package.ggrepel.

(42) Wickham, H. Stringr: Simple, Consistent Wrappers for Common String Operations, 2009, 1.6.0. https://doi.org/10.32614/CRAN.package.stringr.

(43) Yu, G.; Wang, L.-G.; Han, Y.; He, Q.-Y. clusterProfiler: An R Package for Comparing Biological Themes Among Gene Clusters. *OMICS J. Integr. Biol.* **2012**, *16* (5), 284–287. https://doi.org/10.1089/omi.2011.0118.

(44) *org.Hs.eg.db*. Bioconductor. http://bioconductor.org/packages/org.Hs.eg.db/ (accessed 2025-11-04).

(45) Hochstrasser, H.; Tomiuk, J.; Walter, U.; Behnke, S.; Spiegel, J.; Krüger, R.; Becker, G.; Riess, O.; Berg, D. Functional Relevance of Ceruloplasmin Mutations in Parkinson's Disease. *FASEB J.* **2005**, *19* (13), 1851–1853. https://doi.org/10.1096/fj.04-3486fje.

(46) Choudhary, S.; Xiao, T.; Vergara, L. A.; Srivastava, S.; Nees, D.; Piatigorsky, J.; Ansari, N. H. Role of Aldehyde Dehydrogenase Isozymes in the Defense of Rat Lens and Human Lens Epithelial Cells against Oxidative Stress. *Invest. Ophthalmol. Vis. Sci.* **2005**, *46* (1), 259–267. https://doi.org/10.1167/iovs.04-0120.

(47) Parmentier, M.; Lefort, A. Structure of the Human Brain Calcium-Binding Protein Calretinin and Its Expression in Bacteria. *Eur. J. Biochem.* **1991**, *196* (1), 79–85. https://doi.org/10.1111/j.1432-1033.1991.tb15788.x.

(48) Liyanage, N. P. M.; Fernando, M. R.; Lou, M. F. REGULATION OF THE BIOAVAILABILITY OF THIOREDOXIN IN THE LENS BY A SPECIFIC THIOREDOXIN-BINDING PROTEIN (TBP-2). *Exp. Eye Res.* **2007**, *85* (2), 270–279. https://doi.org/10.1016/j.exer.2007.05.001.

(49) *Genetic and transcriptional evolution alters cancer cell line drug response | Nature*. https://www.nature.com/articles/s41586-018-0409-3 (accessed 2025-12-19).

(50) Bortel, P.; Hagn, G.; Skos, L.; Bileck, A.; Paulitschke, V.; Paulitschke, P.; Gleiter, L.; Mohr, T.; Gerner, C.; Meier-Menches, S. M. Memory Effects of Prior Subculture May Impact the Quality of Multiomic Perturbation Profiles. *Proc. Natl. Acad. Sci.* **2024**, *121* (29), e2313851121. https://doi.org/10.1073/pnas.2313851121.

(51) Greene, A. W.; Grenier, K.; Aguileta, M. A.; Muise, S.; Farazifard, R.; Haque, M. E.; McBride, H. M.; Park, D. S.; Fon, E. A. Mitochondrial Processing Peptidase Regulates PINK1 Processing, Import and Parkin Recruitment. *EMBO Rep.* **2012**, *13* (4), 378–385. https://doi.org/10.1038/embor.2012.14.

(52) Colla, S.; Zhan, F.; Xiong, W.; Wu, X.; Xu, H.; Stephens, O.; Yaccoby, S.; Epstein, J.; Barlogie, B.; Shaughnessy, J. D., Jr. The Oxidative Stress Response Regulates DKK1 Expression through the JNK Signaling Cascade in Multiple Myeloma Plasma Cells. *Blood* **2007**, *109* (10), 4470–4477. https://doi.org/10.1182/blood-2006-11-056747.

(53) Balch, W. E.; Morimoto, R. I.; Dillin, A.; Kelly, J. W. Adapting Proteostasis for Disease Intervention. *Science* **2008**, *319* (5865), 916–919. https://doi.org/10.1126/science.1141448.

(54) Baker, S. K.; Strickland, S. A Critical Role for Plasminogen in Inflammation. *J. Exp. Med.* **2020**, *217* (4), e20191865. https://doi.org/10.1084/jem.20191865.

(55) Kim, D.; Baek, J.-H. Macrophages and Fibroblasts in Cardiac Fibrosis: Interactions and Transformation. *Explor. Immunol.* **2025**, *5*, 1003211. https://doi.org/10.37349/ei.2025.1003211.
(56) Lou, Y.; Tian, X.; Sun, C.; Song, M.; Han, M.; Zhao, Y.; Song, Y.; Song, X.; Zhang, W.; Chen, Y. H.; Wang, H. TNFAIP8 Protein Functions as a Tumor Suppressor in Inflammation-Associated Colorectal Tumorigenesis. *Cell Death Dis.* **2022**, *13* (4), 311. https://doi.org/10.1038/s41419-022-04769-x.
(57) Förstermann, U.; Sessa, W. C. Nitric Oxide Synthases: Regulation and Function. *Eur. Heart J.* **2012**, *33* (7), 829–837. https://doi.org/10.1093/eurheartj/ehr304.
(58) Chen, S.-Y.; Wu, J.; Chen, Y.; Wang, Y.-E.; Setayeshpour, Y.; Federico, C.; Mestre, A. A.; Lin, C.-C.; Chi, J.-T. NINJ1 Regulates Ferroptosis via xCT Antiporter Interaction and CoA Modulation. *Cell Death Dis.* **2024**, *15* (10), 755. https://doi.org/10.1038/s41419-024-07135-1.
(59) Kamata, H.; Tsuchiya, Y.; Asano, T. IκBβ Is a Positive and Negative Regulator of NF-κB Activity during Inflammation. *Cell Res.* **2010**, *20* (11), 1178–1180. https://doi.org/10.1038/cr.2010.147.
(60) The UniProt Consortium. UniProt: The Universal Protein Knowledgebase in 2023. *Nucleic Acids Res.* **2023**, *51* (D1), D523–D531. https://doi.org/10.1093/nar/gkac1052.

Supplementary Information

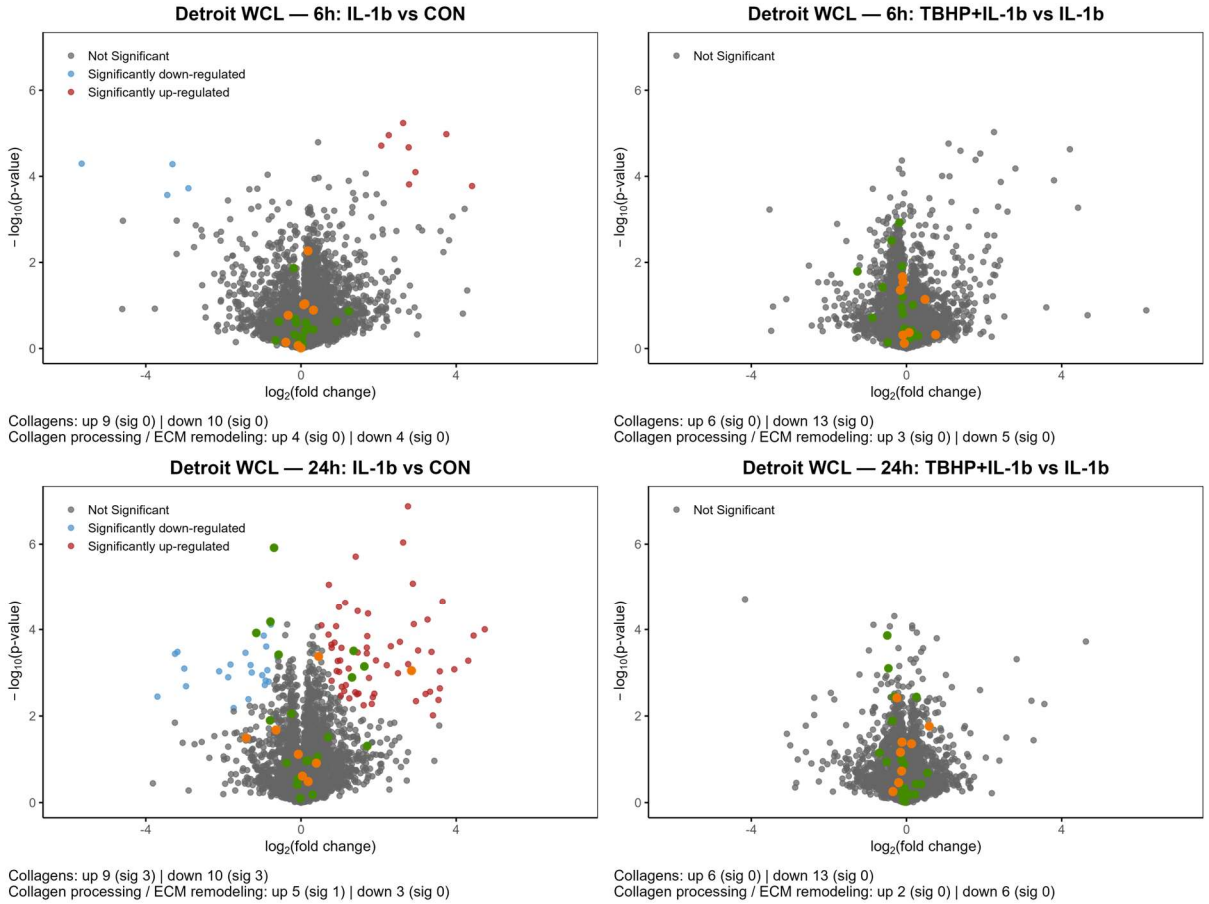

Figure S 1 Volcano plots for the IL-1β *vs* CON (left) and TBHP + IL-1β *vs* IL-1β (right) comparison for the Detroit 551 time-course experiment WCL at 6 h (top) and 24 h (bottom). Significantly upregulated proteins are shown in red, significantly downregulated proteins in blue, and non-significant proteins in grey. Collagens are highlighted in green, while proteins involved in collagen processing and extracellular matrix remodeling are shown in orange Numbers below the plots indicate the numbers of collagens and collagen-/ECM-remodeling-related proteins showing positive (up) or negative (down) log_2 fold changes, numbers in the parentheses (sig) indicate how many of these were significant.

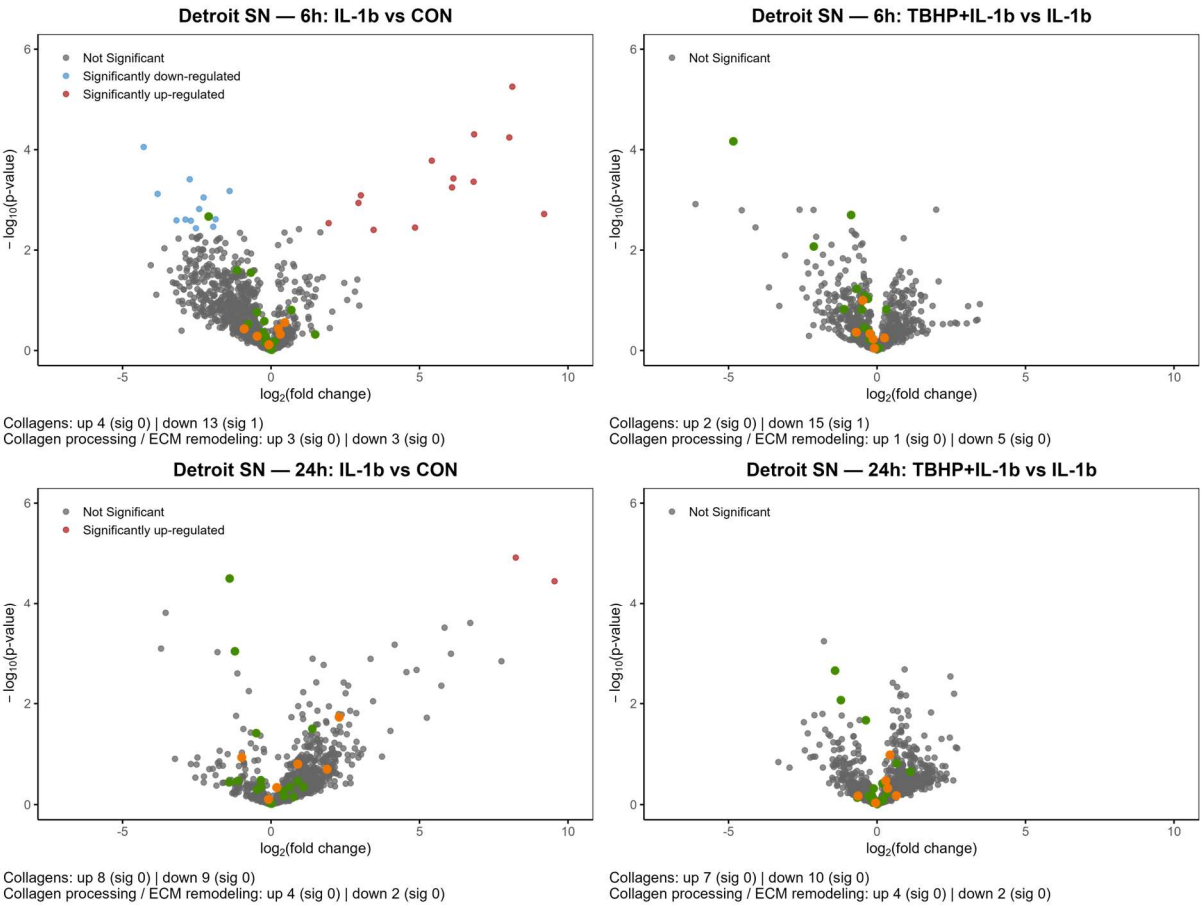

Figure S 2 Volcano plots for the IL-1β *vs* CON (left) and TBHP + IL-1β *vs* IL-1β (right) comparison for the Detroit 551 time-course experiment secretome at 6 h (top) and 24 h (bottom). Significantly upregulated proteins are shown in red, significantly downregulated proteins in blue, and non-significant proteins in grey. Collagens are highlighted in green, while proteins involved in collagen processing and extracellular matrix remodeling are shown in orange. Numbers below the plots indicate the numbers of collagens and collagen-/ECM-remodeling-related proteins showing positive (up) or negative (down) log_2 fold changes, numbers in the parentheses (sig) indicate how many of these were significant.

Table S 1 List of regulated proteins for the TBHP *vs* CON comparison for Detroit 551 – 4 h – 100 proteins (Top 50 up- and downregulated proteins according to difference)

-Log (P-value)	Difference	Majority protein IDs	Protein names	Gene names
4.06	6.3	P02679	Fibrinogen gamma chain	FGG
5.12	4.4	Q13490	Baculoviral IAP repeat-containing protein 2	BIRC2
1.43	3.0	P56385	ATP synthase subunit e, mitochondrial	ATP5I
3.09	2.8	P57721	Poly(rC)-binding protein 3	PCBP3
1.99	2.7	P53805	Calcipressin-1	RCAN1
2.65	2.5	P69905	Hemoglobin subunit alpha	HBA1
1.03	2.5	Q8WX92	Negative elongation factor B	NELFB
1.64	2.2	Q14117	Dihydropyrimidinase	DPYS
1.38	2.1	Q9Y3B7	39S ribosomal protein L11, mitochondrial	MRPL11
1.71	2.1	P49207	60S ribosomal protein L34	RPL34
1.72	2.0	Q15155	Nodal modulator 1	NOMO1
1.81	2.0	F5H284;Q9Y536;P0DN26;A0A075B759	Peptidyl-prolyl cis-trans isomerase A-like 4D;Peptidyl-prolyl cis-trans isomerase A-like 4A/B/C;Peptidyl-prolyl cis-trans isomerase	PPIAL4D;PPIAL4A;PPIAL4E
1.78	1.9	O43768	Alpha-endosulfine	ENSA
2.11	1.8	Q9GZU8	Protein FAM192A	FAM192A
2.03	1.7	Q9UKF7	Cytoplasmic phosphatidylinositol transfer protein 1	PITPNC1
3.84	1.7	P62714	Serine/threonine-protein phosphatase 2A catalytic subunit beta isoform	PPP2CB
1.13	1.6	Q96LR5;Q969T4	Ubiquitin-conjugating enzyme E2 E2;Ubiquitin-conjugating enzyme E2 E3	UBE2E2;UBE2E3
0.93	1.6	Q9Y6I9	Testis-expressed sequence 264 protein	TEX264
1.12	1.6	Q58FG0	Putative heat shock protein HSP 90-alpha A5	HSP90AA5P
1.32	1.6	Q96QS3	Homeobox protein ARX	ARX
1.33	1.5	A0A2R8Y4L2		
1.20	1.5	O60869	Endothelial differentiation-related factor 1	EDF1
0.98	1.5	A4UGR9	Xin actin-binding repeat-containing protein 2	XIRP2
1.24	1.5	Q7Z7F7	39S ribosomal protein L55, mitochondrial	MRPL55
3.52	1.5	Q9UKE5	TRAF2 and NCK-interacting protein kinase	TNIK
2.74	1.5	Q9NWU1	3-oxoacyl-[acyl-carrier-protein] synthase, mitochondrial	OXSM
1.42	1.4	P35443	Thrombospondin-4	THBS4
1.39	1.3	Q16563	Synaptophysin-like protein 1	SYPL1
3.31	1.3	Q9BR61	Acyl-CoA-binding domain-containing protein 6	ACBD6
1.16	1.3	Q16720	Plasma membrane calcium-transporting ATPase 3	ATP2B3
2.53	1.3	Q13442	28 kDa heat- and acid-stable phosphoprotein	PDAP1
1.07	1.3	Q9Y3B8	Oligoribonuclease, mitochondrial	REXO2
1.37	1.3	O75503	Ceroid-lipofuscinosis neuronal protein 5	CLN5
1.00	1.2	Q712K3	Ubiquitin-conjugating enzyme E2 R2	UBE2R2
1.04	1.2	Q9BUI4	DNA-directed RNA polymerase III subunit RPC3	POLR3C
2.08	1.2	Q6STE5;Q96GM5	SWI/SNF-related matrix-associated actin-dependent regulator of chromatin subfamily D member 3;SWI/SNF-related matrix-associated actin-dependent regulator of chromatin subfamily D member 1	SMARCD3;SMARCD1
1.64	1.2	Q9UBP9	PTB domain-containing engulfment adapter protein 1	GULP1
1.41	1.2	Q9UHB7	AF4/FMR2 family member 4	AFF4
1.11	1.2	Q9NXN4	Ganglioside-induced differentiation-associated protein 2	GDAP2
2.34	1.2	Q8TCT9	Minor histocompatibility antigen H13	HM13
1.01	1.2	P62310	U6 snRNA-associated Sm-like protein LSm3	LSM3
1.42	1.2	P38936	Cyclin-dependent kinase inhibitor 1	CDKN1A
1.21	1.2	Q9NWZ8	Gem-associated protein 8	GEMIN8
2.09	1.1	P36639	7,8-dihydro-8-oxoguanine triphosphatase	NUDT1
1.45	1.1	Q8N128	Protein FAM177A1	FAM177A1
1.99	1.1	O14548	Cytochrome c oxidase subunit 7A-related protein, mitochondrial	COX7A2L
1.23	1.1	Q58FF3	Putative endoplasmin-like protein	HSP90B2P
2.39	1.1	Q08170	Serine/arginine-rich splicing factor 4	SRSF4
2.47	1.1	O94907	Dickkopf-related protein 1	DKK1
1.70	-1.4	P07951	Tropomyosin beta chain	TPM2
1.20	-1.4	P17509	Homeobox protein Hox-B6	HOXB6
3.39	-1.4	P31273;P17481	Homeobox protein Hox-C8;Homeobox protein Hox-B8	HOXC8;HOXB8
1.16	-1.4	Q9Y5Q0	Fatty acid desaturase 3	FADS3
1.12	-1.4	Q9BYK8	Helicase with zinc finger domain 2	HELZ2
1.85	-1.4	Q9Y6A1	Protein O-mannosyl-transferase 1	POMT1
1.93	-1.5	Q9Y291	28S ribosomal protein S33, mitochondrial	MRPS33
1.26	-1.5	Q9H0F6	Sharpin	SHARPIN
2.38	-1.5	Q03169	Tumor necrosis factor alpha-induced protein 2	TNFAIP2
1.19	-1.5	Q13367	AP-3 complex subunit beta-2	AP3B2
1.22	-1.5	Q4ADV7	RAB6A-GEF complex partner protein 1	RIC1
2.40	-1.5	Q6ZQR2	Uncharacterized protein C9orf171	C9orf171

0.92	-1.6	Q9UBY8	Protein CLN8	CLN8
1.47	-1.6	Q9NQX3	Gephyrin;Molybdopterin adenylyltransferase;Molybdopterin molybdenumtransferase	GPHN
3.17	-1.6	Q2KHT3	Protein CLEC16A	CLEC16A
2.43	-1.6	P51648	Fatty aldehyde dehydrogenase	ALDH3A2
1.45	-1.6	Q86YQ8	Copine-8	CPNE8
4.12	-1.6	Q9BU02	Thiamine-triphosphatase	THTPA
1.46	-1.6	Q86YP4	Transcriptional repressor p66-alpha	GATAD2A
1.40	-1.7	Q9H0Q0	Protein FAM49A	FAM49A
1.28	-1.7	Q13895	Bystin	BYSL
1.16	-1.7	Q9NYB0	Telomeric repeat-binding factor 2-interacting protein 1	TERF2IP
1.30	-1.7	Q8TCF1	AN1-type zinc finger protein 1	ZFAND1
6.47	-1.7	Q9BV57	1,2-dihydroxy-3-keto-5-methylthiopentene dioxygenase	ADI1
1.73	-1.8	P20585	DNA mismatch repair protein Msh3	MSH3
3.66	-1.8	Q9NQZ5	StAR-related lipid transfer protein 7, mitochondrial	STARD7
0.90	-1.8	Q9Y243	RAC-gamma serine/threonine-protein kinase	AKT3
3.24	-1.8	O00625	Pirin	PIR
1.94	-1.8	Q96Q15	Serine/threonine-protein kinase SMG1	SMG1
3.52	-1.9	Q96P16	Regulation of nuclear pre-mRNA domain-containing protein 1A	RPRD1A
1.43	-1.9	Q9HCE5	N6-adenosine-methyltransferase subunit METTL14	METTL14
1.41	-1.9	P34972	Cannabinoid receptor 2	CNR2
3.17	-1.9	P50747	Biotin--protein ligase;Biotin--[methylmalonyl-CoA-carboxytransferase] ligase;Biotin--[propionyl-CoA-carboxylase [ATP-hydrolyzing]] ligase;Biotin--[methylcrotonoyl-CoA-carboxylase] ligase;Biotin--[acetyl-CoA-carboxylase] ligase	HLCS
1.23	-2.0	Q9BSD7	Cancer-related nucleoside-triphosphatase	NTPCR
1.19	-2.0	Q9Y618	Nuclear receptor corepressor 2	NCOR2
1.29	-2.1	O94880	PHD finger protein 14	PHF14
1.84	-2.2	Q969V6	MKL/myocardin-like protein 1	MKL1
1.18	-2.3	Q9BY89	Uncharacterized protein KIAA1671	KIAA1671
2.98	-2.4	Q96SZ6	CDK5 regulatory subunit-associated protein 1	CDK5RAP1
1.31	-2.5	Q9H773	dCTP pyrophosphatase 1	DCTPP1
0.88	-2.5	Q15025	TNFAIP3-interacting protein 1	TNIP1
1.45	-2.5	P98196	Probable phospholipid-transporting ATPase IH	ATP11A
0.99	-2.5	P35916	Vascular endothelial growth factor receptor 3	FLT4
2.76	-2.6	Q09019	Dystrophia myotonica WD repeat-containing protein	DMWD
1.81	-2.6	Q9HCD6	Protein TANC2	TANC2
1.66	-2.6	Q2Y0W8	Electroneutral sodium bicarbonate exchanger 1	SLC4A8
1.76	-2.9	Q12866	Tyrosine-protein kinase Mer	MERTK
2.66	-3.1	Q16787	Laminin subunit alpha-3	LAMA3
3.70	-3.9	P20648	Potassium-transporting ATPase alpha chain 1	ATP4A
2.61	-3.9	O14966	Ras-related protein Rab-7L1	RAB29
2.18	-4.2	Q9Y5F9	Protocadherin gamma-B6	PCDHGB6

Table S 2 List of regulated proteins for the IL-1β *vs* CON comparison for Detroit 551 – 4 h

-Log (P-value)	Difference	Majority protein IDs	Protein names	Gene names
4,49	6.4	P02679	Fibrinogen gamma chain	FGG
4,82	5.0	Q13490	Baculoviral IAP repeat-containing protein 2	BIRC2
4,48	4.4	P26022	Pentraxin-related protein PTX3	PTX3
3,55	4.4	P19876;P19875	C-X-C motif chemokine 3;GRO-gamma(5-73);C-X-C motif chemokine 2;GRO-beta(5-73)	CXCL3;CXCL2
3,79	3.9	P09341	Growth-regulated alpha protein;GRO-alpha(4-73);GRO-alpha(5-73);GRO-alpha(6-73)	CXCL1
3,96	3.2	P31431	Syndecan-4	SDC4
4,96	3.1	P05231	Interleukin-6	IL6
2,49	2.7	P57721	Poly(rC)-binding protein 3	PCBP3
3,45	2.6	Q03169	Tumor necrosis factor alpha-induced protein 2	TNFAIP2
4,60	2.3	P08476	Inhibin beta A chain	INHBA
4,73	2.2	P01584	Interleukin-1 beta	IL1B
3,52	2.1	Q6STE5;Q96GM5	SWI/SNF-related matrix-associated actin-dependent regulator of chromatin subfamily D member 3;SWI/SNF-related matrix-associated actin-dependent regulator of chromatin subfamily D member 1	SMARCD3;SMARCD1
2,49	2.0	Q9GZU8	Protein FAM192A	FAM192A
4,19	1.8	P05362	Intercellular adhesion molecule 1	ICAM1
2,26	1.7	Q16720	Plasma membrane calcium-transporting ATPase 3	ATP2B3
2,27	1.5	Q9UII4	E3 ISG15--protein ligase HERC5	HERC5
2,43	1.4	P00749	Urokinase-type plasminogen activator;Urokinase-type plasminogen activator long chain A;Urokinase-type plasminogen activator short chain A;Urokinase-type plasminogen activator chain B	PLAU
4,91	1.4	Q9UKE5	TRAF2 and NCK-interacting protein kinase	TNIK
2,51	1.4	Q8WWZ4	ATP-binding cassette sub-family A member 10	ABCA10
3,43	1.3	P35354	Prostaglandin G/H synthase 2	PTGS2
3,17	1.2	Q08170	Serine/arginine-rich splicing factor 4	SRSF4
2,48	1.2	Q92543	Sorting nexin-19	SNX19
2,83	1.1	Q9Y3M8	StAR-related lipid transfer protein 13	STARD13
3,05	0.7	Q15043	Zinc transporter ZIP14	SLC39A14
3,22	-0.7	Q92859	Neogenin	NEO1
3,07	-0.7	Q01196	Runt-related transcription factor 1	RUNX1
2,96	-0.8	P41134	DNA-binding protein inhibitor ID-1	ID1
2,83	-1.0	P19883	Follistatin	FST
2,39	-1.3	P29372	DNA-3-methyladenine glycosylase	MPG
3,97	-1.3	Q96SZ6	CDK5 regulatory subunit-associated protein 1	CDK5RAP1
3,01	-1.7	Q6P3X3	Tetratricopeptide repeat protein 27	TTC27
3,57	-1.9	Q9BUR4	Telomerase Cajal body protein 1	WRAP53
2,65	-2.6	Q15653	NF-kappa-B inhibitor beta	NFKBIB

Table S 3 List of regulated proteins for the IL-1β *vs* CON comparison for NHDF – 4 h

-Log (P-value)	Difference	Majority protein IDs	Protein names	Gene names
4,29	5.5	P01584	Interleukin-1 beta	IL1B
4,60	4.3	Q9NR00	Uncharacterized protein C8orf4	C8orf4
3,78	3.8	Q9UQN3	Charged multivesicular body protein 2b	CHMP2B
3,31	3.3	Q13077	TNF receptor-associated factor 1	TRAF1
4,06	2.0	P09341	Growth-regulated alpha protein;GRO-alpha(4-73);GRO-alpha(5-73);GRO-alpha(6-73)	CXCL1
3,23	1.6	P09603	Macrophage colony-stimulating factor 1;Processed macrophage colony-stimulating factor 1	CSF1
3,55	1.5	P05362	Intercellular adhesion molecule 1	ICAM1
3,72	-1.4	Q6EMK4	Vasorin	VASN
2,76	-3.0	P34810	Macrosialin	CD68

Table S 4 List of regulated proteins for the IL-1β *vs* CON comparison for Detroit 551 – WCL – 6 h

-Log (P-value)	Difference	Majority protein IDs	Protein names	Gene names
3,78	4.4	Q9UJJ9	N-acetylglucosamine-1-phosphotransferase subunit gamma	GNPTG
4,98	3.7	P26022	Pentraxin-related protein PTX3	PTX3
4,10	3.0	Q9BXJ4	Complement C1q tumor necrosis factor-related protein 3	C1QTNF3
3,81	2.8	P31431	Syndecan-4	SDC4
4,67	2.8	O94886	CSC1-like protein 1	TMEM63A
5,24	2.6	P30825	High affinity cationic amino acid transporter 1	SLC7A1
4,96	2.3	Q12979	Active breakpoint cluster region-related protein	ABR
4,71	2.1	P19876;P19875	C-X-C motif chemokine 3;GRO-gamma(5-73);C-X-C motif chemokine 2;GRO-beta(5-73)	CXCL3;CXCL2
3,72	-2.9	P18065	Insulin-like growth factor-binding protein 2	IGFBP2
4,28	-3.3	O43150	Arf-GAP with SH3 domain, ANK repeat and PH domain-containing protein 2	ASAP2
3,57	-3.4	Q96 h20	Vacuolar-sorting protein SNF8	SNF8
4,30	-5.7	Q9ULI3	Protein HEG homolog 1	HEG1

Table S 5 List of regulated proteins for the IL-1β *vs* CON comparison for Detroit 551 – WCL – 24 h

-Log (P-value)	Difference	Majority protein IDs	Protein names	Gene names
4.00	4.7	P35354	Prostaglandin G/H synthase 2	PTGS2
3.86	4.4	Q8NEW0	Zinc transporter 7	SLC30A7
3.28	4.3	P49916	DNA ligase 3	LIG3
3.08	4.0	P01024	Complement C3;Complement C3 beta chain;C3-beta-c;Complement C3 alpha chain;C3a anaphylatoxin;Acylation stimulating protein;Complement C3b alpha chain;Complement C3c alpha chain fragment 1;Complement C3dg fragment;Complement C3g fragment;Complement C3d fragment;Complement C3f fragment;Complement C3c alpha chain fragment 2	C3
4.66	3.6	Q00653	Nuclear factor NF-kappa-B p100 subunit;Nuclear factor NF-kappa-B p52 subunit	NFKB2
2.64	3.6	Q9H0U3	Magnesium transporter protein 1	MAGT1
3.03	3.6	P20591	Interferon-induced GTP-binding protein Mx1;Interferon-induced GTP-binding protein Mx1, N-terminally processed	MX1
2.37	3.5	P25774	Cathepsin S	CTSS
2.02	3.4	Q7Z2X4	PTB-containing, cubilin and LRP1-interacting protein	PID1
3.48	3.4	Q5TCZ1	SH3 and PX domain-containing protein 2A	SH3PXD2A
2.56	3.3	O14684	Prostaglandin E synthase	PTGES
4.23	3.3	P21580	Tumor necrosis factor alpha-induced protein 3;A20p50;A20p37	TNFAIP3
2.51	3.2	P05161	Ubiquitin-like protein ISG15	ISG15
3.51	3.0	Q8IW52	SLIT and NTRK-like protein 4	SLITRK4
2.34	3.0	Q03169	Tumor necrosis factor alpha-induced protein 2	TNFAIP2
4.13	2.9	P42830	C-X-C motif chemokine 5;ENA-78(8-78);ENA-78(9-78)	CXCL5
5.08	2.9	Q01201	Transcription factor RelB	RELB
3.05	2.8	P03956	Interstitial collagenase;22 kDa interstitial collagenase;27 kDa interstitial collagenase	MMP1
3.20	2.8	P09341	Growth-regulated alpha protein;GRO-alpha(4-73);GRO-alpha(5-73);GRO-alpha(6-73)	CXCL1
6.88	2.8	Q9C002	Normal mucosa of esophagus-specific gene 1 protein	NMES1
6.04	2.6	P05362	Intercellular adhesion molecule 1	ICAM1
3.71	2.6	Q9UPQ7	E3 ubiquitin-protein ligase PDZRN3	PDZRN3
2.99	2.5	Q24JP5	Transmembrane protein 132A	TMEM132A
3.61	2.3	Q15043	Zinc transporter ZIP14	SLC39A14
3.17	2.2	P19320	Vascular cell adhesion protein 1	VCAM1
3.28	1.9	Q9UBS3	DnaJ homolog subfamily B member 9	DNAJB9
2.52	1.9	Q5VZF2	Muscleblind-like protein 2	MBNL2
2.44	1.9	Q7KYR7	Butyrophilin subfamily 2 member A1	BTN2A1
2.28	1.8	O43353	Receptor-interacting serine/threonine-protein kinase 2	RIPK2
2.88	1.8	P01889	HLA class I histocompatibility antigen, B-7 alpha chain	HLA-B
4.37	1.7	O60488	Long-chain-fatty-acid--CoA ligase 4	ACSL4
3.85	1.7	P35442	Thrombospondin-2	THBS2
3.58	1.7	O95760	Interleukin-33;Interleukin-33 (95-270);Interleukin-33 (99-270);Interleukin-33 (109-270)	IL33
3.45	1.7	O75762	Transient receptor potential cation channel subfamily A member 1	TRPA1
3.15	1.6	Q02388	Collagen alpha-1(VII) chain	COL7A1
2.25	1.6	O94885	SAM and SH3 domain-containing protein 1	SASH1
2.52	1.5	Q9P0J1	[Pyruvate dehydrogenase [acetyl-transferring]]-phosphatase 1, mitochondrial	PDP1
3.47	1.5	P15291	Beta-1,4-galactosyltransferase 1;Lactose synthase A protein;N-acetyllactosamine synthase;Beta-N-acetylglucosaminylglycopeptide beta-1,4-	B4GALT1

			galactosyltransferase;Beta-N-acetylglucosaminyl-glycolipid beta-1,4-galactosyltransferase;Processed beta-1,4-galactosyltransferase 1	
4.43	1.5	P32189;Q14409	Glycerol kinase;Putative glycerol kinase 3	GK;GK3P
2.50	1.4	P05231	Interleukin-6	IL6
5.71	1.4	P43490	Nicotinamide phosphoribosyltransferase	NAMPT
2.55	1.4	O60462	Neuropilin-2	NRP2
3.51	1.4	Q07092	Collagen alpha-1(XVI) chain	COL16A1
2.89	1.3	P27658	Collagen alpha-1(VIII) chain;Vastatin	COL8A1
2.41	1.2	P48723	Heat shock 70 kDa protein 13	HSPA13
3.10	1.2	P08174	Complement decay-accelerating factor	CD55
2.71	1.2	Q9Y4 h2	Insulin receptor substrate 2	IRS2
4.63	1.1	P04179	Superoxide dismutase [Mn], mitochondrial	SOD2
2.58	1.1	Q02297	Pro-neuregulin-1, membrane-bound isoform;Neuregulin-1	NRG1
2.68	1.1	P19838	Nuclear factor NF-kappa-B p105 subunit;Nuclear factor NF-kappa-B p50 subunit	NFKB1
3.58	1.0	Q13219	Pappalysin-1	PAPPA
2.47	1.0	Q8N5I4	Dehydrogenase/reductase SDR family member on chromosome X	DHRSX
3.28	1.0	Q8WUJ3	Cell migration-inducing and hyaluronan-binding protein	CEMIP
3.02	1.0	Q01650	Large neutral amino acids transporter small subunit 1	SLC7A5
4.53	1.0	P02786	Transferrin receptor protein 1;Transferrin receptor protein 1, serum form	TFRC
3.27	0.9	P23458	Tyrosine-protein kinase JAK1	JAK1
3.04	0.9	Q7LBR1	Charged multivesicular body protein 1b	CHMP1B
4.08	0.9	P47712	Cytosolic phospholipase A2;Phospholipase A2;Lysophospholipase	PLA2G4A
3.70	0.9	P17676	CCAAT/enhancer-binding protein beta	CEBPB
3.58	0.8	Q8N556	Actin filament-associated protein 1	AFAP1
2.81	0.8	Q9HD67	Unconventional myosin-X	MYO10
3.65	0.8	P15121	Aldose reductase	AKR1B1
5.06	0.7	P05120	Plasminogen activator inhibitor 2	SERPINB2
3.88	0.7	Q16719	Kynureninase	KYNU
4.10	0.5	Q96K37	Solute carrier family 35 member E1	SLC35E1
3.36	-0.6	P00750	Tissue-type plasminogen activator;Tissue-type plasminogen activator chain A;Tissue-type plasminogen activator chain B	PLAT
5.92	-0.7	P08123	Collagen alpha-2(I) chain	COL1A2
4.11	-0.8	Q8IVN8	Somatomedin-B and thrombospondin type-1 domain-containing protein	SBSPON
4.18	-0.8	P02461	Collagen alpha-1(III) chain	COL3A1
2.79	-0.8	Q96RU3	Formin-binding protein 1	FNBP1
3.06	-0.9	Q9UHD2	Serine/threonine-protein kinase TBK1	TBK1
3.61	-0.9	P23229	Integrin alpha-6;Integrin alpha-6 heavy chain;Integrin alpha-6 light chain;Processed integrin alpha-6	ITGA6
2.82	-0.9	P17936	Insulin-like growth factor-binding protein 3	IGFBP3
2.72	-0.9	O14495	Lipid phosphate phosphohydrolase 3	PPAP2B
3.86	-1.0	P13726	Tissue factor	F3
2.94	-1.0	Q8TDZ2	Protein-methionine sulfoxide oxidase MICAL1	MICAL1
3.92	-1.2	P02452	Collagen alpha-1(I) chain	COL1A1
3.00	-1.3	P18065	Insulin-like growth factor-binding protein 2	IGFBP2
3.18	-1.3	P14210	Hepatocyte growth factor;Hepatocyte growth factor alpha chain;Hepatocyte growth factor beta chain	HGF
2.39	-1.4	O94907	Dickkopf-related protein 1	DKK1
3.46	-1.4	P10398	Serine/threonine-protein kinase A-Raf	ARAF
2.18	-1.7	O75382	Tripartite motif-containing protein 3	TRIM3
3.19	-1.8	Q9UJY4	ADP-ribosylation factor-binding protein GGA2	GGA2
2.90	-1.9	P16234	Platelet-derived growth factor receptor alpha	PDGFRA
3.03	-2.1	Q96MW1	Coiled-coil domain-containing protein 43	CCDC43
2.69	-3.0	Q99836	Myeloid differentiation primary response protein MyD88	MYD88
3.10	-3.0	Q5RI15	Cytochrome c oxidase protein 20 homolog	COX20
3.48	-3.2	P21741	Midkine	MDK
3.44	-3.2	P11310	Medium-chain specific acyl-CoA dehydrogenase, mitochondrial	ACADM
2.45	-3.7	Q92805	Golgin subfamily A member 1	GOLGA1

Table S 6 List of regulated proteins for the IL-1β *vs* CON comparison for Detroit 551 – WCL – 48 h

-Log (P-value)	Difference	Majority protein IDs	Protein names	Gene names
6.63	6.4	P35354	Prostaglandin G/H synthase 2	PTGS2
4.07	4.2	P25774	Cathepsin S	CTSS
3.98	4.1	Q5TCZ1	SH3 and PX domain-containing protein 2A	SH3PXD2A
4.11	3.9	Q8IW52	SLIT and NTRK-like protein 4	SLITRK4
4.52	3.9	Q00653	Nuclear factor NF-kappa-B p100 subunit;Nuclear factor NF-kappa-B p52 subunit	NFKB2
3.71	3.9	P01024	Complement C3;Complement C3 beta chain;C3-beta-c;Complement C3 alpha chain;C3a anaphylatoxin;Acylation stimulating	C3

			protein;Complement C3b alpha chain;Complement C3c alpha chain fragment 1;Complement C3dg fragment;Complement C3g fragment;Complement C3d fragment;Complement C3f fragment;Complement C3c alpha chain fragment 2	
3.39	3.6	P03956	Interstitial collagenase;22 kDa interstitial collagenase;27 kDa interstitial collagenase	MMP1
5.30	3.4	Q9C002	Normal mucosa of esophagus-specific gene 1 protein	NMES1
3.33	3.2	P05231	Interleukin-6	IL6
2.41	3.1	P42830	C-X-C motif chemokine 5;ENA-78(8-78);ENA-78(9-78)	CXCL5
2.52	3.0	A5A3E0;P0CG38	POTE ankyrin domain family member F;POTE ankyrin domain family member I	POTEF;POTEI
3.74	2.9	P09341	Growth-regulated alpha protein;GRO-alpha(4-73);GRO-alpha(5-73);GRO-alpha(6-73)	CXCL1
3.16	2.9	O75762	Transient receptor potential cation channel subfamily A member 1	TRPA1
2.95	2.8	Q01201	Transcription factor RelB	RELB
2.84	2.8	Q24JP5	Transmembrane protein 132A	TMEM132A
2.40	2.8	Q8NBZ7	UDP-glucuronic acid decarboxylase 1	UXS1
2.17	2.7	P08254	Stromelysin-1	MMP3
2.43	2.6	Q7Z2X4	PTB-containing, cubilin and LRP1-interacting protein	PID1
3.09	2.6	P21580	Tumor necrosis factor alpha-induced protein 3;A20p50;A20p37	TNFAIP3
3.34	2.6	Q9H7R5	Zinc finger protein 665	ZNF665
1.81	2.5	Q13015	Protein AF1q	MLLT11
2.50	2.5	O95470	Sphingosine-1-phosphate lyase 1	SGPL1
1.75	2.4	Q9H8H3	Methyltransferase-like protein 7A	METTL7A
2.60	2.3	P18510	Interleukin-1 receptor antagonist protein	IL1RN
3.56	2.2	O43353	Receptor-interacting serine/threonine-protein kinase 2	RIPK2
2.77	2.2	Q92478	C-type lectin domain family 2 member B	CLEC2B
4.02	2.1	Q01432	AMP deaminase 3	AMPD3
3.43	2.1	P19876;P19875	C-X-C motif chemokine 3;GRO-gamma(5-73);C-X-C motif chemokine 2;GRO-beta(5-73)	CXCL3;CXCL2
1.86	2.1	Q7L5N7	Lysophosphatidylcholine acyltransferase 2	LPCAT2
3.04	2.1	Q07092	Collagen alpha-1(XVI) chain	COL16A1
2.40	2.1	P05161	Ubiquitin-like protein ISG15	ISG15
2.14	2.1	Q9P121	Neurotrimin	NTM
2.47	2.0	P08572	Collagen alpha-2(IV) chain;Canstatin	COL4A2
4.44	1.9	P05362	Intercellular adhesion molecule 1	ICAM1
1.72	1.9	Q9NP84	Tumor necrosis factor receptor superfamily member 12A	TNFRSF12A
5.38	1.9	O60488	Long-chain-fatty-acid--CoA ligase 4	ACSL4
1.93	1.9	Q11201	CMP-N-acetylneuraminate-beta-galactosamide-alpha-2,3-sialyltransferase 1	ST3GAL1
3.39	1.9	Q7KYR7	Butyrophilin subfamily 2 member A1	BTN2A1
5.28	1.9	P32189;Q14409	Glycerol kinase;Putative glycerol kinase 3	GK;GK3P
3.41	1.9	Q15043	Zinc transporter ZIP14	SLC39A14
2.62	1.9	Q96CN7	Isochorismatase domain-containing protein 1	ISOC1
2.32	1.8	P53814	Smoothelin	SMTN
6.31	1.8	P43490	Nicotinamide phosphoribosyltransferase	NAMPT
5.37	1.7	Q9UBS3	DnaJ homolog subfamily B member 9	DNAJB9
4.58	1.7	P01889	HLA class I histocompatibility antigen, B-7 alpha chain	HLA-B
5.87	1.7	P04179	Superoxide dismutase [Mn], mitochondrial	SOD2
3.39	1.6	Q9UPQ7	E3 ubiquitin-protein ligase PDZRN3	PDZRN3
2.22	1.5	P80297	Metallothionein-1X	MT1X
4.83	1.4	P27658	Collagen alpha-1(VIII) chain;Vastatin	COL8A1
3.10	1.4	P42229	Signal transducer and activator of transcription 5A	STAT5A
2.02	1.4	Q8WYL5	Protein phosphatase Slingshot homolog 1	SSH1
3.01	1.4	P02795	Metallothionein-2	MT2A
2.63	1.4	Q96AD5	Patatin-like phospholipase domain-containing protein 2	PNPLA2
2.70	1.4	P09038	Fibroblast growth factor 2	FGF2
2.29	1.3	Q96KC8	DnaJ homolog subfamily C member 1	DNAJC1
1.96	1.3	Q9GZT9	Egl nine homolog 1	EGLN1
2.47	1.3	Q8NHQ8	Ras association domain-containing protein 8	RASSF8
1.83	1.3	Q16790	Carbonic anhydrase 9	CA9
3.50	1.3	P47712	Cytosolic phospholipase A2;Phospholipase A2;Lysophospholipase	PLA2G4A
2.23	1.3	Q13438	Protein OS-9	OS9
3.53	1.2	Q96MX6	WD repeat-containing protein 92	WDR92
1.88	1.2	Q02297	Pro-neuregulin-1, membrane-bound isoform;Neuregulin-1	NRG1
2.66	1.1	P33121	Long-chain-fatty-acid--CoA ligase 1	ACSL1
3.89	1.1	P35442	Thrombospondin-2	THBS2
3.78	1.1	P43235	Cathepsin K	CTSK
2.26	1.1	O95786	Probable ATP-dependent RNA helicase DDX58	DDX58
3.60	1.1	Q96NE9	FERM domain-containing protein 6	FRMD6

2.49	1.0	Q15633	RISC-loading complex subunit TARBP2	TARBP2
2.34	1.0	P04732	Metallothionein-1E	MT1E
4.05	1.0	Q9UPU9	Protein Smaug homolog 1	SAMD4A
2.41	1.0	Q96RD7	Pannexin-1	PANX1
3.74	1.0	P19838	Nuclear factor NF-kappa-B p105 subunit;Nuclear factor NF-kappa-B p50 subunit	NFKB1
3.82	1.0	P98155	Very low-density lipoprotein receptor	VLDLR
3.36	1.0	Q9HC07	Transmembrane protein 165	TMEM165
2.87	1.0	P52823	Stanniocalcin-1	STC1
2.04	1.0	P0DPI2		
2.03	1.0	P02462	Collagen alpha-1(IV) chain;Arresten	COL4A1
3.25	1.0	P05121	Plasminogen activator inhibitor 1	SERPINE1
2.65	0.9	P05120	Plasminogen activator inhibitor 2	SERPINB2
3.10	0.9	P05412	Transcription factor AP-1	JUN
4.04	0.9	Q9Y6N7	Roundabout homolog 1	ROBO1
3.98	0.9	P02786	Transferrin receptor protein 1;Transferrin receptor protein 1, serum form	TFRC
2.36	0.8	P00533	Epidermal growth factor receptor	EGFR
3.43	0.8	P43304	Glycerol-3-phosphate dehydrogenase, mitochondrial	GPD2
3.79	0.8	P08174	Complement decay-accelerating factor	CD55
2.95	0.8	Q7LBR1	Charged multivesicular body protein 1b	CHMP1B
4.35	0.8	P20020	Plasma membrane calcium-transporting ATPase 1	ATP2B1
4.41	0.8	O60462	Neuropilin-2	NRP2
2.21	0.8	O94808	Glutamine--fructose-6-phosphate aminotransferase [isomerizing] 2	GFPT2
3.34	0.8	Q9Y2H6	Fibronectin type-III domain-containing protein 3A	FNDC3A
2.47	0.8	Q8WZA9	Immunity-related GTPase family Q protein	IRGQ
3.76	0.8	Q13217	DnaJ homolog subfamily C member 3	DNAJC3
3.83	0.8	Q16719	Kynureninase	KYNU
3.05	0.7	P15121	Aldose reductase	AKR1B1
2.45	0.7	Q01650	Large neutral amino acids transporter small subunit 1	SLC7A5
2.73	0.7	P51116	Fragile X mental retardation syndrome-related protein 2	FXR2
3.29	0.7	P51153	Ras-related protein Rab-13	RAB13
2.94	0.7	P02794	Ferritin heavy chain;Ferritin heavy chain, N-terminally processed	FTH1
4.44	0.7	Q9NW68	BSD domain-containing protein 1	BSDC1
2.91	0.7	Q96EC8	Protein YIPF6	YIPF6
2.89	0.7	Q96DZ1	Endoplasmic reticulum lectin 1	ERLEC1
2.58	0.7	O00300	Tumor necrosis factor receptor superfamily member 11B	TNFRSF11B
2.77	0.6	Q5SWX8	Protein odr-4 homolog	ODR4
3.08	0.6	Q6PIU2	Neutral cholesterol ester hydrolase 1	NCEH1
3.21	0.6	Q8NC42	E3 ubiquitin-protein ligase RNF149	RNF149
2.57	0.6	Q86XL3	Ankyrin repeat and LEM domain-containing protein 2	ANKLE2
3.41	0.6	Q02952	A-kinase anchor protein 12	AKAP12
3.10	0.6	O15344	E3 ubiquitin-protein ligase Midline-1	MID1
3.33	0.6	Q9UBY9	Heat shock protein beta-7	HSPB7
2.75	0.6	Q99470	Stromal cell-derived factor 2	SDF2
2.75	0.6	O00391	Sulfhydryl oxidase 1	QSOX1
2.84	0.6	P48449	Lanosterol synthase	LSS
4.16	0.6	P08195	4F2 cell-surface antigen heavy chain	SLC3A2
3.29	0.6	P04439	HLA class I histocompatibility antigen, A-3 alpha chain	HLA-A
3.07	0.5	Q03405	Urokinase plasminogen activator surface receptor	PLAUR
3.87	0.5	Q9Y4L1	Hypoxia up-regulated protein 1	HYOU1
3.76	0.5	Q96KG9	N-terminal kinase-like protein	SCYL1
2.99	0.5	Q96 hD1	Cysteine-rich with EGF-like domain protein 1	CRELD1
5.12	0.5	O00469	Procollagen-lysine,2-oxoglutarate 5-dioxygenase 2	PLOD2
3.85	0.5	P55145	Mesencephalic astrocyte-derived neurotrophic factor	MANF
3.01	0.5	Q14195	Dihydropyrimidinase-related protein 3	DPYSL3
3.18	0.5	P10321	HLA class I histocompatibility antigen, Cw-7 alpha chain	HLA-C
3.94	0.5	Q9HD26	Golgi-associated PDZ and coiled-coil motif-containing protein	GOPC
3.59	0.4	P13667	Protein disulfide-isomerase A4	PDIA4
3.37	0.4	P84098	60S ribosomal protein L19	RPL19
3.63	0.4	Q9NWM8	Peptidyl-prolyl cis-trans isomerase FKBP14	FKBP14
3.56	0.4	P11021	78 kDa glucose-regulated protein	HSPA5
4.13	-0.4	P48681	Nestin	NES
4.40	-0.4	P98082	Disabled homolog 2	DAB2
4.65	-0.5	Q9HCJ6	Synaptic vesicle membrane protein VAT-1 homolog-like	VAT1L
3.16	-0.5	Q4L180	Filamin A-interacting protein 1-like	FILIP1L
3.01	-0.5	P98095	Fibulin-2	FBLN2
4.39	-0.5	Q96TA1	Niban-like protein 1	FAM129B
4.59	-0.5	P05783	Keratin, type I cytoskeletal 18	KRT18
3.50	-0.5	P49023	Paxillin	PXN
3.34	-0.5	Q13425	Beta-2-syntrophin	SNTB2

3.71	-0.6	P27105	Erythrocyte band 7 integral membrane protein	STOM
2.84	-0.6	P24593	Insulin-like growth factor-binding protein 5	IGFBP5
3.20	-0.6	P01137	Transforming growth factor beta-1;Latency-associated peptide	TGFB1
2.68	-0.6	Q9H9H4	Vacuolar protein sorting-associated protein 37B	VPS37B
4.31	-0.6	Q3SY69	Mitochondrial 10-formyltetrahydrofolate dehydrogenase	ALDH1L2
2.99	-0.6	Q6DKJ4	Nucleoredoxin	NXN
5.36	-0.6	Q09666	Neuroblast differentiation-associated protein AHNAK	AHNAK
2.53	-0.6	P16401	Histone H1.5	HIST1H1B
2.96	-0.7	Q9H4X1	Regulator of cell cycle RGCC	RGCC
2.43	-0.7	P21926	CD9 antigen	CD9
3.20	-0.7	O14558	Heat shock protein beta-6	HSPB6
4.42	-0.7	Q15758	Neutral amino acid transporter B(0)	SLC1A5
2.60	-0.7	Q5JPI3	Uncharacterized protein C3orf38	C3orf38
3.53	-0.7	Q8TED1	Probable glutathione peroxidase 8	GPX8
2.48	-0.7	O75084;Q14332	Frizzled-7;Frizzled-2	FZD7;FZD2
2.28	-0.7	P11388	DNA topoisomerase 2-alpha	TOP2A
3.30	-0.7	P04216	Thy-1 membrane glycoprotein	THY1
2.67	-0.7	Q8NFJ5	Retinoic acid-induced protein 3	GPRC5A
2.51	-0.7	P29373	Cellular retinoic acid-binding protein 2	CRABP2
3.89	-0.7	Q8N3V7	Synaptopodin	SYNPO
2.62	-0.7	Q53H82	Beta-lactamase-like protein 2	LACTB2
2.97	-0.8	O43310	CBP80/20-dependent translation initiation factor	CTIF
3.28	-0.8	P08123	Collagen alpha-2(I) chain	COL1A2
4.94	-0.8	Q8NDI1	EH domain-binding protein 1	EHBP1
2.24	-0.8	Q9BRK3	Matrix-remodeling-associated protein 8	MXRA8
3.23	-0.8	Q68CZ2	Tensin-3	TNS3
4.32	-0.8	Q9HCU0	Endosialin	CD248
4.35	-0.8	Q6UVK1	Chondroitin sulfate proteoglycan 4	CSPG4
3.88	-0.8	Q9NUQ6	SPATS2-like protein	SPATS2L
5.34	-0.8	Q14126	Desmoglein-2	DSG2
3.18	-0.8	Q16678	Cytochrome P450 1B1	CYP1B1
3.56	-0.8	P02461	Collagen alpha-1(III) chain	COL3A1
4.05	-0.9	P09619	Platelet-derived growth factor receptor beta	PDGFRB
2.91	-0.9	Q7Z4I7	LIM and senescent cell antigen-like-containing domain protein 2	LIMS2
2.15	-0.9	Q8IWU6	Extracellular sulfatase Sulf-1	SULF1
2.54	-0.9	Q15024	Exosome complex component RRP42	EXOSC7
2.38	-0.9	Q9P2K8	Eukaryotic translation initiation factor 2-alpha kinase 4	EIF2AK4
2.24	-0.9	P52735	Guanine nucleotide exchange factor VAV2	VAV2
3.27	-0.9	Q6EMK4	Vasorin	VASN
2.75	-0.9	Q6UWE0	E3 ubiquitin-protein ligase LRSAM1	LRSAM1
2.91	-0.9	P35520	Cystathionine beta-synthase	CBS
5.42	-1.0	P20908	Collagen alpha-1(V) chain	COL5A1
2.04	-1.0	P27216	Annexin A13	ANXA13
2.01	-1.0	Q9Y606	tRNA pseudouridine synthase A, mitochondrial	PUS1
2.87	-1.0	Q6XZF7	Dynamin-binding protein	DNMBP
1.96	-1.0	Q15847	Adipogenesis regulatory factor	ADIRF
2.34	-1.0	Q16666	Gamma-interferon-inducible protein 16	IFI16
3.43	-1.0	Q76M96	Coiled-coil domain-containing protein 80	CCDC80
2.39	-1.1	P31431	Syndecan-4	SDC4
1.91	-1.1	Q66K79	Carboxypeptidase Z	CPZ
2.71	-1.1	Q9Y625	Glypican-6;Secreted glypican-6	GPC6
3.15	-1.1	Q9UKX5	Integrin alpha-11	ITGA11
2.24	-1.2	Q15036	Sorting nexin-17	SNX17
2.76	-1.2	Q96PE1	G-protein coupled receptor 124	GPR124
3.01	-1.2	P35052	Glypican-1;Secreted glypican-1	GPC1
1.91	-1.2	O15119	T-box transcription factor TBX3	TBX3
3.32	-1.3	P13726	Tissue factor	F3
2.57	-1.3	O76074	cGMP-specific 3,5-cyclic phosphodiesterase	PDE5A
4.74	-1.3	Q9UKU9	Angiopoietin-related protein 2	ANGPTL2
2.04	-1.4	Q9BXR0	Queuine tRNA-ribosyltransferase	QTRT1
2.40	-1.4	Q9Y6K8	Adenylate kinase isoenzyme 5	AK5
1.92	-1.4	Q99988	Growth/differentiation factor 15	GDF15
2.08	-1.4	Q9BYX2	TBC1 domain family member 2A	TBC1D2
2.81	-1.5	Q01628;Q01629;P13164	Interferon-induced transmembrane protein 3;Interferon-induced transmembrane protein 2;Interferon-induced transmembrane protein 1	IFITM3;IFITM2;IFITM1
1.92	-1.6	O95084	Serine protease 23	PRSS23
2.87	-1.6	P17936	Insulin-like growth factor-binding protein 3	IGFBP3
2.65	-1.6	Q13137	Calcium-binding and coiled-coil domain-containing protein 2	CALCOCO2
1.73	-1.6	Q9UKG9	Peroxisomal carnitine O-octanoyltransferase	CROT

3.23	-1.6	P14210	Hepatocyte growth factor;Hepatocyte growth factor alpha chain;Hepatocyte growth factor beta chain	HGF
4.76	-1.7	P02452	Collagen alpha-1(I) chain	COL1A1
1.86	-1.7	Q8WW01	tRNA-splicing endonuclease subunit Sen15	TSEN15
3.30	-1.7	Q4LDE5	Sushi, von Willebrand factor type A, EGF and pentraxin domain-containing protein 1	SVEP1
2.33	-1.8	Q9NX14	NADH dehydrogenase [ubiquinone] 1 beta subcomplex subunit 11, mitochondrial	NDUFB11
2.62	-1.8	P49736	DNA replication licensing factor MCM2	MCM2
1.92	-1.8	Q9H000	Probable E3 ubiquitin-protein ligase makorin-2	MKRN2
2.11	-1.8	O94907	Dickkopf-related protein 1	DKK1
2.73	-1.8	Q15113	Procollagen C-endopeptidase enhancer 1	PCOLCE
2.67	-1.9	P43007	Neutral amino acid transporter A	SLC1A4
1.89	-1.9	O14908	PDZ domain-containing protein GIPC1	GIPC1
3.84	-1.9	Q9UKI2	Cdc42 effector protein 3	CDC42EP3
1.97	-2.0	Q8IZV5	Retinol dehydrogenase 10	RDH10
2.34	-2.0	Q9H788	SH2 domain-containing protein 4A	SH2D4A
1.78	-2.1	Q9BZF9	Uveal autoantigen with coiled-coil domains and ankyrin repeats	UACA
2.28	-2.2	Q9H3M7	Thioredoxin-interacting protein	TXNIP
1.91	-2.2	P21246	Pleiotrophin	PTN
2.58	-2.3	P16402;P10412	Histone H1.3;Histone H1.4	HIST1H1D;HIST1H1E
2.00	-2.5	Q96RR4	Calcium/calmodulin-dependent protein kinase kinase 2	CAMKK2
3.69	-2.6	O14495	Lipid phosphate phosphohydrolase 3	PPAP2B
3.06	-2.9	P40189	Interleukin-6 receptor subunit beta	IL6ST
2.18	-3.1	Q53EL6	Programmed cell death protein 4	PDCD4
2.69	-3.1	P47895	Aldehyde dehydrogenase family 1 member A3	ALDH1A3
3.67	-3.2	P16234	Platelet-derived growth factor receptor alpha	PDGFRA
3.12	-3.6	P21741	Midkine	MDK
2.95	-3.7	Q05707	Collagen alpha-1(XIV) chain	COL14A1
4.47	-4.1	Q99836	Myeloid differentiation primary response protein MyD88	MYD88

Table S 7 List of regulated proteins for the IL-1β *vs* CON comparison for Detroit 551 – SN – 6 h

-Log (P-value)	Difference	Majority protein IDs	Protein names	Gene names
2.72	9.2	P09341	Growth-regulated alpha protein;GRO-alpha(4-73);GRO-alpha(5-73);GRO-alpha(6-73)	CXCL1
5.25	8.1	P26022	Pentraxin-related protein PTX3	PTX3
4.24	8.0	P19876	C-X-C motif chemokine 3;GRO-gamma(5-73)	CXCL3
4.31	6.8	P05231	Interleukin-6	IL6
3.36	6.8	P10145	Interleukin-8;MDNCF-a;Interleukin-8;IL-8(5-77);IL-8(6-77);IL-8(7-77);IL-8(8-77);IL-8(9-77)	CXCL8
3.43	6.1	P13500	C-C motif chemokine 2	CCL2
3.25	6.1	P15018	Leukemia inhibitory factor	LIF
3.78	5.4	P09603	Macrophage colony-stimulating factor 1;Processed macrophage colony-stimulating factor 1	CSF1
2.45	4.8	P08476	Inhibin beta A chain	INHBA
2.40	3.5	P42830	C-X-C motif chemokine 5;ENA-78(8-78);ENA-78(9-78)	CXCL5
3.09	3.0	P31431	Syndecan-4	SDC4
2.94	2.9	P09919	Granulocyte colony-stimulating factor	CSF3
2.54	1.9	P17050	Alpha-N-acetylgalactosaminidase	NAGA
3.18	-1.4	P07195	L-lactate dehydrogenase B chain	LDHB
2.61	-1.9	P13473	Lysosome-associated membrane glycoprotein 2	LAMP2
2.47	-1.9	O95394	Phosphoacetylglucosamine mutase	PGM3
2.67	-2.1	P12107	Collagen alpha-1(XI) chain	COL11A1
3.05	-2.3	Q9NY33	Dipeptidyl peptidase 3	DPP3
2.82	-2.4	Q9UHI8	A disintegrin and metalloproteinase with thrombospondin motifs 1	ADAMTS1
2.43	-2.5	P08238	Heat shock protein HSP 90-beta	HSP90AB1
2.58	-2.7	O75223	Gamma-glutamylcyclotransferase	GGCT
3.41	-2.7	Q9ULV4	Coronin-1C	CORO1C
2.61	-2.9	P02792	Ferritin light chain	FTL
2.59	-3.2	P50395	Rab GDP dissociation inhibitor beta	GDI2
3.12	-3.8	Q8NDC0	MAPK-interacting and spindle-stabilizing protein-like	MAPK1IP1L
4.05	-4.3	P31150	Rab GDP dissociation inhibitor alpha	GDI1

Table S 8 List of regulated proteins for the IL-1β *vs* CON comparison for Detroit 551 – SN – 24 h

-Log (P-value)	Difference	Majority protein IDs	Protein names	Gene names
4.45	9.5	P09341	Growth-regulated alpha protein;GRO-alpha(4-73);GRO-alpha(5-73);GRO-alpha(6-73)	CXCL1
4.92	8.2	P05231	Interleukin-6	IL6

Table S 9 List of regulated proteins for the IL-1β *vs* CON comparison for Detroit 551 – SN – 48 h

-Log(P-value)	Difference	Majority protein IDs	Protein names	Gene names
3.76	8.1	P42830	C-X-C motif chemokine 5;ENA-78(8-78);ENA-78(9-78)	CXCL5
3.54	7.1	P05231	Interleukin-6	IL6
3.62	6.8	P09341	Growth-regulated alpha protein;GRO-alpha(4-73);GRO-alpha(5-73);GRO-alpha(6-73)	CXCL1
3.05	6.4	P15018	Leukemia inhibitory factor	LIF
3.63	6.3	P10145	Interleukin-8;MDNCF-a;Interleukin-8;IL-8(5-77);IL-8(6-77);IL-8(7-77);IL-8(8-77);IL-8(9-77)	CXCL8
2.80	5.1	P13500	C-C motif chemokine 2	CCL2
2.93	5.1	P08254	Stromelysin-1	MMP3
2.98	5.1	P19876	C-X-C motif chemokine 3;GRO-gamma(5-73)	CXCL3
3.79	-2.0	P08123	Collagen alpha-2(I) chain	COL1A2
2.98	-2.4	P49788	Retinoic acid receptor responder protein 1	RARRES1
4.50	-2.5	P02452	Collagen alpha-1(I) chain	COL1A1
3.20	-3.2	Q9NRR1	Cytokine-like protein 1	CYTL1
3.27	-3.9	P12107	Collagen alpha-1(XI) chain	COL11A1
3.91	-3.9	O95965	Integrin beta-like protein 1	ITGBL1
2.79	-4.3	P80511	Protein S100-A12;Calcitermin	S100A12
3.43	-5.8	P16278	Beta-galactosidase	GLB1

Table S 10 List of regulated proteins for the TBHP + IL-1β *vs* IL-1β comparison for Detroit 551 – WCL – 48 h

-Log (P-value)	Difference	Majority protein IDs	Protein names	Gene names
2.41	5.2	P49754	Vacuolar protein sorting-associated protein 41 homolog	VPS41
3.80	4.1	Q9BTC0	Death-inducer obliterator 1	DIDO1
2.19	4.0	P09914	Interferon-induced protein with tetratricopeptide repeats 1	IFIT1
2.89	3.9	P19883	Follistatin	FST
3.47	3.7	Q6T4R5	Nance-Horan syndrome protein	NHS
3.10	3.3	O14949	Cytochrome b-c1 complex subunit 8	UQCRQ
2.22	2.8	Q05481	Zinc finger protein 91	ZNF91
1.99	2.7	P00749	Urokinase-type plasminogen activator;Urokinase-type plasminogen activator long chain A;Urokinase-type plasminogen activator short chain A;Urokinase-type plasminogen activator chain B	PLAU
2.84	2.4	Q9NNW5	WD repeat-containing protein 6	WDR6
2.17	2.4	P23508	Colorectal mutant cancer protein	MCC
3.04	2.4	Q9BQ39	ATP-dependent RNA helicase DDX50	DDX50
3.23	2.3	Q9H2V7	Protein spinster homolog 1	SPNS1
3.00	2.3	Q8TBX8	Phosphatidylinositol 5-phosphate 4-kinase type-2 gamma	PIP4K2C
2.49	2.3	Q7Z5L7	Podocan	PODN
3.55	2.3	Q92934	Bcl2-associated agonist of cell death	BAD
2.68	2.2	Q9NQ66	1-phosphatidylinositol 4,5-bisphosphate phosphodiesterase beta-1	PLCB1
3.52	2.2	Q9NX14	NADH dehydrogenase [ubiquinone] 1 beta subcomplex subunit 11, mitochondrial	NDUFB11
2.44	2.1	O43896	Kinesin-like protein KIF1C	KIF1C
2.19	2.1	O60739	Eukaryotic translation initiation factor 1b	EIF1B
2.57	2.0	Q9NRG1	Phosphoribosyltransferase domain-containing protein 1	PRTFDC1
2.69	1.9	Q99836	Myeloid differentiation primary response protein MyD88	MYD88
2.42	1.9	Q969N2	GPI transamidase component PIG-T	PIGT
2.76	1.9	P62310	U6 snRNA-associated Sm-like protein LSm3	LSM3
3.29	1.8	Q96C86	m7GpppX diphosphatase	DCPS
2.45	1.8	Q96DE0	U8 snoRNA-decapping enzyme	NUDT16
2.23	1.8	P86791;P86790	Vacuolar fusion protein CCZ1 homolog;Vacuolar fusion protein CCZ1 homolog B	CCZ1;CCZ1B
2.21	1.7	Q7L0Y3	Mitochondrial ribonuclease P protein 1	TRMT10C
2.24	1.7	Q9HCC0	Methylcrotonoyl-CoA carboxylase beta chain, mitochondrial	MCCC2
2.30	1.7	O60476	Mannosyl-oligosaccharide 1,2-alpha-mannosidase IB	MAN1A2
2.26	1.6	P26440	Isovaleryl-CoA dehydrogenase, mitochondrial	IVD
2.10	1.5	Q12946;Q12947	Forkhead box protein F1;Forkhead box protein F2	FOXF1;FOXF2
2.20	1.5	Q92982	Ninjurin-1	NINJ1
2.78	1.4	Q8WUX9	Charged multivesicular body protein 7	CHMP7

3.34	1.4	Q9BXR0	Queuine tRNA-ribosyltransferase	QTRT1
2.44	1.4	Q9H9Q4	Non-homologous end-joining factor 1	NHEJ1
2.58	1.4	Q96CN9	GRIP and coiled-coil domain-containing protein 1	GCC1
2.92	1.3	O75880	Protein SCO1 homolog, mitochondrial	SCO1
3.62	1.3	Q8NFD5	AT-rich interactive domain-containing protein 1B	ARID1B
2.28	1.3	P82930	28S ribosomal protein S34, mitochondrial	MRPS34
2.78	1.3	Q15389	Angiopoietin-1	ANGPT1
2.66	1.3	P27216	Annexin A13	ANXA13
2.96	1.2	P57764	Gasdermin-D	GSDMD
2.73	1.2	P03956	Interstitial collagenase;22 kDa interstitial collagenase;27 kDa interstitial collagenase	MMP1
2.27	1.2	Q9BX40	Protein LSM14 homolog B	LSM14B
2.38	1.2	Q9NP81	Serine--tRNA ligase, mitochondrial	SARS2
2.43	1.2	Q9BYD1	39S ribosomal protein L13, mitochondrial	MRPL13
2.27	1.2	Q96I15	Selenocysteine lyase	SCLY
2.41	1.1	Q96ND0	Protein FAM210A	FAM210A
2.56	1.1	Q9BPW8	Protein NipSnap homolog 1	NIPSNAP1
2.90	1.1	Q9ULJ3	Zinc finger and BTB domain-containing protein 21	ZBTB21
2.62	1.1	Q9UQB8	Brain-specific angiogenesis inhibitor 1-associated protein 2	BAIAP2
2.69	1.1	O75179	Ankyrin repeat domain-containing protein 17	ANKRD17
2.32	1.0	Q9BYN0	Sulfiredoxin-1	SRXN1
2.54	1.0	Q96EY7	Pentatricopeptide repeat domain-containing protein 3, mitochondrial	PTCD3
2.58	1.0	P56134	ATP synthase subunit f, mitochondrial	ATP5J2
2.58	1.0	Q9BTZ2	Dehydrogenase/reductase SDR family member 4	DHRS4
2.59	0.9	Q08623	Pseudouridine-5-phosphatase	HDHD1
2.53	0.9	Q5T6V5	UPF0553 protein C9orf64	C9orf64
2.46	0.9	Q86TU7	Histone-lysine N-methyltransferase setd3	SETD3
2.63	0.9	Q8N183	Mimitin, mitochondrial	NDUFAF2
3.66	0.8	P08579	U2 small nuclear ribonucleoprotein B	SNRPB2
2.66	0.8	Q8WU76	Sec1 family domain-containing protein 2	SCFD2
2.69	0.8	P19876;P19875	C-X-C motif chemokine 3;GRO-gamma(5-73);C-X-C motif chemokine 2;GRO-beta(5-73)	CXCL3;CXCL2
3.36	0.7	Q00169	Phosphatidylinositol transfer protein alpha isoform	PITPNA
2.95	0.7	Q6EMK4	Vasorin	VASN
2.93	0.7	Q9UJS0	Calcium-binding mitochondrial carrier protein Aralar2	SLC25A13
3.22	0.7	P48723	Heat shock 70 kDa protein 13	HSPA13
3.02	0.7	O75762	Transient receptor potential cation channel subfamily A member 1	TRPA1
3.50	0.7	P23786	Carnitine O-palmitoyltransferase 2, mitochondrial	CPT2
3.39	0.7	Q9H9H4	Vacuolar protein sorting-associated protein 37B	VPS37B
3.46	0.6	P50148	Guanine nucleotide-binding protein G(q) subunit alpha	GNAQ
3.32	0.6	Q9UIJ7	GTP:AMP phosphotransferase AK3, mitochondrial	AK3
4.00	0.5	P33897	ATP-binding cassette sub-family D member 1	ABCD1
4.05	0.5	P35232	Prohibitin	PHB
3.23	-0.7	O95218	Zinc finger Ran-binding domain-containing protein 2	ZRANB2
2.76	-0.9	Q15836	Vesicle-associated membrane protein 3	VAMP3
2.48	-0.9	Q16513	Serine/threonine-protein kinase N2	PKN2
5.06	-0.9	Q9Y3E1	Hepatoma-derived growth factor-related protein 3	HDGFRP3
2.75	-0.9	Q3SYG4	Protein PTHB1	BBS9
2.59	-0.9	O15127	Secretory carrier-associated membrane protein 2	SCAMP2
3.41	-1.0	Q14126	Desmoglein-2	DSG2
2.20	-1.2	Q7Z3G6	Prickle-like protein 2	PRICKLE2
3.59	-1.3	Q16790	Carbonic anhydrase 9	CA9
2.25	-1.5	O43292	Glycosylphosphatidylinositol anchor attachment 1 protein	GPAA1
2.59	-1.8	Q8N128	Protein FAM177A1	FAM177A1
4.43	-1.8	P31431	Syndecan-4	SDC4
2.07	-1.9	Q9BXT2	Voltage-dependent calcium channel gamma-6 subunit	CACNG6
3.44	-2.1	Q9BUN8	Derlin-1	DERL1
2.07	-2.2	P19320	Vascular cell adhesion protein 1	VCAM1
2.55	-3.0	P23434	Glycine cleavage system H protein, mitochondrial	GCSH
1.91	-3.2	Q969M3	Protein YIPF5	YIPF5

Table S 11 List of regulated proteins for the TBHP + IL-1β *vs* IL-1β comparison for Detroit 551 – SN – 6 h

-Log (P-value)	Difference	Majority protein IDs	Protein names	Gene names
4.17	-4.8	P02458	Collagen alpha-1(II) chain;Collagen alpha-1(II) chain;Chondrocalcin	COL2A1

Table S 12 Collagen and collagen-associated proteins - WCL

Majority protein IDs	Gene names	Protein names	Time-point	Comparison	log2FC direction	Significant
P12107	COL11A1	Collagen alpha-1(XI) chain	6 h	IL-1b vs CON	up	
Q99715	COL12A1	Collagen alpha-1(XII) chain	6 h	IL-1b vs CON	up	
Q05707	COL14A1	Collagen alpha-1(XIV) chain	6 h	IL-1b vs CON	down	
Q07092	COL16A1	Collagen alpha-1(XVI) chain	6 h	IL-1b vs CON	up	
P39060	COL18A1	Collagen alpha-1(XVIII) chain;Endostatin	6 h	IL-1b vs CON	up	
P02452	COL1A1	Collagen alpha-1(I) chain	6 h	IL-1b vs CON	down	
P08123	COL1A2	Collagen alpha-2(I) chain	6 h	IL-1b vs CON	down	
P02461	COL3A1	Collagen alpha-1(III) chain	6 h	IL-1b vs CON	down	
P02462	COL4A1	Collagen alpha-1(IV) chain;Arresten	6 h	IL-1b vs CON	up	
P08572	COL4A2	Collagen alpha-2(IV) chain;Canstatin	6 h	IL-1b vs CON	down	
Q9Y5P4	COL4A3BP	Collagen type IV alpha-3-binding protein	6 h	IL-1b vs CON	up	
P20908	COL5A1	Collagen alpha-1(V) chain	6 h	IL-1b vs CON	down	
P05997	COL5A2	Collagen alpha-2(V) chain	6 h	IL-1b vs CON	up	
P25940	COL5A3	Collagen alpha-3(V) chain	6 h	IL-1b vs CON	down	
P12109	COL6A1	Collagen alpha-1(VI) chain	6 h	IL-1b vs CON	up	
P12110	COL6A2	Collagen alpha-2(VI) chain	6 h	IL-1b vs CON	down	
P12111	COL6A3	Collagen alpha-3(VI) chain	6 h	IL-1b vs CON	down	
Q02388	COL7A1	Collagen alpha-1(VII) chain	6 h	IL-1b vs CON	down	
P27658	COL8A1	Collagen alpha-1(VIII) chain;Vastatin	6 h	IL-1b vs CON	up	
Q8NBJ5	COLGALT1	Procollagen galactosyltransferase 1	6 h	IL-1b vs CON	up	
Q96CG8	CTHRC1	Collagen triple helix repeat-containing protein 1	6 h	IL-1b vs CON	down	
P03956	MMP1	Interstitial collagenase;22 kDa interstitial collagenase;27 kDa interstitial collagenase	6 h	IL-1b vs CON	down	
P08253	MMP2	72 kDa type IV collagenase;PEX	6 h	IL-1b vs CON	down	
Q15113	PCOLCE	Procollagen C-endopeptidase enhancer 1	6 h	IL-1b vs CON	down	
Q02809	PLOD1	Procollagen-lysine,2-oxoglutarate 5-dioxygenase 1	6 h	IL-1b vs CON	up	
O00469	PLOD2	Procollagen-lysine,2-oxoglutarate 5-dioxygenase 2	6 h	IL-1b vs CON	up	
O60568	PLOD3	Procollagen-lysine,2-oxoglutarate 5-dioxygenase 3	6 h	IL-1b vs CON	up	
P12107	COL11A1	Collagen alpha-1(XI) chain	6 h	TBHP + IL-1b vs IL-1b	up	
Q99715	COL12A1	Collagen alpha-1(XII) chain	6 h	TBHP + IL-1b vs IL-1b	down	
Q05707	COL14A1	Collagen alpha-1(XIV) chain	6 h	TBHP + IL-1b vs IL-1b	up	
Q07092	COL16A1	Collagen alpha-1(XVI) chain	6 h	TBHP + IL-1b vs IL-1b	down	
P39060	COL18A1	Collagen alpha-1(XVIII) chain;Endostatin	6 h	TBHP + IL-1b vs IL-1b	up	
P02452	COL1A1	Collagen alpha-1(I) chain	6 h	TBHP + IL-1b vs IL-1b	down	
P08123	COL1A2	Collagen alpha-2(I) chain	6 h	TBHP + IL-1b vs IL-1b	up	
P02461	COL3A1	Collagen alpha-1(III) chain	6 h	TBHP + IL-1b vs IL-1b	down	
P02462	COL4A1	Collagen alpha-1(IV) chain;Arresten	6 h	TBHP + IL-1b vs IL-1b	down	
P08572	COL4A2	Collagen alpha-2(IV) chain;Canstatin	6 h	TBHP + IL-1b vs IL-1b	down	
Q9Y5P4	COL4A3BP	Collagen type IV alpha-3-binding protein	6 h	TBHP + IL-1b vs IL-1b	up	
P20908	COL5A1	Collagen alpha-1(V) chain	6 h	TBHP + IL-1b vs IL-1b	down	
P05997	COL5A2	Collagen alpha-2(V) chain	6 h	TBHP + IL-1b vs IL-1b	down	
P25940	COL5A3	Collagen alpha-3(V) chain	6 h	TBHP + IL-1b vs IL-1b	down	
P12109	COL6A1	Collagen alpha-1(VI) chain	6 h	TBHP + IL-1b vs IL-1b	down	
P12110	COL6A2	Collagen alpha-2(VI) chain	6 h	TBHP + IL-1b vs IL-1b	up	
P12111	COL6A3	Collagen alpha-3(VI) chain	6 h	TBHP + IL-1b vs IL-1b	down	
Q02388	COL7A1	Collagen alpha-1(VII) chain	6 h	TBHP + IL-1b vs IL-1b	down	
P27658	COL8A1	Collagen alpha-1(VIII) chain;Vastatin	6 h	TBHP + IL-1b vs IL-1b	down	

Q8NBJ5	COLGALT1	Procollagen galactosyltransferase 1	6 h	TBHP + IL-1b vs IL-1b	down	
Q96CG8	CTHRC1	Collagen triple helix repeat-containing protein 1	6 h	TBHP + IL-1b vs IL-1b	up	
P03956	MMP1	Interstitial collagenase;22 kDa interstitial collagenase;27 kDa interstitial collagenase	6 h	TBHP + IL-1b vs IL-1b	up	
P08253	MMP2	72 kDa type IV collagenase;PEX	6 h	TBHP + IL-1b vs IL-1b	down	
Q15113	PCOLCE	Procollagen C-endopeptidase enhancer 1	6 h	TBHP + IL-1b vs IL-1b	up	
Q02809	PLOD1	Procollagen-lysine,2-oxoglutarate 5-dioxygenase 1	6 h	TBHP + IL-1b vs IL-1b	down	
O00469	PLOD2	Procollagen-lysine,2-oxoglutarate 5-dioxygenase 2	6 h	TBHP + IL-1b vs IL-1b	down	
O60568	PLOD3	Procollagen-lysine,2-oxoglutarate 5-dioxygenase 3	6 h	TBHP + IL-1b vs IL-1b	down	
P12107	COL11A1	Collagen alpha-1(XI) chain	24 h	IL-1b vs CON	down	
Q99715	COL12A1	Collagen alpha-1(XII) chain	24 h	IL-1b vs CON	down	
Q05707	COL14A1	Collagen alpha-1(XIV) chain	24 h	IL-1b vs CON	down	
Q07092	COL16A1	Collagen alpha-1(XVI) chain	24 h	IL-1b vs CON	up	yes
P39060	COL18A1	Collagen alpha-1(XVIII) chain;Endostatin	24 h	IL-1b vs CON	up	
P02452	COL1A1	Collagen alpha-1(I) chain	24 h	IL-1b vs CON	down	yes
P08123	COL1A2	Collagen alpha-2(I) chain	24 h	IL-1b vs CON	down	yes
P02461	COL3A1	Collagen alpha-1(III) chain	24 h	IL-1b vs CON	down	yes
P02462	COL4A1	Collagen alpha-1(IV) chain;Arresten	24 h	IL-1b vs CON	up	
P08572	COL4A2	Collagen alpha-2(IV) chain;Canstatin	24 h	IL-1b vs CON	up	
Q9Y5P4	COL4A3BP	Collagen type IV alpha-3-binding protein	24 h	IL-1b vs CON	up	
P20908	COL5A1	Collagen alpha-1(V) chain	24 h	IL-1b vs CON	down	
P05997	COL5A2	Collagen alpha-2(V) chain	24 h	IL-1b vs CON	up	
P25940	COL5A3	Collagen alpha-3(V) chain	24 h	IL-1b vs CON	up	
P12109	COL6A1	Collagen alpha-1(VI) chain	24 h	IL-1b vs CON	down	
P12110	COL6A2	Collagen alpha-2(VI) chain	24 h	IL-1b vs CON	down	
P12111	COL6A3	Collagen alpha-3(VI) chain	24 h	IL-1b vs CON	down	
Q02388	COL7A1	Collagen alpha-1(VII) chain	24 h	IL-1b vs CON	up	yes
P27658	COL8A1	Collagen alpha-1(VIII) chain;Vastatin	24 h	IL-1b vs CON	up	yes
Q8NBJ5	COLGALT1	Procollagen galactosyltransferase 1	24 h	IL-1b vs CON	up	
Q96CG8	CTHRC1	Collagen triple helix repeat-containing protein 1	24 h	IL-1b vs CON	down	
P03956	MMP1	Interstitial collagenase;22 kDa interstitial collagenase;27 kDa interstitial collagenase	24 h	IL-1b vs CON	up	yes
P08253	MMP2	72 kDa type IV collagenase;PEX	24 h	IL-1b vs CON	up	
Q15113	PCOLCE	Procollagen C-endopeptidase enhancer 1	24 h	IL-1b vs CON	down	
Q02809	PLOD1	Procollagen-lysine,2-oxoglutarate 5-dioxygenase 1	24 h	IL-1b vs CON	up	
O00469	PLOD2	Procollagen-lysine,2-oxoglutarate 5-dioxygenase 2	24 h	IL-1b vs CON	up	
O60568	PLOD3	Procollagen-lysine,2-oxoglutarate 5-dioxygenase 3	24 h	IL-1b vs CON	down	
P12107	COL11A1	Collagen alpha-1(XI) chain	24 h	TBHP + IL-1b vs IL-1b	down	
Q99715	COL12A1	Collagen alpha-1(XII) chain	24 h	TBHP + IL-1b vs IL-1b	down	
Q05707	COL14A1	Collagen alpha-1(XIV) chain	24 h	TBHP + IL-1b vs IL-1b	down	
Q07092	COL16A1	Collagen alpha-1(XVI) chain	24 h	TBHP + IL-1b vs IL-1b	down	
P39060	COL18A1	Collagen alpha-1(XVIII) chain;Endostatin	24 h	TBHP + IL-1b vs IL-1b	down	
P02452	COL1A1	Collagen alpha-1(I) chain	24 h	TBHP + IL-1b vs IL-1b	down	
P08123	COL1A2	Collagen alpha-2(I) chain	24 h	TBHP + IL-1b vs IL-1b	down	
P02461	COL3A1	Collagen alpha-1(III) chain	24 h	TBHP + IL-1b vs IL-1b	down	
P02462	COL4A1	Collagen alpha-1(IV) chain;Arresten	24 h	TBHP + IL-1b vs IL-1b	up	
P08572	COL4A2	Collagen alpha-2(IV) chain;Canstatin	24 h	TBHP + IL-1b vs IL-1b	up	
Q9Y5P4	COL4A3BP	Collagen type IV alpha-3-binding protein	24 h	TBHP + IL-1b vs IL-1b	down	
P20908	COL5A1	Collagen alpha-1(V) chain	24 h	TBHP + IL-1b vs IL-1b	down	
P05997	COL5A2	Collagen alpha-2(V) chain	24 h	TBHP + IL-1b vs IL-1b	down	

P25940	COL5A3	Collagen alpha-3(V) chain	24 h	TBHP + IL-1b vs IL-1b	down	
P12109	COL6A1	Collagen alpha-1(VI) chain	24 h	TBHP + IL-1b vs IL-1b	up	
P12110	COL6A2	Collagen alpha-2(VI) chain	24 h	TBHP + IL-1b vs IL-1b	up	
P12111	COL6A3	Collagen alpha-3(VI) chain	24 h	TBHP + IL-1b vs IL-1b	up	
Q02388	COL7A1	Collagen alpha-1(VII) chain	24 h	TBHP + IL-1b vs IL-1b	down	
P27658	COL8A1	Collagen alpha-1(VIII) chain;Vastatin	24 h	TBHP + IL-1b vs IL-1b	up	
Q8NBJ5	COLGALT1	Procollagen galactosyltransferase 1	24 h	TBHP + IL-1b vs IL-1b	down	
Q96CG8	CTHRC1	Collagen triple helix repeat-containing protein 1	24 h	TBHP + IL-1b vs IL-1b	down	
P03956	MMP1	Interstitial collagenase;22 kDa interstitial collagenase;27 kDa interstitial collagenase	24 h	TBHP + IL-1b vs IL-1b	up	
P08253	MMP2	72 kDa type IV collagenase;PEX	24 h	TBHP + IL-1b vs IL-1b	up	
Q15113	PCOLCE	Procollagen C-endopeptidase enhancer 1	24 h	TBHP + IL-1b vs IL-1b	down	
Q02809	PLOD1	Procollagen-lysine,2-oxoglutarate 5-dioxygenase 1	24 h	TBHP + IL-1b vs IL-1b	down	
O00469	PLOD2	Procollagen-lysine,2-oxoglutarate 5-dioxygenase 2	24 h	TBHP + IL-1b vs IL-1b	down	
O60568	PLOD3	Procollagen-lysine,2-oxoglutarate 5-dioxygenase 3	24 h	TBHP + IL-1b vs IL-1b	down	
P12107	COL11A1	Collagen alpha-1(XI) chain	48 h	IL-1b vs CON	down	
Q99715	COL12A1	Collagen alpha-1(XII) chain	48 h	IL-1b vs CON	down	
Q05707	COL14A1	Collagen alpha-1(XIV) chain	48 h	IL-1b vs CON	down	yes
Q07092	COL16A1	Collagen alpha-1(XVI) chain	48 h	IL-1b vs CON	up	yes
P39060	COL18A1	Collagen alpha-1(XVIII) chain;Endostatin	48 h	IL-1b vs CON	up	
P02452	COL1A1	Collagen alpha-1(I) chain	48 h	IL-1b vs CON	down	yes
P08123	COL1A2	Collagen alpha-2(I) chain	48 h	IL-1b vs CON	down	yes
P02461	COL3A1	Collagen alpha-1(III) chain	48 h	IL-1b vs CON	down	yes
P02462	COL4A1	Collagen alpha-1(IV) chain;Arresten	48 h	IL-1b vs CON	up	yes
P08572	COL4A2	Collagen alpha-2(IV) chain;Canstatin	48 h	IL-1b vs CON	up	yes
Q9Y5P4	COL4A3BP	Collagen type IV alpha-3-binding protein	48 h	IL-1b vs CON	down	
P20908	COL5A1	Collagen alpha-1(V) chain	48 h	IL-1b vs CON	down	yes
P05997	COL5A2	Collagen alpha-2(V) chain	48 h	IL-1b vs CON	down	
P25940	COL5A3	Collagen alpha-3(V) chain	48 h	IL-1b vs CON	down	
P12109	COL6A1	Collagen alpha-1(VI) chain	48 h	IL-1b vs CON	down	
P12110	COL6A2	Collagen alpha-2(VI) chain	48 h	IL-1b vs CON	down	
P12111	COL6A3	Collagen alpha-3(VI) chain	48 h	IL-1b vs CON	down	
Q02388	COL7A1	Collagen alpha-1(VII) chain	48 h	IL-1b vs CON	up	
P27658	COL8A1	Collagen alpha-1(VIII) chain;Vastatin	48 h	IL-1b vs CON	up	yes
Q8NBJ5	COLGALT1	Procollagen galactosyltransferase 1	48 h	IL-1b vs CON	down	
Q96CG8	CTHRC1	Collagen triple helix repeat-containing protein 1	48 h	IL-1b vs CON	down	
P03956	MMP1	Interstitial collagenase;22 kDa interstitial collagenase;27 kDa interstitial collagenase	48 h	IL-1b vs CON	up	yes
P08253	MMP2	72 kDa type IV collagenase;PEX	48 h	IL-1b vs CON	up	
Q15113	PCOLCE	Procollagen C-endopeptidase enhancer 1	48 h	IL-1b vs CON	down	yes
Q02809	PLOD1	Procollagen-lysine,2-oxoglutarate 5-dioxygenase 1	48 h	IL-1b vs CON	up	
O00469	PLOD2	Procollagen-lysine,2-oxoglutarate 5-dioxygenase 2	48 h	IL-1b vs CON	up	yes
O60568	PLOD3	Procollagen-lysine,2-oxoglutarate 5-dioxygenase 3	48 h	IL-1b vs CON	down	
P12107	COL11A1	Collagen alpha-1(XI) chain	48 h	TBHP + IL-1b vs IL-1b	down	
Q99715	COL12A1	Collagen alpha-1(XII) chain	48 h	TBHP + IL-1b vs IL-1b	up	
Q05707	COL14A1	Collagen alpha-1(XIV) chain	48 h	TBHP + IL-1b vs IL-1b	down	
Q07092	COL16A1	Collagen alpha-1(XVI) chain	48 h	TBHP + IL-1b vs IL-1b	up	
P39060	COL18A1	Collagen alpha-1(XVIII) chain;Endostatin	48 h	TBHP + IL-1b vs IL-1b	down	
P02452	COL1A1	Collagen alpha-1(I) chain	48 h	TBHP + IL-1b vs IL-1b	down	
P08123	COL1A2	Collagen alpha-2(I) chain	48 h	TBHP + IL-1b vs IL-1b	down	

P02461	COL3A1	Collagen alpha-1(III) chain	48 h	TBHP + IL-1b vs IL-1b	down	
P02462	COL4A1	Collagen alpha-1(IV) chain;Arresten	48 h	TBHP + IL-1b vs IL-1b	up	
P08572	COL4A2	Collagen alpha-2(IV) chain;Canstatin	48 h	TBHP + IL-1b vs IL-1b	up	
Q9Y5P4	COL4A3BP	Collagen type IV alpha-3-binding protein	48 h	TBHP + IL-1b vs IL-1b	up	
P20908	COL5A1	Collagen alpha-1(V) chain	48 h	TBHP + IL-1b vs IL-1b	down	
P05997	COL5A2	Collagen alpha-2(V) chain	48 h	TBHP + IL-1b vs IL-1b	down	
P25940	COL5A3	Collagen alpha-3(V) chain	48 h	TBHP + IL-1b vs IL-1b	up	
P12109	COL6A1	Collagen alpha-1(VI) chain	48 h	TBHP + IL-1b vs IL-1b	up	
P12110	COL6A2	Collagen alpha-2(VI) chain	48 h	TBHP + IL-1b vs IL-1b	down	
P12111	COL6A3	Collagen alpha-3(VI) chain	48 h	TBHP + IL-1b vs IL-1b	up	
Q02388	COL7A1	Collagen alpha-1(VII) chain	48 h	TBHP + IL-1b vs IL-1b	down	
P27658	COL8A1	Collagen alpha-1(VIII) chain;Vastatin	48 h	TBHP + IL-1b vs IL-1b	up	
Q8NBJ5	COLGALT1	Procollagen galactosyltransferase 1	48 h	TBHP + IL-1b vs IL-1b	up	
Q96CG8	CTHRC1	Collagen triple helix repeat-containing protein 1	48 h	TBHP + IL-1b vs IL-1b	down	
P03956	MMP1	Interstitial collagenase;22 kDa interstitial collagenase;27 kDa interstitial collagenase	48 h	TBHP + IL-1b vs IL-1b	up	yes
P08253	MMP2	72 kDa type IV collagenase;PEX	48 h	TBHP + IL-1b vs IL-1b	up	
Q15113	PCOLCE	Procollagen C-endopeptidase enhancer 1	48 h	TBHP + IL-1b vs IL-1b	down	
Q02809	PLOD1	Procollagen-lysine,2-oxoglutarate 5-dioxygenase 1	48 h	TBHP + IL-1b vs IL-1b	down	
O00469	PLOD2	Procollagen-lysine,2-oxoglutarate 5-dioxygenase 2	48 h	TBHP + IL-1b vs IL-1b	down	
O60568	PLOD3	Procollagen-lysine,2-oxoglutarate 5-dioxygenase 3	48 h	TBHP + IL-1b vs IL-1b	down	

Table S 13 Collagen and collagen-associated proteins - SN

Majority protein IDs	Gene names	Protein names	Time-point	Comparison	log2FC direction	Significant
P12107	COL11A1	Collagen alpha-1(XI) chain	6 h	IL-1b vs CON	down	yes
Q99715	COL12A1	Collagen alpha-1(XII) chain	6 h	IL-1b vs CON	down	
P39060	COL18A1	Collagen alpha-1(XVIII) chain;Endostatin	6 h	IL-1b vs CON	up	
P02452	COL1A1	Collagen alpha-1(I) chain	6 h	IL-1b vs CON	down	
P08123	COL1A2	Collagen alpha-2(I) chain	6 h	IL-1b vs CON	up	
P02458	COL2A1	Collagen alpha-1(II) chain;Collagen alpha-1(II) chain;Chondrocalcin	6 h	IL-1b vs CON	up	
P02461	COL3A1	Collagen alpha-1(III) chain	6 h	IL-1b vs CON	down	
P02462	COL4A1	Collagen alpha-1(IV) chain;Arresten	6 h	IL-1b vs CON	down	
P08572	COL4A2	Collagen alpha-2(IV) chain;Canstatin	6 h	IL-1b vs CON	down	
P20908	COL5A1	Collagen alpha-1(V) chain	6 h	IL-1b vs CON	down	
P05997	COL5A2	Collagen alpha-2(V) chain	6 h	IL-1b vs CON	down	
P25940	COL5A3	Collagen alpha-3(V) chain	6 h	IL-1b vs CON	down	
P12109	COL6A1	Collagen alpha-1(VI) chain	6 h	IL-1b vs CON	down	
P12110	COL6A2	Collagen alpha-2(VI) chain	6 h	IL-1b vs CON	down	
P12111	COL6A3	Collagen alpha-3(VI) chain	6 h	IL-1b vs CON	down	
Q02388	COL7A1	Collagen alpha-1(VII) chain	6 h	IL-1b vs CON	up	
P27658	COL8A1	Collagen alpha-1(VIII) chain;Vastatin	6 h	IL-1b vs CON	down	
Q96CG8	CTHRC1	Collagen triple helix repeat-containing protein 1	6 h	IL-1b vs CON	up	
P03956	MMP1	Interstitial collagenase;22 kDa interstitial collagenase;27 kDa interstitial collagenase	6 h	IL-1b vs CON	up	
P08253	MMP2	72 kDa type IV collagenase;PEX	6 h	IL-1b vs CON	down	
Q15113	PCOLCE	Procollagen C-endopeptidase enhancer 1	6 h	IL-1b vs CON	up	
Q02809	PLOD1	Procollagen-lysine,2-oxoglutarate 5-dioxygenase 1	6 h	IL-1b vs CON	down	
O00469	PLOD2	Procollagen-lysine,2-oxoglutarate 5-dioxygenase 2	6 h	IL-1b vs CON	down	

P12107	COL11A1	Collagen alpha-1(XI) chain	6 h	TBHP + IL-1b vs IL-1b	down	
Q99715	COL12A1	Collagen alpha-1(XII) chain	6 h	TBHP + IL-1b vs IL-1b	down	
P39060	COL18A1	Collagen alpha-1(XVIII) chain;Endostatin	6 h	TBHP + IL-1b vs IL-1b	down	
P02452	COL1A1	Collagen alpha-1(I) chain	6 h	TBHP + IL-1b vs IL-1b	down	
P08123	COL1A2	Collagen alpha-2(I) chain	6 h	TBHP + IL-1b vs IL-1b	down	
P02458	COL2A1	Collagen alpha-1(II) chain;Collagen alpha-1(II) chain;Chondrocalcin	6 h	TBHP + IL-1b vs IL-1b	down	yes
P02461	COL3A1	Collagen alpha-1(III) chain	6 h	TBHP + IL-1b vs IL-1b	down	
P02462	COL4A1	Collagen alpha-1(IV) chain;Arresten	6 h	TBHP + IL-1b vs IL-1b	down	
P08572	COL4A2	Collagen alpha-2(IV) chain;Canstatin	6 h	TBHP + IL-1b vs IL-1b	down	
P20908	COL5A1	Collagen alpha-1(V) chain	6 h	TBHP + IL-1b vs IL-1b	down	
P05997	COL5A2	Collagen alpha-2(V) chain	6 h	TBHP + IL-1b vs IL-1b	down	
P25940	COL5A3	Collagen alpha-3(V) chain	6 h	TBHP + IL-1b vs IL-1b	down	
P12109	COL6A1	Collagen alpha-1(VI) chain	6 h	TBHP + IL-1b vs IL-1b	down	
P12110	COL6A2	Collagen alpha-2(VI) chain	6 h	TBHP + IL-1b vs IL-1b	down	
P12111	COL6A3	Collagen alpha-3(VI) chain	6 h	TBHP + IL-1b vs IL-1b	down	
Q02388	COL7A1	Collagen alpha-1(VII) chain	6 h	TBHP + IL-1b vs IL-1b	up	
P27658	COL8A1	Collagen alpha-1(VIII) chain;Vastatin	6 h	TBHP + IL-1b vs IL-1b	up	
Q96CG8	CTHRC1	Collagen triple helix repeat-containing protein 1	6 h	TBHP + IL-1b vs IL-1b	down	
P03956	MMP1	Interstitial collagenase;22 kDa interstitial collagenase;27 kDa interstitial collagenase	6 h	TBHP + IL-1b vs IL-1b	up	
P08253	MMP2	72 kDa type IV collagenase;PEX	6 h	TBHP + IL-1b vs IL-1b	down	
Q15113	PCOLCE	Procollagen C-endopeptidase enhancer 1	6 h	TBHP + IL-1b vs IL-1b	down	
Q02809	PLOD1	Procollagen-lysine,2-oxoglutarate 5-dioxygenase 1	6 h	TBHP + IL-1b vs IL-1b	down	
O00469	PLOD2	Procollagen-lysine,2-oxoglutarate 5-dioxygenase 2	6 h	TBHP + IL-1b vs IL-1b	down	
P12107	COL11A1	Collagen alpha-1(XI) chain	24 h	IL-1b vs CON	up	
Q99715	COL12A1	Collagen alpha-1(XII) chain	24 h	IL-1b vs CON	up	
P39060	COL18A1	Collagen alpha-1(XVIII) chain;Endostatin	24 h	IL-1b vs CON	up	
P02452	COL1A1	Collagen alpha-1(I) chain	24 h	IL-1b vs CON	down	
P08123	COL1A2	Collagen alpha-2(I) chain	24 h	IL-1b vs CON	down	
P02458	COL2A1	Collagen alpha-1(II) chain;Collagen alpha-1(II) chain;Chondrocalcin	24 h	IL-1b vs CON	down	
P02461	COL3A1	Collagen alpha-1(III) chain	24 h	IL-1b vs CON	down	
P02462	COL4A1	Collagen alpha-1(IV) chain;Arresten	24 h	IL-1b vs CON	down	
P08572	COL4A2	Collagen alpha-2(IV) chain;Canstatin	24 h	IL-1b vs CON	down	
P20908	COL5A1	Collagen alpha-1(V) chain	24 h	IL-1b vs CON	down	
P05997	COL5A2	Collagen alpha-2(V) chain	24 h	IL-1b vs CON	down	
P25940	COL5A3	Collagen alpha-3(V) chain	24 h	IL-1b vs CON	up	
P12109	COL6A1	Collagen alpha-1(VI) chain	24 h	IL-1b vs CON	up	
P12110	COL6A2	Collagen alpha-2(VI) chain	24 h	IL-1b vs CON	up	
P12111	COL6A3	Collagen alpha-3(VI) chain	24 h	IL-1b vs CON	up	
Q02388	COL7A1	Collagen alpha-1(VII) chain	24 h	IL-1b vs CON	down	
P27658	COL8A1	Collagen alpha-1(VIII) chain;Vastatin	24 h	IL-1b vs CON	up	
Q96CG8	CTHRC1	Collagen triple helix repeat-containing protein 1	24 h	IL-1b vs CON	up	
P03956	MMP1	Interstitial collagenase;22 kDa interstitial collagenase;27 kDa interstitial collagenase	24 h	IL-1b vs CON	up	
P08253	MMP2	72 kDa type IV collagenase;PEX	24 h	IL-1b vs CON	down	
Q15113	PCOLCE	Procollagen C-endopeptidase enhancer 1	24 h	IL-1b vs CON	down	
Q02809	PLOD1	Procollagen-lysine,2-oxoglutarate 5-dioxygenase 1	24 h	IL-1b vs CON	up	
O00469	PLOD2	Procollagen-lysine,2-oxoglutarate 5-dioxygenase 2	24 h	IL-1b vs CON	up	

P12107	COL11A1	Collagen alpha-1(XI) chain	24 h	TBHP + IL-1b vs IL-1b	down	
Q99715	COL12A1	Collagen alpha-1(XII) chain	24 h	TBHP + IL-1b vs IL-1b	down	
P39060	COL18A1	Collagen alpha-1(XVIII) chain;Endostatin	24 h	TBHP + IL-1b vs IL-1b	up	
P02452	COL1A1	Collagen alpha-1(I) chain	24 h	TBHP + IL-1b vs IL-1b	down	
P08123	COL1A2	Collagen alpha-2(I) chain	24 h	TBHP + IL-1b vs IL-1b	up	
P02458	COL2A1	Collagen alpha-1(II) chain;Collagen alpha-1(II) chain;Chondrocalcin	24 h	TBHP + IL-1b vs IL-1b	down	
P02461	COL3A1	Collagen alpha-1(III) chain	24 h	TBHP + IL-1b vs IL-1b	down	
P02462	COL4A1	Collagen alpha-1(IV) chain;Arresten	24 h	TBHP + IL-1b vs IL-1b	up	
P08572	COL4A2	Collagen alpha-2(IV) chain;Canstatin	24 h	TBHP + IL-1b vs IL-1b	down	
P20908	COL5A1	Collagen alpha-1(V) chain	24 h	TBHP + IL-1b vs IL-1b	down	
P05997	COL5A2	Collagen alpha-2(V) chain	24 h	TBHP + IL-1b vs IL-1b	up	
P25940	COL5A3	Collagen alpha-3(V) chain	24 h	TBHP + IL-1b vs IL-1b	down	
P12109	COL6A1	Collagen alpha-1(VI) chain	24 h	TBHP + IL-1b vs IL-1b	up	
P12110	COL6A2	Collagen alpha-2(VI) chain	24 h	TBHP + IL-1b vs IL-1b	up	
P12111	COL6A3	Collagen alpha-3(VI) chain	24 h	TBHP + IL-1b vs IL-1b	down	
Q02388	COL7A1	Collagen alpha-1(VII) chain	24 h	TBHP + IL-1b vs IL-1b	down	
P27658	COL8A1	Collagen alpha-1(VIII) chain;Vastatin	24 h	TBHP + IL-1b vs IL-1b	up	
Q96CG8	CTHRC1	Collagen triple helix repeat-containing protein 1	24 h	TBHP + IL-1b vs IL-1b	up	
P03956	MMP1	Interstitial collagenase;22 kDa interstitial collagenase;27 kDa interstitial collagenase	24 h	TBHP + IL-1b vs IL-1b	up	
P08253	MMP2	72 kDa type IV collagenase;PEX	24 h	TBHP + IL-1b vs IL-1b	up	
Q15113	PCOLCE	Procollagen C-endopeptidase enhancer 1	24 h	TBHP + IL-1b vs IL-1b	down	
Q02809	PLOD1	Procollagen-lysine,2-oxoglutarate 5-dioxygenase 1	24 h	TBHP + IL-1b vs IL-1b	down	
O00469	PLOD2	Procollagen-lysine,2-oxoglutarate 5-dioxygenase 2	24 h	TBHP + IL-1b vs IL-1b	up	
P12107	COL11A1	Collagen alpha-1(XI) chain	48 h	IL-1b vs CON	down	yes
Q99715	COL12A1	Collagen alpha-1(XII) chain	48 h	IL-1b vs CON	down	
P39060	COL18A1	Collagen alpha-1(XVIII) chain;Endostatin	48 h	IL-1b vs CON	down	
P02452	COL1A1	Collagen alpha-1(I) chain	48 h	IL-1b vs CON	down	yes
P08123	COL1A2	Collagen alpha-2(I) chain	48 h	IL-1b vs CON	down	yes
P02458	COL2A1	Collagen alpha-1(II) chain;Collagen alpha-1(II) chain;Chondrocalcin	48 h	IL-1b vs CON	up	
P02461	COL3A1	Collagen alpha-1(III) chain	48 h	IL-1b vs CON	down	
P02462	COL4A1	Collagen alpha-1(IV) chain;Arresten	48 h	IL-1b vs CON	down	
P08572	COL4A2	Collagen alpha-2(IV) chain;Canstatin	48 h	IL-1b vs CON	down	
P20908	COL5A1	Collagen alpha-1(V) chain	48 h	IL-1b vs CON	down	
P05997	COL5A2	Collagen alpha-2(V) chain	48 h	IL-1b vs CON	down	
P25940	COL5A3	Collagen alpha-3(V) chain	48 h	IL-1b vs CON	up	
P12109	COL6A1	Collagen alpha-1(VI) chain	48 h	IL-1b vs CON	down	
P12110	COL6A2	Collagen alpha-2(VI) chain	48 h	IL-1b vs CON	down	
P12111	COL6A3	Collagen alpha-3(VI) chain	48 h	IL-1b vs CON	down	
Q02388	COL7A1	Collagen alpha-1(VII) chain	48 h	IL-1b vs CON	down	
P27658	COL8A1	Collagen alpha-1(VIII) chain;Vastatin	48 h	IL-1b vs CON	up	
Q96CG8	CTHRC1	Collagen triple helix repeat-containing protein 1	48 h	IL-1b vs CON	down	
P03956	MMP1	Interstitial collagenase;22 kDa interstitial collagenase;27 kDa interstitial collagenase	48 h	IL-1b vs CON	up	
P08253	MMP2	72 kDa type IV collagenase;PEX	48 h	IL-1b vs CON	down	
Q15113	PCOLCE	Procollagen C-endopeptidase enhancer 1	48 h	IL-1b vs CON	down	
Q02809	PLOD1	Procollagen-lysine,2-oxoglutarate 5-dioxygenase 1	48 h	IL-1b vs CON	up	
O00469	PLOD2	Procollagen-lysine,2-oxoglutarate 5-dioxygenase 2	48 h	IL-1b vs CON	up	

P12107	COL11A1	Collagen alpha-1(XI) chain	48 h	TBHP + IL-1b vs IL-1b	up	
Q99715	COL12A1	Collagen alpha-1(XII) chain	48 h	TBHP + IL-1b vs IL-1b	up	
P39060	COL18A1	Collagen alpha-1(XVIII) chain;Endostatin	48 h	TBHP + IL-1b vs IL-1b	up	
P02452	COL1A1	Collagen alpha-1(I) chain	48 h	TBHP + IL-1b vs IL-1b	up	
P08123	COL1A2	Collagen alpha-2(I) chain	48 h	TBHP + IL-1b vs IL-1b	up	
P02458	COL2A1	Collagen alpha-1(II) chain;Collagen alpha-1(II) chain;Chondrocalcin	48 h	TBHP + IL-1b vs IL-1b	down	
P02461	COL3A1	Collagen alpha-1(III) chain	48 h	TBHP + IL-1b vs IL-1b	up	
P02462	COL4A1	Collagen alpha-1(IV) chain;Arresten	48 h	TBHP + IL-1b vs IL-1b	up	
P08572	COL4A2	Collagen alpha-2(IV) chain;Canstatin	48 h	TBHP + IL-1b vs IL-1b	up	
P20908	COL5A1	Collagen alpha-1(V) chain	48 h	TBHP + IL-1b vs IL-1b	up	
P05997	COL5A2	Collagen alpha-2(V) chain	48 h	TBHP + IL-1b vs IL-1b	up	
P25940	COL5A3	Collagen alpha-3(V) chain	48 h	TBHP + IL-1b vs IL-1b	up	
P12109	COL6A1	Collagen alpha-1(VI) chain	48 h	TBHP + IL-1b vs IL-1b	up	
P12110	COL6A2	Collagen alpha-2(VI) chain	48 h	TBHP + IL-1b vs IL-1b	up	
P12111	COL6A3	Collagen alpha-3(VI) chain	48 h	TBHP + IL-1b vs IL-1b	up	
Q02388	COL7A1	Collagen alpha-1(VII) chain	48 h	TBHP + IL-1b vs IL-1b	up	
P27658	COL8A1	Collagen alpha-1(VIII) chain;Vastatin	48 h	TBHP + IL-1b vs IL-1b	up	
Q96CG8	CTHRC1	Collagen triple helix repeat-containing protein 1	48 h	TBHP + IL-1b vs IL-1b	up	
P03956	MMP1	Interstitial collagenase;22 kDa interstitial collagenase;27 kDa interstitial collagenase	48 h	TBHP + IL-1b vs IL-1b	up	
P08253	MMP2	72 kDa type IV collagenase;PEX	48 h	TBHP + IL-1b vs IL-1b	up	
Q15113	PCOLCE	Procollagen C-endopeptidase enhancer 1	48 h	TBHP + IL-1b vs IL-1b	up	
Q02809	PLOD1	Procollagen-lysine,2-oxoglutarate 5-dioxygenase 1	48 h	TBHP + IL-1b vs IL-1b	up	
O00469	PLOD2	Procollagen-lysine,2-oxoglutarate 5-dioxygenase 2	48 h	TBHP + IL-1b vs IL-1b	down	

List of Figures

List of Tables

Hilfsmittelverzeichnis

KI-Hilfsmittel	**Einsatz**	**Betroffene Teile der Arbeit**	**Bemerkungen**
OpenAI ChatGPT	Unterstützung bei der Erstellung und Fehlersuche von R-Code, bei der grafischen Darstellung der Daten (PCA-Plots, Loadings-Plots, Volcano-Plots, Dotplots) sowie bei Durchführung des Gene-Ontology-Enrichments.	Kapitel 3.5 (Data Processing) und Kapitel 4 (Results)	In Kapitel 3.5 wurde ChatGPT zur Unterstützung beim Code genutzt. Die daraus resultierenden Abbildungen sind in Kapitel 4 abgebildet.
Grammarly	Sprachliche Korrekturen und Stilverbesserungen	Kapitel 1 (Introduction), Kapitel 4 (Results) und Kapitel 5 (Discussion)	Grammarly wurde vereinzelt zur Unterstützung von Grammatik und Stil verwendet.